NAVIGATION ANALYSIS OF EARTH-MOON LIBRATION POINT MISSIONS

by

Anthony John Gingiss

B.S., Aeronautical & Astronautical Engineering, Purdue University
West Lafayette, Indiana - May 1990

Submitted to the Department of Aeronautics and Astronautics
in Partial Fulfillment of the Requirements for the Degree of

MASTER OF SCIENCE IN AERONAUTICS AND ASTRONAUTICS

at the

MASSACHUSETTS INSTITUTE OF TECHNOLOGY

June 1992

Signature of Author _____
Department of Aeronautics and Astronautics
June 1, 1992

Certified by _____
Professor Richard H. Battin
Department of Aeronautics & Astronautics
Thesis Advisor

Certified by _____
Professor Joseph F. Shea
Department of Aeronautics & Astronautics
Thesis Advisor

Certified by _____
Kenneth M. Spratlin
Charles Stark Draper Laboratory, Inc.
Technical Supervisor

Certified by _____
Stanley W. Shepperd
Charles Stark Draper Laboratory, Inc.
Technical Supervisor

Approved by _____
Professor Harold Y. Wachman
Chairman, Departmental Committee on Graduate Studies
Department of Aeronautics and Astronautics

NAVIGATION ANALYSIS OF EARTH-MOON LIBRATION POINT MISSIONS

by

Anthony John Gingiss

Submitted to the
Department of Aeronautics and Astronautics
on May 15, 1992.

In partial fulfillment of the requirements for the degree of
Master of Science in Aeronautics and Astronautics

Abstract

The Restricted Three-Body Problem is examined to determine the performance of navigation for libration point missions. The environments in the vicinities of the three collinear libration points are examined to determine the primary perturbation effects to be considered (e.g. solar radiation pressure, J2, etc.). Navigation analysis is performed for an onboard system which uses a Kalman filter for state estimation. Various measurement types are investigated to determine the optimal choice of measurement systems for this class of problems.

Application of navigation methods to several possible libration point missions is presented. Navigation analysis is performed using a computer simulation which integrates the three-body equations of motion and accounts for specified environmental perturbations. The navigation system performance is evaluated with additional discussion of the impact of environmental perturbations. Limitations in the application of current guidance and navigation methods to this problem are presented and areas of further warranted research identified.

Thesis Supervisor:	Dr. Richard H. Battin Adjunct Professor of Aeronautics and Astronautics
Thesis Supervisor:	Dr. Joseph F. Shea Adjunct Professor of Aeronautics and Astronautics
Technical Supervisor:	Kenneth M. Spratlin Group Leader, The Charles Stark Draper Laboratory, Inc.
Technical Supervisor:	Stanley W. Shepperd Staff Engineer, The Charles Stark Draper Laboratory, Inc.

Acknowledgments

I would like to take this opportunity to thank some of the many people who have made my graduate studies such a valuable experience.

To the Charles Stark Draper Laboratory for making my studies at MIT possible through the Draper Lab Fellowship. To Tim , Vicki , Doug , Tony, Barbara, Lori and the rest of the Guidance and Navigation Analysis Division for making my time at Draper an enjoyable one. To Stan Shepperd and Ken Spratlin whose technical support, expertise and general assistance with my thesis was invaluable.

To Prof. K.C. Howell at Purdue University and Profs. J.F. Shea and R.H. Battin at MIT for their abilities as educators. They have, through their love and enthusiasm of what they do, helped me more clearly see the path which I have chosen to follow.

Finally to my parents, who have always taught me that if I pursue my dreams, they may come true. With each passing year, I more fully realize the wisdom in what they have taught me. It is because of their unending love and support that I have made it thus far.

This report was prepared at the Charles Stark Draper Laboratory, Inc. under Corporate Sponsored Research funding.

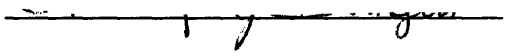

Anthony J. Gingiss

Table of Contents

Description **Page**

List of Figures

Description **Page**

List of Tables

Description **Page**

List of Symbols

Symbol	Description
A	Area
$\vec{a}_d$	Disturbing acceleration
$\vec{a}$	Acceleration vector
a_{eff}	Effective acceleration
a_{Moon}	Semi-major axis of the Moon's orbit
$\vec{b}$	Measurement geometry vector
β_d	Doppler bias
β_r	Range bias
β_{rr}	Range rate bias
E	Covariance matrix
F	Dynamics matrix
$\vec{F}_{SRP}$	Force due to Solar radiation pressure
G	Gravity gradient matrix
I	Identity matrix
J_k	Kth Mass potential coefficient
L_{Factor}	Ratio of $\frac{\text{distance to the libration point from Earth}}{\text{distance to the Moon from Earth}}$
m_i	Mass of i
μ_i	Gravitational constant of i
$P_k(v)$	Kth Legendre polynomial with independent variable v
$P'_k(v)$	Derivative of kth Legendre polynomial with repect to v
Q	Noise matrix
q	Noise
$\vec{R}_{ij}$	Position vector from point i to point j
r_{eq}	Equatorial radius
σ_i	Standard deviation of i
σ_i^2	Variance of i
τ	Time constant
$\vec{V}_i$	Velocity of i
$\vec{\omega}_P$	Rotation vector of planet P
χ	Distance ratio
$\vec{x}$	State vector
$\delta\vec{x}$	State dispersion

Subscript

1WR	One-way range
2WR	Two-way range
B	Beacon
cm	Center of mass
D	Doppler
I	Inertial
LOS	Line of sight
max	Maximum
nom	Nominal
NS	NavSat
p, SC	Spacecraft
REL	Relative

Superscript

^	Unit vector
—	Expected value
—	Vector
.	First derivative with respect to time
..	Second derivative with respect to time
0	Initial time
f	Final time
T	Transpose

Acronym

CT	Crosstrack
DR	Downrange
Lpoint	Libration point
LEO	Low Earth Orbit
LLO	Low Lunar Orbit
LVLH	Local vertical, local horizontal coordinate system
NavSat	Navigation satellite
NavSite	Navigation site
VT	Vertical

CHAPTER 1
Introduction

1.1 Background and Motivation

On July 20, 1989 , the 20th anniversary of the Apollo Moon landing, President George Bush asked Vice President Dan Quayle to lead the National Space Council in charting a new and continuous course to the Moon, Mars and beyond. President Bush provided specifics to the goal contained in the 1988 Presidential Directive on National Space Policy. In President Bush's words, he wanted the U.S. to make

> "... a long-range continuing commitment. First for the coming decade, for the 1990s, Space Station Freedom, our critical next step in all our space endeavors. And next, for the next century, back to the Moon, back to the future, and this time back to stay. And then a journey into tomorrow, a journey to another planet, a manned mission to Mars. Each mission should and will lay the groundwork for the next."

During a several year period surrounding this directive, several government advisory committees convened to make recommendations on the future of the U.S. space program. The first of these, *Report of the 90-Day Study on Human Exploration of the Moon and Mars* (The 90 Day Study) was presented to the administrator of NASA, Admiral Richard H. Truly on November 20, 1989. It was an internal NASA report designed to serve as a database for the Space Council to refer to as it considered strategic planning issues. The second, *America At The Threshold: America's Space Exploration Initiative* (SEI / The Stafford Report) was released in May of 1991. SEI made direct recommendations on the direction of U.S. space policy by outlining specific mission goals and the necessary technologies for the response to President Bush's "challenge". One of the primary emphases of these two reports was making clear the necessity of the establishment of a Moon/Mars Initiative in the future of the U.S. space program.

Both of these reports maintain that the Moon is a necessary precursor step in man's ultimate journey to Mars. The colonization of the Moon on a temporary or permanent basis

involves scientific development and research in many different areas. Two key areas presented in the two studies are:

1) **Telecommunication and Navigation Systems**

The function of telecommunications and navigation is to provide the ability to monitor and control mission elements, provide radiometric data, acquire telemetered data from engineering and science measurements, and provide the ability to communicate, receive, and distribute this information. A primary component in the development of an operational telecommunications system is the implementation of Lunar and Mars telecommunication relay networks. This system must provide the means to monitor and control distributed mission elements and to acquire system data from remote locations at high data rates and high reliability levels.

2) **Orbital Assembly, Storage and Rendezvous Techniques**

The process of constructing a Lunar base and Mars-bound spacecraft require the handling and integration of large quantities of raw materials. Materials for the construction of a Mars vehicle would entail the integration of components from Earth-launched spacecraft and Lunar-based spacecraft carrying raw materials and/or personnel and equipment from in-situ Lunar sites. In order to effect the successful integration of these components and materials, a well refined system of orbital assembly, storage and rendezvous techniques will be required.

Utilization of the libration points can provide unique solutions to the problems presented in the colonization of the Moon. The focus of this thesis analysis of navigation techniques for use in libration point missions; specifically, to determine the feasibility of utilizing current navigation techniques and hardware in the navigation of a spacecraft to, from or at a libration point. In addition, guidance and station-keeping techniques will be discussed based upon the results of the initial navigation studies.

1.2 The Restricted 3-Body Problem

1.2.1 What is a Libration Point?

In celestial mechanics, the 3-body problem consists of three masses gravitationally attracting each other in space. This unrestricted three-body is not the important case for our problem but a variant of it is. We will examine the restricted three-body problem, which is of considerable importance in celestial mechanics. In the restricted three-body problem, two of the three bodies have much larger masses than the third. As a result, the motions of the two larger bodies are unaffected by the third body. The larger bodies will however govern the motion of the small body. The system consisting of the Earth, the Moon and a spacecraft is the one of interest here.

The important simplification of the restricted three-body problem is that we can solve for the motion of the larger masses (primaries) by first solving the two-body problem without considering the small body. After solving the two-body problem, one can calculate the motion of the small body in the calculated gravitational field of the two larger bodies. The simplest form of the three-body problem involves the primaries moving on circular paths. For this circular restricted three-body problem, there are five points in the plane of the motion of the two primaries where the forces acting on the small body are balanced. These five points are called libration or Lagrange points after Joseph Louis Lagrange who was the first to discover these particular solutions to the circular restricted three-body problem. The forces which are in balance at the libration points are the gravitational attraction of the two large masses on the small mass and the centrifugal force on the small mass revolving with the two primaries about their common center of mass.

Three of the libration points are on the line connecting the two primaries and are called the collinear libration points. The locations of the three collinear libration points are calculated by solving Lagrange's quintic equation

$$(m_1+m_2)\chi^5+(3m_1+2m_2)\chi^4+(3m_1+m_2)\chi^3 -(m_2+3m_3)\chi^2-(2m_2+3m_3)\chi-(m_2+m_3)=0 \qquad (1.1)^1$$

$$\chi=\frac{r_{23}}{r_{12}}$$

---

[1] R.H. Battin, An Introduction to the Mathematics and Methods of Astrodynamics, Equation 8.7

$$\overline{R}_{Earth-LPoint} = L_{Factor}\overline{R}_{Earth-Moon}$$
$$L_{Factor} = f(\chi)$$

where r_{23} is the distance from the second to the third mass, r_{12} is the distance from the first to the second mass and the three masses (m_1, m_2, m_3) are the mass of the Earth, Moon and spacecraft (≈ 0) . The masses must be interchanged to solve for the three values of L_{factor} which is a function of the single real root of the equation.

The other two libration points are located at the two points which form equilateral triangles with the two primary bodies and hence the name "equilateral points". The five points are all fixed in the synodic system, which is the rotating system in which the primaries are fixed.

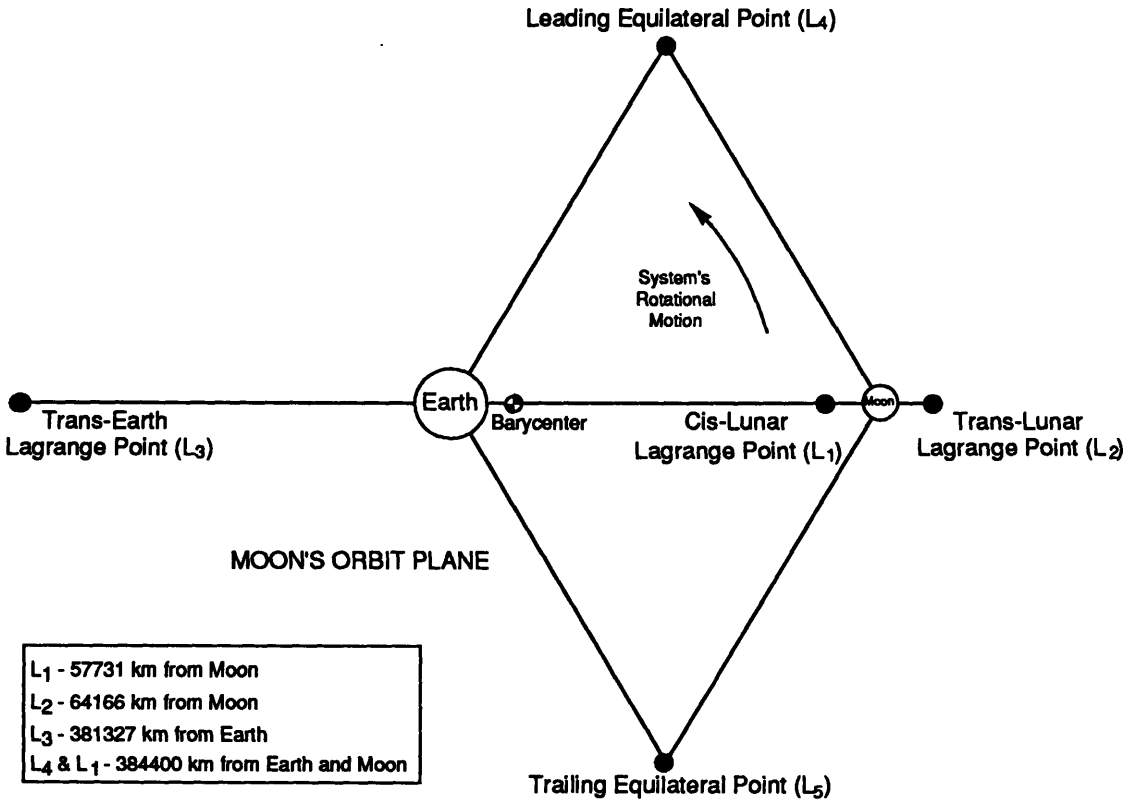

Figure 1.1 : Earth-Moon Libration Point Geometry

The three collinear libration points are unstable in the sense that if the small mass is placed at one of these points, a small disturbance will cause the mass to depart from the

point. The instability of these collinear points can be counteracted via the use of station-keeping thrusters or other low thrust devices. By linear analysis, the equilateral points have been shown to be stable in many cases[2] which means that the small mass will oscillate about these libration points when disturbed. Small asteroids have been observed at the triangular points of the Jupiter-Sun system. These Trojan Asteroids, as they were named, are proof that equilateral libration points can be stable. A libration is an oscillatory motion about an equilibrium point, and hence the term libration point is used.

The motion of a spacecraft in the vicinity of one of the collinear points has a sinusoidal and an exponential component. There are certain initial conditions which can eliminate the effects of the exponential term with two types of resultant motions: *lissajous figures* and *halo orbits*. In a lissajous figure, the motion out of the Earth-Moon plane is not phased with the in-plane motion. In a halo orbit, both the in-plane and out-of-plane motions have the same phase, creating a "halo" like motion. The existence of these closed curves about the collinear points allow for interesting solutions to the problem of Earth-Moon telecommunications. Figure 1.2 shows the halo orbit geometry and Figure 1.3 an actual L1 halo orbit [3].

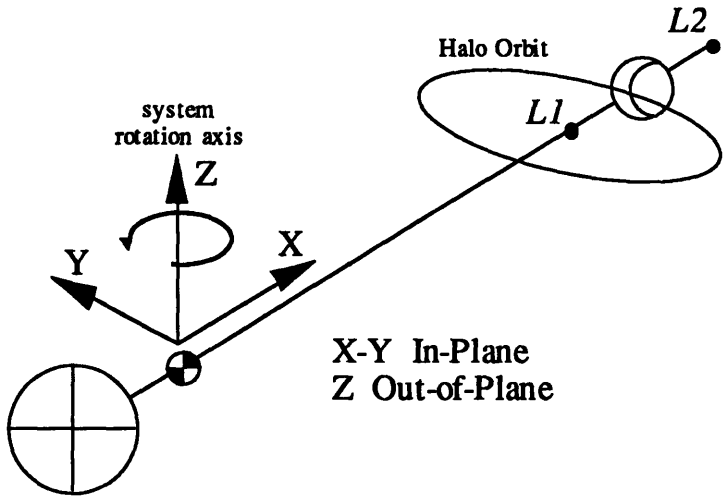

Figure 1.2 : Halo Orbit Geometry

---

[2] R.H. Battin, An Introduction to the Mathematics and Methods of Astrodynamics, Section 8.3

[3] Compliments of K.C. Howell and J.L. Bell, Purdue University

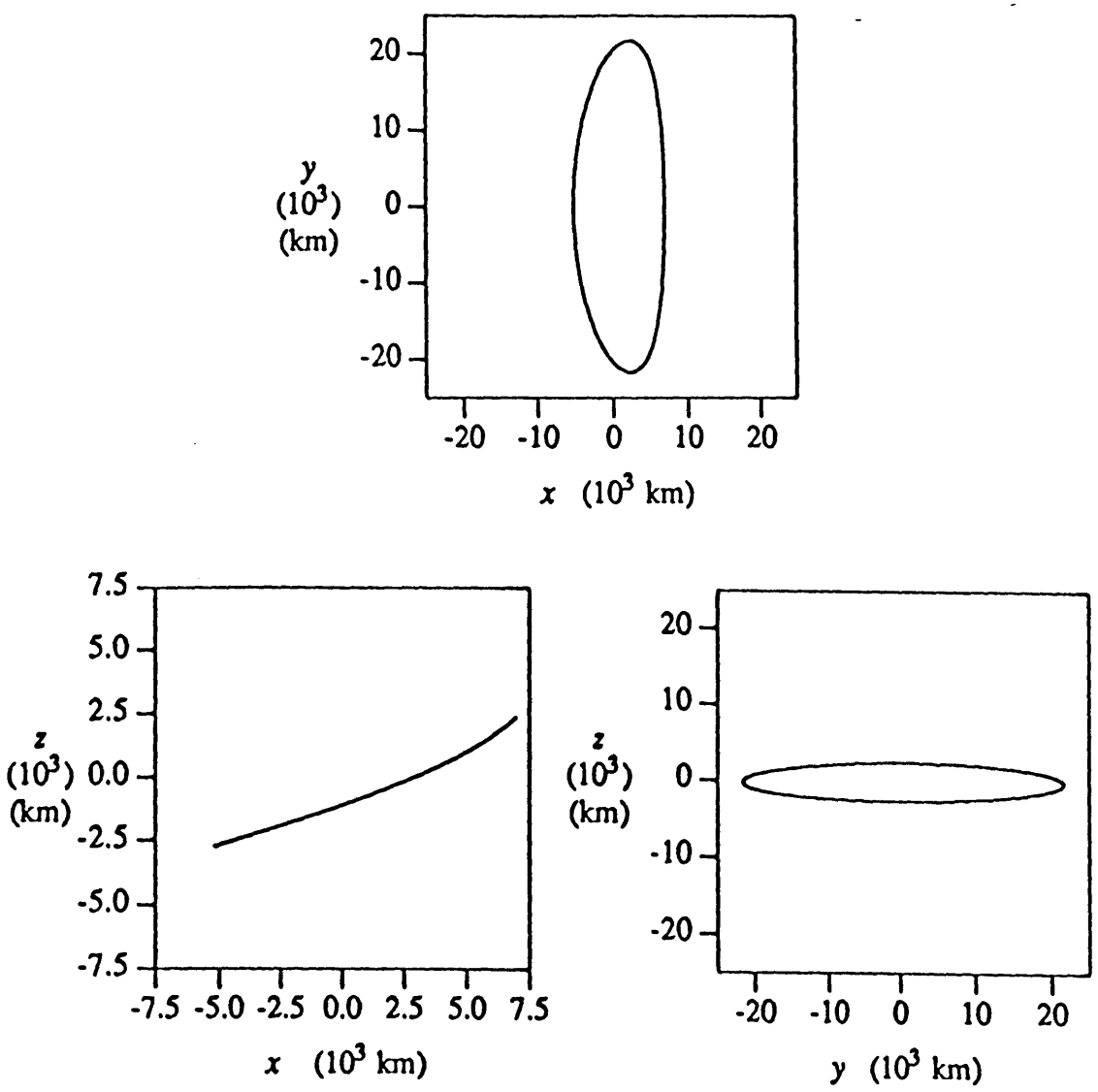

Figure 1.3 : L1 Halo Orbit

1.3 Navigation Analysis

The role of the navigation system is to minimize the uncertainties in the spacecraft state (by optimal estimation) to allow the spacecraft (through the guidance system) to meet the mission goals. The navigation system estimates the state with the aid of inertial instruments and by taking external measurements. The following sections briefly describe navigation analysis.

1.3.1 Measurements and the Kalman Filter

Instruments onboard the spacecraft are used to take measurements which provide information about the position and/or velocity of the spacecraft. Through the use of a Kalman filter, these pieces of information are weighed according to their relative accuracy and incorporated into the state estimation process in an optimal way. If the measurements provide enough information, the state uncertainties can be systematically decreased to a level comparable to the accuracy of the measurements. It is however possible for the effects of the orbital dynamics to "outweigh" the effects of the measurements resulting in either no decrease or possibly an increase in the state uncertainties. We are trying to systematically determine which measurement types will reduce the state uncertainties to acceptable levels over reasonable time intervals for missions at or near Earth-Moon libration points.

The measurement types to be studied are two-way ranging, one-way ranging and Doppler systems. These will be implemented with Earth and Moon based beacons and Lunar navigation satellites in an attempt to ascertain the types of configurations with the greatest potential to reduce state uncertainties for various libration point missions. The Linear Covariance Analysis section of Chapter 2 will discuss in further detail the implementation of these systems. The variations of configuration will be discussed in Chapter 3 along with issues of station-keeping burn modeling.

1.3.2 Covariance Matrices

A covariance matrix is a statistical representation of the state uncertainties for all components of the navigation state, and the correlation of each component to every other. The principle diagonals are the variances of each state element, and the off diagonals are the

cross correlations and are symmetric about the diagonal. Equation 1.2 shows the 6x6 covariance matrix for a navigation state consisting of the spacecraft position and velocity.

$$E = \begin{bmatrix} \sigma_{R_x}^2 & \sigma_{R_yR_x} & \cdot & \cdot & \cdot & \\ \sigma_{R_xR_y} & \sigma_{R_y}^2 & & & & \\ \cdot & & \sigma_{R_z}^2 & & & \\ \cdot & & & \sigma_{V_x}^2 & & \\ \cdot & & & & \sigma_{V_y}^2 & \\ & & & & & \sigma_{V_z}^2 \end{bmatrix} \tag{1.2}$$

The states of a covariance matrix usually include the spacecraft position and velocity along with all other important components making up the navigation state. In our case, surface beacon navigation site (NavSite) and navigation satellite (NavSat) states along with any relevant measurement instrument states will be included in the covariance.

Normally the state uncertainties, and therefore the covariance matrix, grow over time. This implies that for the state of Equation 1.2, the knowledge about the spacecraft position and velocity are degrading with passing time. The navigation system is designed to bound the covariance by taking external measurements as described above.

1.3.3 The Covariance Ellipsoid

A helpful representation of the covariance matrix is that of an n-dimensional ellipsoid, where n is the number of states. This ellipsoid is an equi-probability surface, where the length from the center to any perpendicular tangent represents the standard deviation of the position in that direction. When a measurement is taken, the covariance ellipsoid shrinks along the direction of the information. This direction is defined as the measurement geometry vector and is described in further detail in Section 2.6. For a simple example, let us assume that we have a two-dimensional covariance consisting of two spacecraft position states. This covariance can be represented by a two-dimensional ellipsoid (an ellipse). Figure 1.4 is a graphical representation of how the process works for this ellipse. In the figure, $\hat{x}$ and $\hat{y}$ are principle axes and $\hat{u}$ is the direction of the measurement.

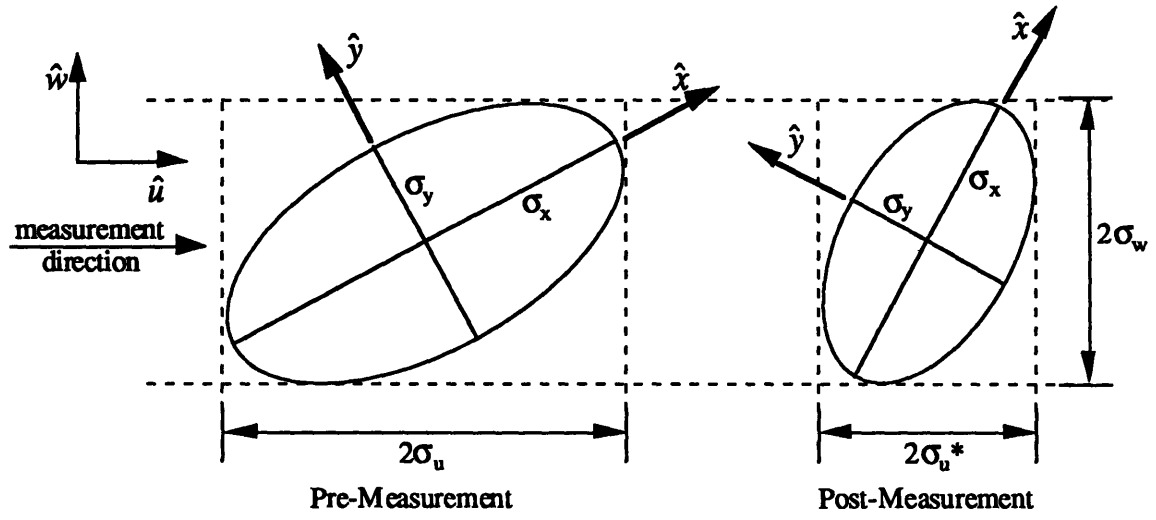

Figure 1.4 : Covariance Ellipsoid and Measurements

1.4 Applications

Libration points remain fixed with respect to the rotating frame defined by the two primary bodies. This is the unique feature of libration points which provides interesting alternatives to the problems of Earth-Moon communications and transport. The following sections present applications for libration point missions which capitalize on the unique properties that libration points possess.

Trans-Lunar (L2) Halo Orbit Telecommunications Relay

A stated requirement for a Lunar habitat is for a 90% or better link connectivity between the Earth and Moon. Virtual 100% link connectivity is easily met for the Earth and Moon except in the case where there are operations on the far side. Gravitational tidal forces have resulted in the Moon always presenting the same face toward the Earth. This means that half of the Moon (the far side) is never visible from the Earth. As a result, a lunar orbiting relay would only provide coverage for the far side over about half of its period since it can only cover below it at any given time. In this case, use of a Trans-Lunar halo orbit would provide a large portion of the far side with telecommunication to the Earth 100% of the time. Coverage would only be dependent on the visibility of the Earth

stations which would still affect a near 100% link connectivity for far side operations. The L2 Halo Relay Network is shown in Figure 1.5.

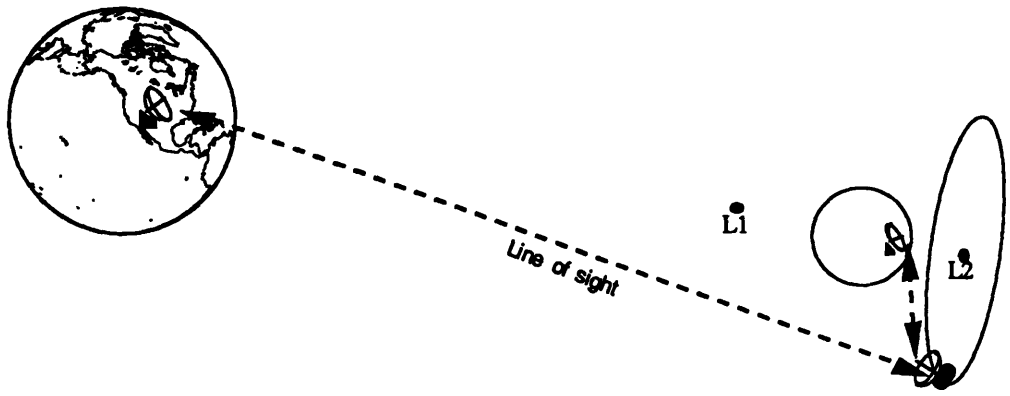

Figure 1.5 : Ground-Based and L2 Halo Relay Telecommunications Network

The spacecraft would have to be placed in a halo orbit of at least a 2065 km amplitude in the out-of-plane direction to allow full view of the Lunar far side and the Earth simultaneously. This however should pose no problem since orbits of 3500+ km amplitude have been shown to be attainable[4].

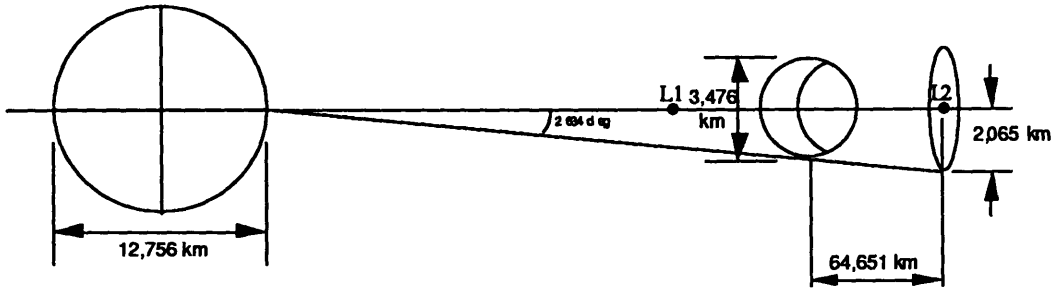

Figure 1.6 : Geometry of Trans-Lunar Halo Orbit

The 90 Day Study presents a telecommunications architecture for the Moon which involves both the classical ground-based antenna on the far side and halo orbit satellite at L2 65,000 km beyond the Moon as shown in Figures 1.5 and 1.6. This will provide

---

[4] Breakwell, J.V. and Brown, J.V., The "Halo" Family of 3-Dimensional Periodic Orbits in the Earth-Moon Restricted 3-Body Problem

coverage for orbiting vehicles, far-side surface terminals and possibly critical orbit insertion of piloted vehicles.

Cis-Lunar (L1) Telecommunications Relay

Telecommunications relay satellites permit the use of lower power and much smaller antennas at surface terminals and in transportation vehicles. Another possible scenario which would allow near-side operations to take advantage of a relay satellite, would be to have another relay satellite "sitting" at L1 as shown in Figure 1.7. This satellite would have constant coverage of the near side of the Moon and the Earth resulting in no loss in link connectivity between the Lunar and Earth stations. An additional benefit of this implementation is the ability to communicate between different points on the near side of the Moon without the use of Earth-based components. This ability to relay signals between near side lunar operations would not be a feature of Lunar-based antenna systems since there is no atmosphere to reflect signals, and the curvature of the Moon limits the line of sight communications range. An L1 relay system would also reduce the overall power and weight for the Moon-based communication antennas due to shorter transmitting distance.

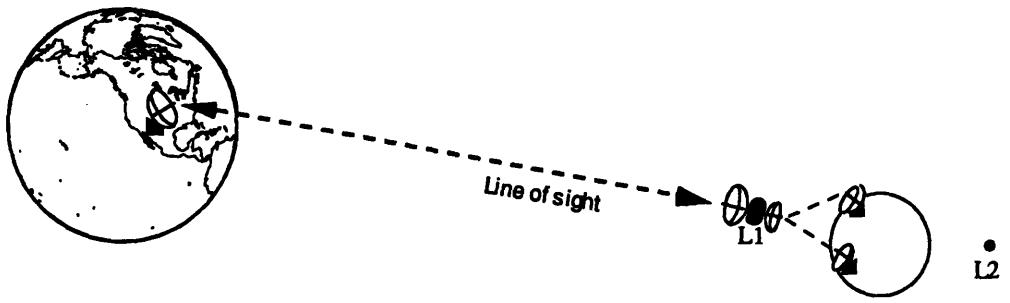

Figure 1.7 : L1 Telecommunications Relay

L1 Transport, Assembly and Storage Node

Another libration point application which is presented in The Stafford Report is the concept of a Lagrange point as an assembly, storage and transport node. Instead of staging missions directly from LEO to Mars, the L1 libration point could be used as an assembly node. This would be especially attractive if reusable vehicles are specified for multiple Mars missions with in-situ Lunar fuel also being available. The L1 libration point can also

be used for storing mission nuclear components, such as nuclear thermal rocket stages, or cargo sent in advance from the surface of the Moon awaiting the arrival of the transport ship. The L1 libration point requires on the order of 2.6 km/s less ΔV than the same vehicle departing from low Earth orbit. Cycling between the Cis-Lunar and Cis-Martian libration points[5] and using L1 as a transport node for Lunar exploration[6] have also been studied.

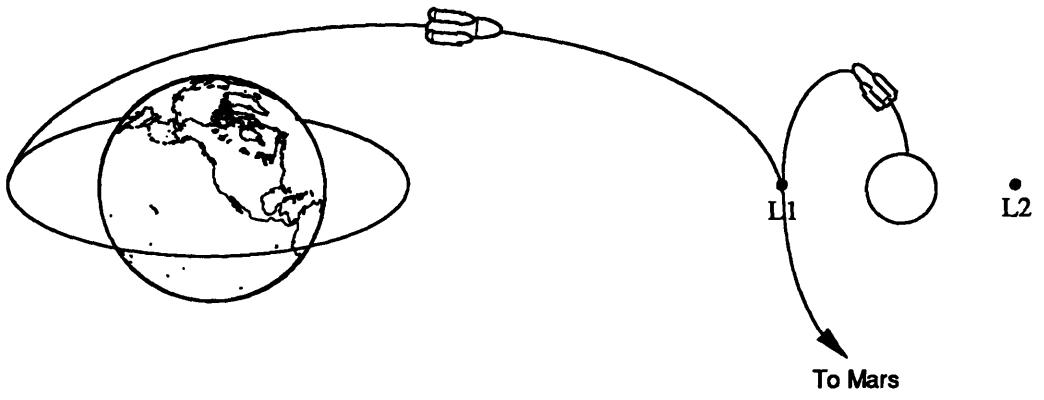

Figure 1.8 : L1 as a Transport, Storage and Assembly Node

1.5 Previous Work

The origin of the study of libration points dates back to 1772 when Joseph-Louis Lagrange submitted "Essai sur le Problém des Trois Corps" (Essay on the Problem of Three Bodies) to the Paris Academy in which he presented the libration point solutions.

On August 12, 1978 a scientific spacecraft called International Sun-Earth Explorer 3 (ISEE-3) was launched towards the interior Sun-Earth libration point (L1). It was placed in a halo orbit about L1 on November 20,1978, thus becoming the first man-made libration point satellite. Its scientific mission involved analysis of the pre-bow shock solar wind environment near the Earth. This mission demonstrated the uniqueness of using libration

---

[5] Sponaugle, S.J., et. al ,Optimal Cycling Between Cislunar and CisMartian Libration Points With Reusable Nuclear Electric Transfer Vehicles

[6] Bond, V.R., et. al , Cislunar Libration Point as a Transportation Node for Lunar Exploration

points as an observing "platform". It also demonstrated the feasibility of these missions and their usefulness for space-based applications. The craft was renamed when R.W. Farquhar of Goddard Space Flight Center designed a trajectory to take the spacecraft away from the Earth to encounter the comet Giacobini-Zinner. The trajectory involved several Moon flybys to gain the velocity necessary to leave Earth's vicinity and according to Dr. Farquhar it is "one of the most complicated things that's ever been done ... in the way of orbital dynamics in moving a spacecraft around". In more current times, the European spacecraft SOHO is set to orbit the interior Earth-Sun libration point in the late 1990s.

Much of the recent work has been done on the problems of station-keeping and orbit determination for Earth-Moon and Earth-Sun libration points. Currently K.C. Howell at Purdue University is performing much of the research in these areas, having produced a significant body of work pertaining to the station-keeping and orbit determination of libration point missions.

This emphasis of this thesis will be on the navigation analysis of libration point missions. With the results of this navigation study, integrated guidance and navigation for future Earth-Moon libration point missions can be analyzed using some of the existing work pertaining to station-keeping and orbit determination.

CHAPTER 2
Analytic Development

2.1 The Restricted 3-Body Equations of Motion

For the purpose of simulation, a set of differential equations describing the motion of a spacecraft in the Earth-Moon system must be derived. The equations are numerically integrated to calculate the state of the spacecraft given a specified set of initial conditions (i.e. time, position and velocity). Figure 2.1 shows the basic geometry of the system consisting of two primary masses orbiting their common center of mass, and a spacecraft moving within the system. Point P is the location of the spacecraft.

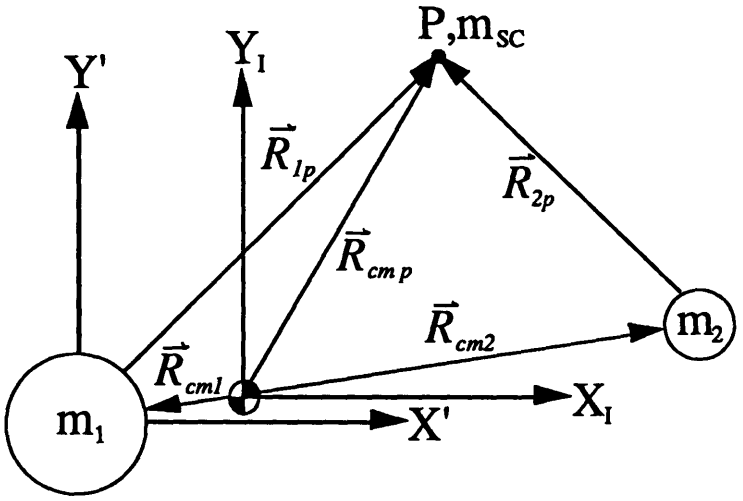

Figure 2.1 : Geometry of the Three-Body System

It should be noted that these equations will be valid for either eccentric or circular Earth-Moon systems, with the motion being determined by the initial conditions of the two primaries. Given circular velocities the primaries will move in circles about the center of mass. Conversely, eccentric position and velocity initial conditions will result in the primaries moving in ellipses about the center of mass.

The derivation of the equations is done via simple application of Newton's second law:

$$\sum \vec{F}_{SC} = m_{SC}\vec{a}_{SC}$$

The forces on the spacecraft are the gravitational attractions of the two primaries:

$$\sum \vec{F}_{SC} = -\frac{Gm_1 m_{SC}}{R_{cm1}^{\ 3}}\vec{R}_{cm1} - \frac{Gm_2 m_{SC}}{R_{cm2}^{\ 3}}\vec{R}_{cm2} \tag{2.1}$$

The acceleration is simply the spacecraft mass multiplied by the second derivative of the position vector $\vec{R}_p$, which has an inertial base point (center of mass). Dividing both sides of the equation by the mass of the spacecraft and substituting μ_1 for Gm_1 and μ_2 for Gm_2 results in the vector equation of motion:

$$\ddot{\vec{R}}_{cm\,p} = -\frac{\mu_1}{R_{cm1}^{\ 3}}\vec{R}_{cm1} - \frac{\mu_2}{R_{cm2}^{\ 3}}\vec{R}_{cm2} \tag{2.2}$$

While this vector equation adequately represents the motion of the spacecraft in the system, we must also have equations representing the motions of the primaries about their inertial center of mass. Again applying Newton's law provides the results:

$$\ddot{\vec{R}}_{cm1} = -\frac{\mu_2}{(R_{cm1} + R_{cm2})^3}(\vec{R}_{cm2} - \vec{R}_{cm1}) \tag{2.3}$$

$$\ddot{\vec{R}}_{cm2} = -\frac{\mu_1}{(R_{cm1} + R_{cm2})^3}(\vec{R}_{cm1} - \vec{R}_{cm2}) \tag{2.4}$$

Simulating the system involves integrating all three (Equations 2.2-2.4) of these vector differential equations simultaneously. To further simplify the numerical complexity of the problem we can center the integration coordinates at one of the primaries. By doing this we need only integrate the relative equations of motion of the other primary and the spacecraft simultaneously.

2.2 Relative Equations of Motion

The geometry involved in writing the system equations of motion relative to the first primary is the same as shown in Figure 2.1, but the axes of integration are now the X' and Y' axes. A new vector $\vec{R}_{12}$ is introduced, where

$$\begin{aligned} \vec{R}_{12} &= \vec{R}_{cm2} - \vec{R}_{cm1} \\ \vec{R}_{2p} &= \vec{R}_{1p} - \vec{R}_{12} \end{aligned} \tag{2.5}$$

By writing $\vec{R}_{1p}$ in terms of $\vec{R}_{cmp}$ and $\vec{R}_{cm1}$, we can calculate the expression for $\ddot{\vec{R}}_{1p}$:

$$\begin{aligned} \vec{R}_{1p} &= \vec{R}_{cmp} - \vec{R}_{cm1} \\ \ddot{\vec{R}}_{1p} &= \ddot{\vec{R}}_{cmp} - \ddot{\vec{R}}_{cm1} \end{aligned} \tag{2.6}$$

By substituting Equations 2.2 and 2.3 for $\ddot{\vec{R}}_{cmp}$ and $\ddot{\vec{R}}_{cm1}$ we have the relative equations of motion for the spacecraft in accelerating but non-rotating coordinates fixed in and translating with the first primary (X'Y' coordinates):

$$\ddot{\vec{R}}_{1p} = -\frac{\mu_1}{R_{1p}^{\,3}}\vec{R}_{1p} - \frac{\mu_2}{R_{2p}^{\,3}}\vec{R}_{2p} - \frac{\mu_2}{R_{12}^{\,3}}\vec{R}_{12} \tag{2.7}$$

Similarly the relative vector equation of motion for $\vec{R}_{12}$ can be derived resulting in:

$$\ddot{\vec{R}}_{12} = -\frac{\mu_1 + \mu_2}{R_{12}^{\,3}}\vec{R}_{12} \tag{2.8}$$

Integration of Equations 2.7 and 2.8 now simulate the motion of the entire system relative to m_1.

2.3 Halo Orbits

To calculate the injection position and velocity for a halo orbit or lissajous figure an analytic model must be developed. A first-order linearized model for the motion of a spacecraft about a collinear libration point can be written as[7]

$$x' = -pa_1 e^{\alpha t} + pa_2 e^{-\alpha t} - kA_y \cos(\lambda t + \phi)$$
$$y' = a_1 e^{\alpha t} + a_2 e^{-\alpha t} - A_y \sin(\lambda t + \phi)$$
$$z' = A_z \sin(\nu t + \psi)$$

where the x'y'z' coordinates are coordinates fixed at the libration point and rotating with the Earth-Moon line-of-sight , with x' and y' being the in-plane components. A_y and A_z are the amplitudes of the motion, ϕ and ψ are phase angles, k is a proportionality constant and λ and ν are the in-plane and out-of-plane frequencies. For the case where the initial conditions are chosen to eliminate the exponential terms, and where λ is equal to ν the result is a halo orbit. For the same conditions where λ is not equal to ν the result is a lissajous figure.

This model can be used to obtain an estimate of halo orbit injection velocity by choosing the initial conditions to eliminate the exponential terms. This linear model is insufficient to predict actual halo orbits, but it can be useful in obtaining lissajous figures about the libration point. For this study, the precise orbit determination of an actual halo orbit was not critical. Calculating a trajectory to keep the spacecraft in the viscinity of the point for a significant period was sufficient to test the navigation performance. For more detailed guidance work to be done, higher-order models must be used. These higher-order models will show that the in-plane and out-of-plane motion are coupled, which constrain the halo orbit geometry.

---

[7] Shepperd, S.W. C.S. Draper Laboratory Inc., personal notes & Howell, K.C. Purdue University, Halo Orbits and Other Libration Point Trajectories

2.4 Perturbations

There are many environmental factors which have the potential to significantly affect the spacecraft state. The principle ones we will consider are the eccentricity of the Earth-Moon system, Solar radiation pressure, Earth and Moon non-spherical mass distribution effects and the disturbing gravitational accelerations of the other planets and the Sun. The effects of these perturbations will be assessed and the results presented at the end of this section. As a reference, Table 2.1 contains the nominal primary accelerations for a spacecraft at L1 in the non-eccentric system.

Table 2.1 : Magnitudes of Primary Accelerations

Primary	a (m/s^2)
Moon	3.7387×10^{-3}
Earth	1.4633×10^{-3}

2.4.1 Earth-Moon Eccentricity

Adding eccentricity to the Earth-Moon system results in a variation of the distance between the two bodies on the order of $2eR_{EM}$ where e is the eccentricity of the system, and R_{EM} is the distance between the two bodies. With the eccentricity being approximately 0.055 there is a change in distance of about 42,284 km over one orbital period. In addition, the eccentric system has a non-constant rotation rate. In essence, the system "pulses", speeding up as the bodies move closer together towards periapse and slowing down towards apoapse.

While libration points are usually examined in the circular restricted 3-body problem, they are still defined in the elliptic problem. The locations of the libration points are still calculated by the equations discussed in Section 1.2 with the L_{factor} remaining constant but the Earth-Moon distance changing. Since the Earth-Moon distance in the elliptic case varies, the locations of the libration points also vary. The libration points move along with the system, maintaining the same geometric constraints. Figure 2.2 shows the relative motion of the Moon and L_1 and L_2 in the Earth-relative circular system. This motion shows the typical 2 by 1 ellipses predicted by Hill's or Clohessy-Wiltshire relative linearized equations of motion.

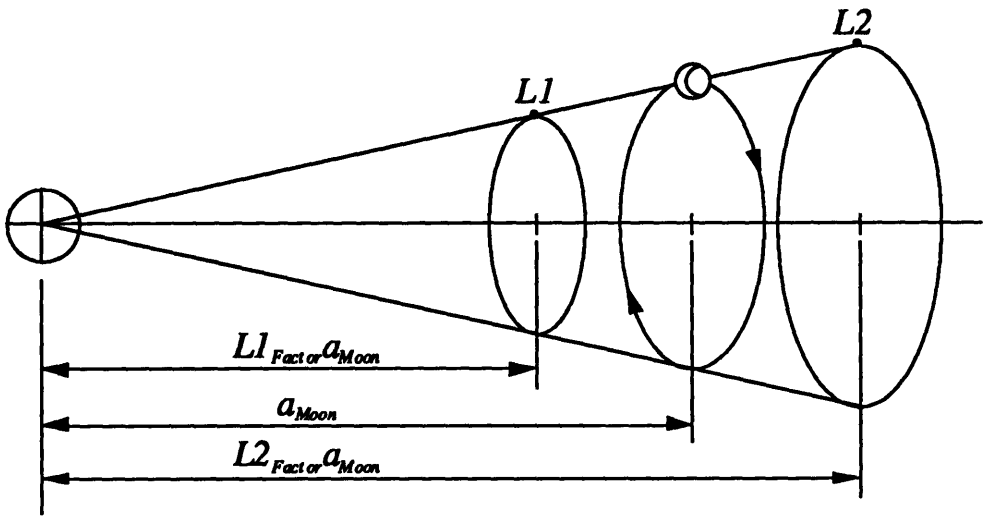

Figure 2.2 : Linearized Eccentric Motion of the Moon and Libration Points Relative to Their Circular Rotating Coordinates

One might expect that in an eccentric system, the libration point would be "pulled out from under" the spacecraft as the system geometry and angular velocity changed. Typically in the circular problem, a spacecraft at a libration point would be initialized as the velocity of the libration point in Earth-centered coordinates which can be expressed as

$$\vec{V}_{Lpoint} = L_{Factor}\vec{V}_{Moon} \tag{2.9}$$

If the spacecraft is always initialized with the velocity defined in Equation 2.9, it will "track" the libration point. Figure 2.3 shows the actual relative motion of the Moon, L1 and L2 in the circular rotating frame.

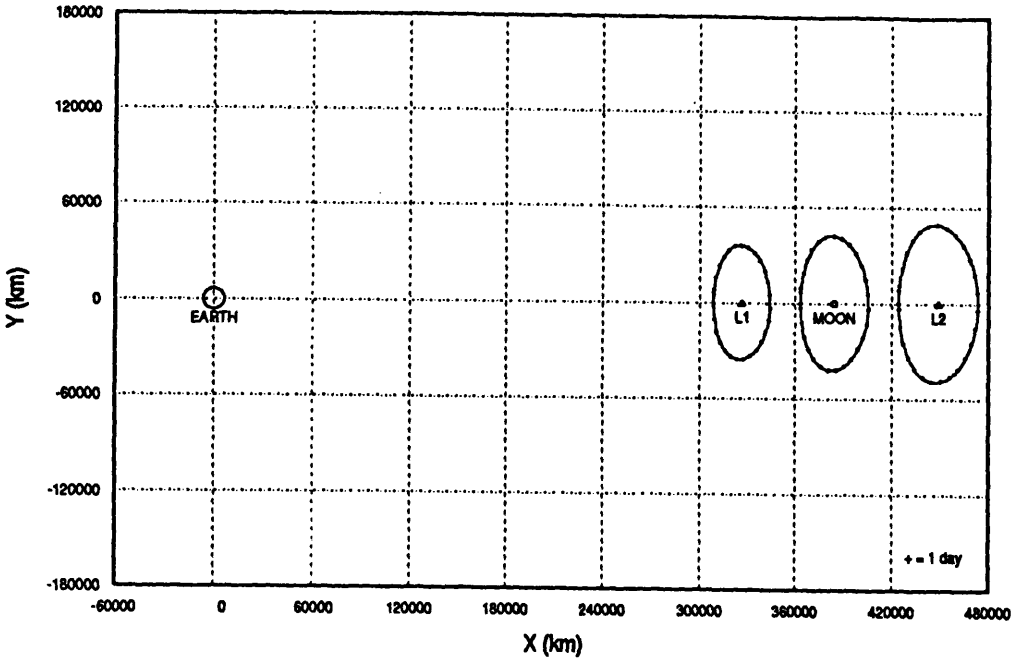

Figure 2.3 : Actual Relative Motion of the Moon and Libration Points

In effect the Moon has, through its gravitational effect on the spacecraft, altered the apparent attraction of the Earth. This is done in such a way as to allow the spacecraft to have the same period as the Moon about the Earth. This is similar to the dumbbell in orbit problem with the moon and spacecraft being the two masses, and the gravitational attraction of the Moon acting as the "tension in the bar". It should be noted that while a spacecraft at the libration point will track the point after adding the eccentric velocity effects, a spacecraft in a large halo or lissajous figure will deviate from the nominal path about the point. Just as linearized halo orbit equations break down with increasing distance from the libration point, so does the Hill's type relative motion. To accurately put a spacecraft in a halo or lissajous figure about a libration point in an eccentric system, the halo and lissajous linearized model to predict injection position and velocity must be of significant order and not make circularizing assumptions as discussed in Section 2.3.

The net effect that eccentricity has on the spacecraft navigation is to result in varying of the gravity gradients of the Earth and Moon experienced at the libration point over the rotational period. This is obviously caused by the change in distance from the libration point to each primary body. To assess these effects it should be sufficient to analyze the performance of a spacecraft tracking the nominal eccentric libration point, with the navigation system under the influence of the "pulsing" gravity gradients.

2.4.2 Solar Radiation Pressure

The next perturbation to be examined is solar radiation pressure. Unlike eccentricity, the effect of solar radiation pressure can be quantified as an effective acceleration on the spacecraft. A simple model of the force exerted by solar radiation on a flat plate is:

$$\vec{F}_{SRP} = PA(\hat{n} \cdot \hat{s})\hat{s} \tag{2.10}$$

where P is the solar constant which has a value of 4.644×10^{-6} N/m^2 at 1 astronomical unit from the Sun. A is the surface area of the "flat plate" spacecraft , $\hat{n}$ is the spacecraft normal direction and $\hat{s}$ is the unit vector from the Sun to the spacecraft.

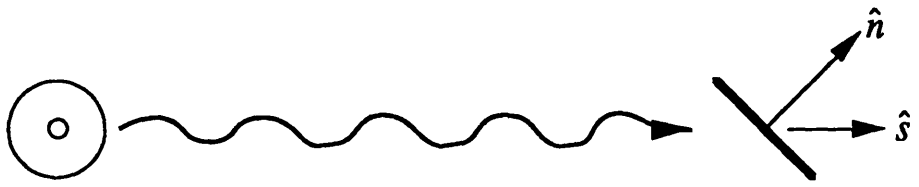

Figure 2.4 : Solar Radiation Pressure Model

For our purposes, two spacecraft configurations will be considered. The specifications of the two spacecraft and their effective accelerations are presented in Table 2.2 below.

Table 2.2 : Solar Radiation Pressure Spacecraft Configurations

Spacecraft	Area (m^2)	Mass (kg)	a_{eff} (m/s^2)
Case 1	10	3500	1.3269×10^{-8}
Case 2	10	250	1.8576×10^{-7}

To calculate the effective acceleration on the spacecraft, the force due to Solar radiation pressure was divided by the spacecraft mass. The effective accelerations for both of these cases are quite small. The typical process noise for a navigation system in trans-Earth space is about 1×10^{-10} m^2/s^3. If we take this number and divide by the time frame between our measurements ,which in this study is typically about 4 hours (14400 sec), and take the square root, we get a number which gives us a "ballpark" acceleration due to noise

of about 8.3×10^{-8} m/s^2. While this is larger than the Case 1 effective acceleration, Case 2's is still somewhat larger. Navigation cases will be run with larger noise levels to test the sensitivity of the system to unmodeled Solar radiation pressure effects greater than those presented in Case 2. It should be noted that the noise is applied spherically (in all directions equally) and is not meant to model the solar radiation pressure. The comparison is being done to show that the noise, which accounts for unmodeled effects, is large enough to account for unmodeled solar radiation pressure (typically ~5% of the total Solar radiation pressure). It should be noted that Solar radiation pressure is a differential perturbation, which means that it only affects the spacecraft, it does not have any effect on the Earth or Moon.

2.4.3 Earth and Moon Mass Distributions

Normally the Earth and Moon are treated as point or spherical mass attracting bodies. In reality the bodies are composed of non-uniform mass distributions which can be represented as a harmonic expansion using Legendre polynomials. A relatively simple mass model is to assume that the bodies are axially symmetric. While this model is not completely accurate, it will account for the major non-spherical mass effects (J_2, J_3 ...). The acceleration at a point external to an axially symmetric mass distribution can be written as[8]

$$\vec{a} = -\frac{\mu}{r^2}\left\{\hat{i}_r - \sum_{k=2}^{\infty} J_k \left(\frac{r_{eq}}{r}\right)^k \left[P'_{k+1}(\cos\phi)\hat{i}_r - P'_k(\cos\phi)\hat{i}_z\right]\right\} \qquad (2.11)$$

$$\cos\phi = \hat{i}_r \cdot \hat{i}_z$$

where μ and r_{eq} are the gravitational constant and equatorial radius of the attracting body, P_k' is the derivative of the kth Legendre polynomial, ϕ is the angle between the body's symmetry axis and the position vector of the spacecraft (co-latitude) and $\hat{i}_r$ and $\hat{i}_z$ are unit vectors in the spacecraft and symmetry axis directions respectively. Figure 2.5 shows the coordinate system for Equation 2.11.

---

[8] Battin, R.H., An Introduction to the Mathematics and Methods of Astrodynamics, Problem 8-20

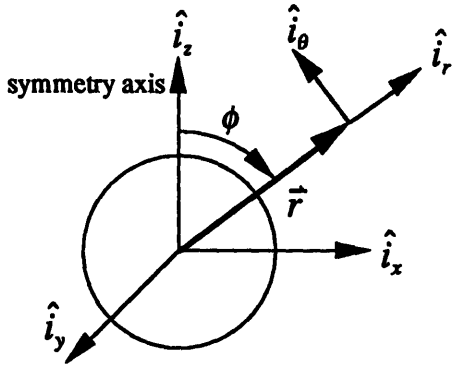

Figure 2.5 : Axial Symmetric Mass Distribution Geometry

By dotting Equation 2.11 with the $\hat{i}_r$ and $\hat{i}_\theta$ directions and subtracting the spherical gravity components:

$$\vec{a}_{spherical} = -\frac{\mu}{r^2}\hat{i}_r$$

we obtain expressions for the radial and tangential components of the disturbing acceleration:

$$a_r = \frac{\mu}{r^2}\left\{\sum_{k=2}^{\infty} J_k \left(\frac{r_{eq}}{r}\right)^k (k+1) P_k(\cos\phi)\right\} \tag{2.12}$$

$$a_\theta = -\frac{\mu}{r^2}\sum_{k=2}^{\infty} J_k \left(\frac{r_{eq}}{r}\right)^k P_k'(\cos\phi)\sin\phi \tag{2.13}$$

The total disturbing acceleration on the spacecraft is the magnitude of these two components:

$$a_{total} = \sqrt{a_r^{\,2} + a_\theta^{\,2}} \tag{2.14}$$

It should be noted that there is no acceleration component in the $\hat{i}_r$ x $\hat{i}_\theta$ direction due to the axial symmetry of the mass model.

For a spacecraft at one of the three collinear libration points, ϕ_{Earth} has a range of about 61.42-71.72° degrees and ϕ_{Moon} has a range of approximately 89-91°. ϕ_{Earth} of 61.42° and ϕ_{Moon} of 89° will maximize Equation 2.14. Table 2.3 presents the relative disturbing accelerations on a spacecraft at L1, due to Earth and Moon J_2, J_3 and J_4 terms using the values of ϕ to maximize the accelerations as discussed above.

Table 2.3 : Disturbing Accelerations Due To J_k Effects at L1

Planet	Term	J_k Value	a_{total} (m/s^2)
Earth	J_2	1.08263×10^{-3}	2.0775×10^{-9}
	J_3	-2.54×10^{-6}	1.2639×10^{-13}
	J_4	-1.61×10^{-8}	1.7016×10^{-17}
Moon	J_2	2.027×10^{-4}	4.0101×10^{-10}
	J_3	≈ 0	≈ 0
	J_4	≈ 0	≈ 0

2.4.4 Sun and Planets Disturbing Accelerations

Another set of perturbations which must be considered are the disturbing accelerations of the Sun and the other planets in the solar system. In the basic model, we have accounted for the gravitational attractions of the Moon and the Earth on the spacecraft. In actuality, the Sun and the other planets are gravitationally attracting the Earth, Moon and spacecraft, perturbing their nominal motion. Figure 2.6 shows the geometry of the problem.

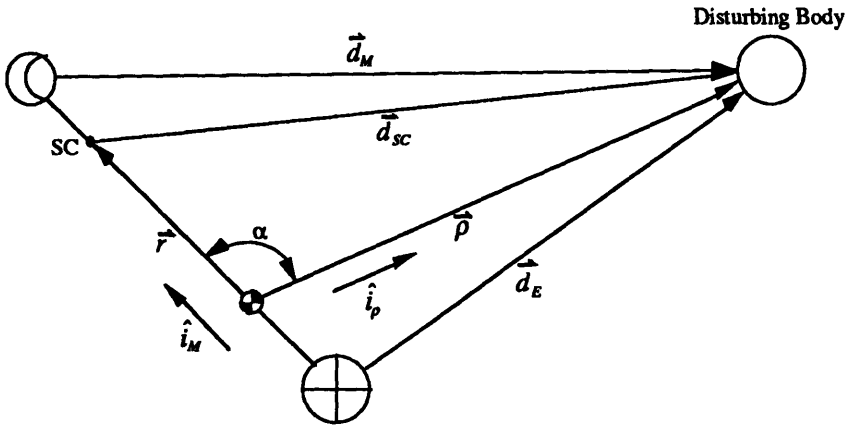

Figure 2.6 : Disturbing Body Geometry

In this figure the spacecraft is shown at L1. The following analysis is equally valid for the spacecraft at any of the other libration points.

An equation for the disturbing acceleration on any body in the Earth-Moon system is:

$$\vec{a}_d = \mu_P \left(\frac{1}{d^3}\vec{d} - \frac{1}{\rho^3}\vec{\rho} \right) \tag{2.15}$$

where μ_P is the gravitational constant of the disturbing planet, $\vec{\rho}$ is the vector from the center of mass of the system to the disturbing body and $\vec{d}$ is the vector from the body to the disturbing planet. This equation can be expanded using Legendre Polynomials into

$$\vec{a}_d = \frac{\mu_P}{\rho} \sum_{k=1}^{\infty} \chi^k \left[P'_{k+1}(v)\hat{i}_\rho - P'_k(v)\hat{i}_M \right] \tag{2.16}[9]$$

Here $\vec{r}$ is the vector from the center of mass of the system to the body of interest and

$$\chi = \frac{\vec{r} \cdot \hat{i}_M}{\rho}$$

$$v = \cos(\alpha) = \hat{i}_M \cdot \hat{i}_\rho$$

In order to quantify the effects of the disturbing acceleration, we will analyze the first two order effects (k=1,2) in Equation 2.16. By substituting for the Legendre polynomials, the first-order effects can be written as:

$$\vec{a}_d = \frac{\mu_P}{\rho} \chi \left[3v\hat{i}_\rho - \hat{i}_M \right] \tag{2.17}$$

Likewise the second-order effects can be written as:

$$\vec{a}_d = \frac{\mu_P}{\rho} \chi^2 \left[\left(\frac{15}{2}v^2 - \frac{3}{2} \right)\hat{i}_\rho - 3v\hat{i}_M \right] \tag{2.18}$$

---

[9] Battin, R.H., An Introduction to the Mathematics and Methods of Astrodynamics,, Equation 8.66

Using Equations 2.17 and 2.18 Table 2.4 presents the magnitudes of the first-order and second-order disturbing accelerations on a spacecraft at L1 due to the Sun and the other planets. To maximize the accelerations, the system was set up so $\hat{i}_M$ and $\hat{i}_\rho$ were parallel.

Table 2.4 : First-Order and Second-Order Disturbing Accelerations

Disturbing Body	First-Order Acceleration (m/s^2)	Second-Order Acceleration (m/s^2)
Sun	2.5504×10^{-05}	1.0969×10^{-07}
Mercury	1.8391×10^{-11}	1.2906×10^{-13}
Venus	2.9479×10^{-09}	4.5826×10^{-11}
Mars	5.7322×10^{-11}	4.7081×10^{-13}
Jupiter	3.2792×10^{-10}	3.3556×10^{-13}
Saturn	1.1772×10^{-11}	5.9403×10^{-15}
Uranus	1.8401×10^{-13}	4.3465×10^{-17}
Neptune	5.3553×10^{-14}	7.9187×10^{-18}
Pluto	3.3065×10^{-18}	3.6703×10^{-22}

From these numbers the Sun seems to be the only disturbing body with a significant effect on the system, having a first-order effect roughly two orders of magnitude less than the primary body accelerations.

Analyzing the first-order disturbing acceleration on the Earth, Moon and spacecraft, we see that the accelerations are parallel. In addition, the sign of the acceleration changes (due to the χ term) depending on which side of the center of mass the body is on along the Earth-Moon line-of-sight. The magnitude of the disturbing acceleration also scales linearly with distance from the center of mass. This acceleration geometry will cause the same sort of "pulsing" of the system as eccentricity does. The system will speed up and slow down as the Earth and the Moon move closer and farther apart, but the ratio of the Earth to libration point and Moon to libration point distances will remain constant. Figure 2.7 shows the first-order disturbing acceleration geometry

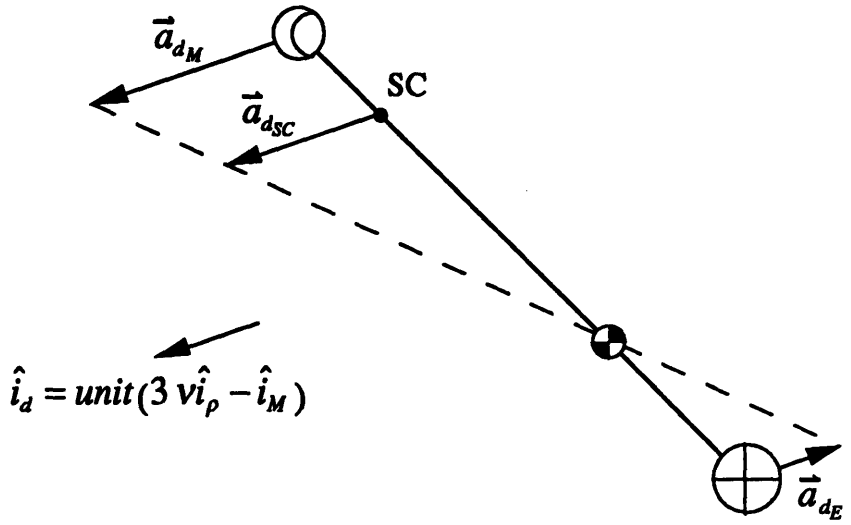

Figure 2.7 : First-Order Disturbing Acceleration Geometry

Being similar to the eccentric case, the net effect of the first-order disturbing accelerations on the navigation can be accounted for by adding the gravity gradient of the disturbing body into the navigation dynamics. For station-keeping purposes, the spacecraft velocity should be initialized using a model which accounts for the first-order disturbing accelerations of the disturbing body. If this is done, the spacecraft will still track the nominal libration point as in the eccentric case. It should also be noted that while the first-order disturbing effects are similar to the eccentric effects, they have about an order of magnitude less effect on the system geometry. Most of these accelerations are inconsequential, only the Sun has a disturbing acceleration of appreciable size compared to the primary body accelerations.

Having accounted for the first-order effects, the second-order effects become the primary disturbing accelerations of concern. By examining the second-order disturbing acceleration (Equation 2.18) for the Earth, Moon and spacecraft we see that these accelerations are also parallel. Unlike the first-order effects, the second-order accelerations do not change sign across the center of mass (due to the χ^2 term), or scale linearly with distance from the center of mass. Thus the second-order effects produce a "bending mode" on the system which does not preserve the geometry or distance ratios.

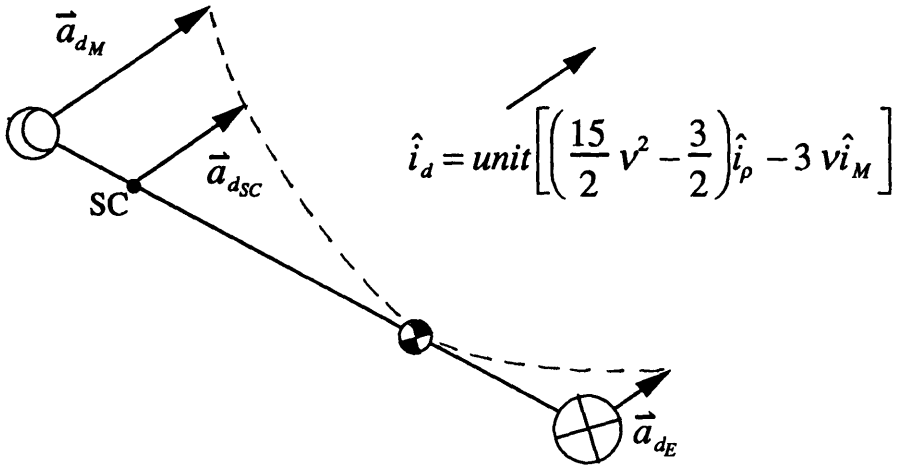

Figure 2.8 : Second-Order Disturbing Acceleration Geometry

The second-order effects are approximately two orders of magnitude less than the first-order effects and therefore about four orders of magnitude smaller than the primary body accelerations. Due to the minute size of these effects, they will be neglected in our analysis.

2.4.5 Summary of Perturbations

Figure 2.9 shows the primary accelerations of the Earth and Moon, second-order disturbing accelerations due to the Sun and planets and the accelerations due to Earth and Moon distributed mass effects and solar radiation pressure perturbations.

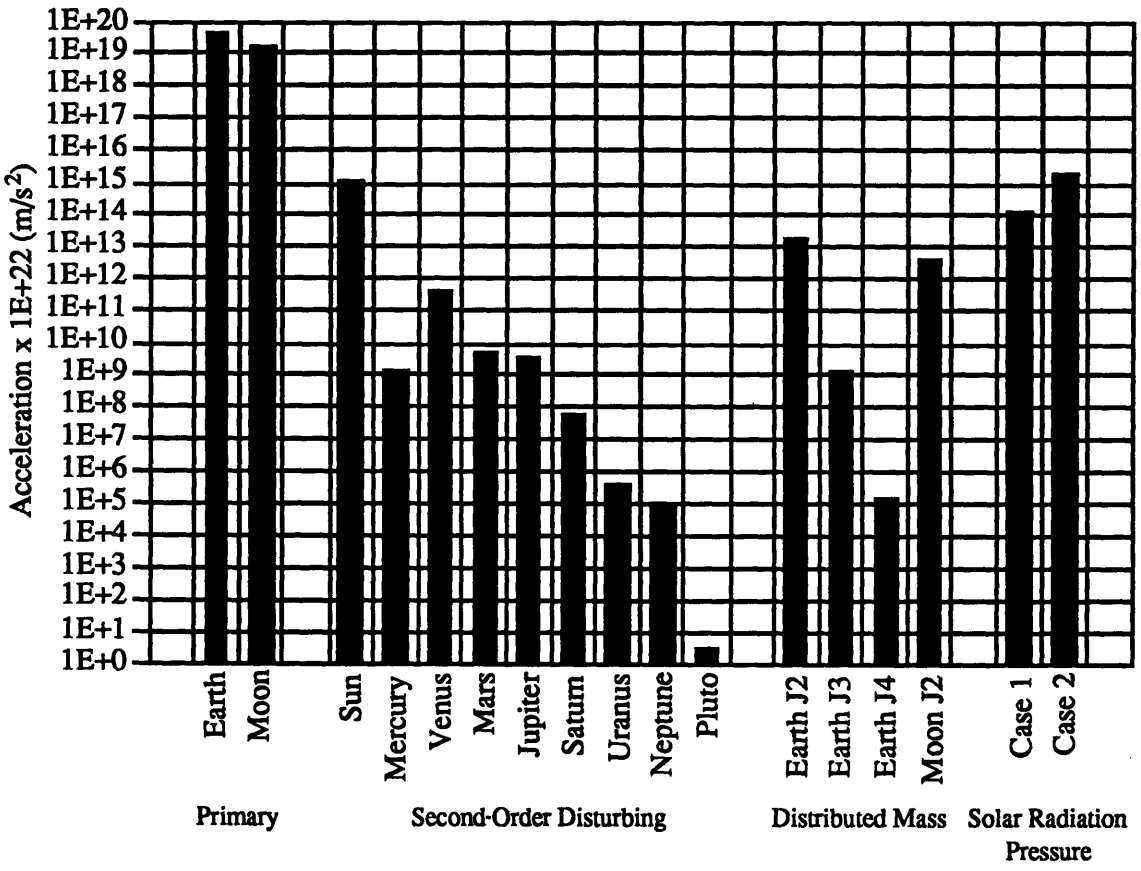

Figure 2.9 : Summary of Accelerations Due To Perturbations at L1

Analysis will be done to the account for the unmodeled effects of the second-order disturbing accelerations and solar radiation pressure. Eccentric effects on the navigation will be evaluated by propagating the spacecraft at the eccentric libration point under the influence of the varying Earth and Moon gravity gradients. The effects of the first-order disturbances due to the Sun will be analyzed by adding the gravity gradient of the Sun into the navigation dynamics. In addition, analysis will be done to account for the effects of vehicle burns which can be appreciable and must be taken into account. Specifics of these cases will be discussed in Chapter 3.

2.5 Linear Covariance Analysis

Linear covariance analysis is a process in which the state uncertainties are analyzed. It is assumed that there are no state dispersions or, in other words, that the actual state corresponds to the nominal trajectory. The error dynamics are simulated and measurements taken to observe the effects on the spacecraft's state uncertainties. The results are assumed to be valid on any trajectory neighboring the nominal.

2.5.1 Covariance Propagation

When the actual state errors are propagated, the covariance matrix must also be propagated simultaneously. The linearized differential equations of motion for the spacecraft state and covariance are:

$$\begin{aligned} \dot{\vec{x}} &= F\vec{x} + q \\ \dot{E} &= FE + EF^T + Q \end{aligned} \tag{2.19}$$

where E is the covariance matrix, Q is the process noise matrix and F is the dynamics matrix which, for a position and velocity state, is defined by:

$$F = \left[\begin{array}{c|c} 0 & I \\ \hline G & 0 \end{array}\right] \tag{2.20}$$

Here G is the three-dimensional gradient of the gravitational field experienced by the spacecraft and is the sum of the Earth and Moon gravity gradients:

$$G = G_E + G_M \tag{2.21}$$

A first-order model which approximates the gravity gradient is given by:

$$G_P = \frac{\mu_P}{r_P^3}\left[3\hat{i}_{r_P}\hat{i}_{r_P}^T - I\right] \tag{2.21}$$

Where r_P is the position vector of the vehicle with respect to the primary, μ_P is the gravitational constant of the primary and I is the 3-dimensional identity matrix.

Through the integration of the covariance we can examine the state uncertainties behavior over time. The process noise matrix (Q) is used to account for all of the unmodeled effects which are not explicitly in the filter. It should be noted that all of the covariance equations were calculated using linearizing assumptions.

2.5.2 Monte Carlo Analysis

Occasionally to verify the validity of the linearizing assumptions for covariance integration, a Monte Carlo analysis is done. Monte Carlo analysis involve integrating a significant sample of dispersed trajectories over a period of time and then collecting the statistics on how these trajectories vary from the nominal. The initial states of the trajectories, which are random Gaussian dispersions about the nominal state are calculated using:

$$\vec{x} = \begin{bmatrix} \vec{R} \\ \vec{V} \end{bmatrix}$$

$$\vec{x}_i^{\,0} = \vec{x}_{nom} + \delta\vec{x}_i^{\,0} \tag{2.22}$$

$$\delta\vec{x}_i^{\,0} = \begin{bmatrix} \sigma_R \vec{v}_{rndg} \\ \sigma_V \vec{v}_{rndg} \end{bmatrix}$$

where $\vec{x}_i^{\,0}$ and $\delta\vec{x}_i^{\,0}$ is the state and state dispersion at the initial time, σ_R and σ_V are the position and velocity uncertainties and $\vec{v}_{rndg}$ is a 3-dimensional Gaussian random vector (σ=1). This is valid only for an initially diagonal covariance! The states of each of these trajectories are integrated to the desired time, and the dispersions from the nominal are calculated using:

$$\delta\vec{x}_i^{\,f} = \int_0^T \dot{\vec{x}}_i dt - \vec{x}_{nom} \tag{2.23}$$

The covariance at the terminal time can be calculated using:

$$E^f = \overline{\delta\vec{x}\delta\vec{x}^T} = \frac{1}{n-1}\sum_{i=1}^{n} \delta\vec{x}_i \delta\vec{x}_i^T \tag{2.24}$$

Assuming a zero mean.

This covariance can be compared to the integrated result to test the validity of the linearized propagation equations.

2.6 Measurements

2.6.1 Measurement Updates

The measurement process is comprised of several main components. They are : computation of the measurement geometry vector, weighting of the measurement, and the incorporation of the measurement information into the covariance.

Each measurement type has a measurement geometry vector ($\vec{b}$) associated with it . This vector describes how the measurement information affects the state components. For an optimal filter where all state components are being estimated, the actual state would be updated after a measurement using:

$$\begin{aligned} \vec{x}^* &= \vec{x} + \delta R\, \vec{w} \\ \delta R &= \vec{x}^T \delta \vec{x} \end{aligned} \tag{2.25}$$

The covariance would be updated using:

$$\begin{aligned} E^* &= \left(I - \vec{w}\vec{b}^T\right)E \\ \vec{w} &= \frac{E\vec{b}}{\vec{b}^T E\vec{b} + \alpha^2} \end{aligned} \tag{2.26}$$

where α^2 is the measurement noise variance.

Many times when a state will not be incorporated in an onboard system, or is unpredictable and difficult to model, we do not estimate it in the covariance analysis. For example we might not wish to estimate clock drift, beacon location accuracy, etc. These states are referred to as consider states. They are referred to as consider states because, while they are not being estimated, they are still being considered by the filter for the information they contain. For a suboptimal filter, the update for the covariance is given by the Joseph form:

$$E^* = SES^T + \alpha^2 \hat{w}\hat{w}^T$$

$$S = I - \hat{w}\vec{b}^T$$

$$\hat{w} = \underbrace{\begin{bmatrix} 1 & & & & \\ & 1 & & & \\ & & \ddots & & \\ & & & 0 & \\ & & & & 1 \\ & & & & & 1 \end{bmatrix}}_{I_W} \vec{w} \tag{2.27}$$

where I_W is a diagonal weighting matrix where a 1 indicates that the state is being estimated, and a 0 indicates a consider state.

2.6.2 Measurement Types

The principle types of measurements we will be analyzing are: Two-way ranging, One-way ranging and Doppler. Each of the measurements has a measurement geometry vector[10] and a block in the covariance dynamics matrix (F) and process noise matrix (Q)[11] which govern the behavior and integration of the measurement into the covariance matrix. These measurement types will be implemented using either Moon-based beacons (NavSites) or a navigation satellite (NavSat). When a beacon is used, three covariance states are needed to represent the beacon location uncertainty. When a NavSat is used, six covariance states are needed to represent the satellites position and velocity uncertainties. In each case, some additional states will be needed to model any relevant instrument biases. The dynamics block for the addition of a beacon or NavSat will be of the form:

$$F = \begin{bmatrix} F_i & \\ & F_m \end{bmatrix}$$

where F_i is the dynamics matrix of the NavSite or NavSat and F_m is the dynamics matrix for the instrument biases. The following sections present a description of the error model used for each of the measurement types.

---

[10] Refer to beginning of Section 2.6 for more detail about measurement geometry vectors

[11] Section 2.5

Two-Way Range

Two-way ranging measures the distance between the spacecraft and a NavSite or NavSat by essentially "pinging" the beacon using radio transmissions. The spacecraft transmits a coded pulse sequence to the beacon which retransmits it back to the spacecraft. The transit time is used to measure the range between the two stations[12]. Although the measurement is really a time delay, it can be thought of as a range bias and will be modeled as such. The accuracy of this measurement is dependent on the stability of the onboard clock and biases due to unmodeled electronic delays or other environmental factors. Over the short transit times for Lunar ranging, the clock stability (drift) is not a problem. The composite bias is thus the only state that must be modeled in the filter.

The addition of two-way ranging will add one state per beacon to the covariance matrix. Thus, the covariance block is for a two-way ranging system is of the form

$$\begin{bmatrix} E_i & \\ & \sigma_{\beta_r}{}^2 \end{bmatrix}$$

where the E_i is the NavSite or NavSat covariance block and $\sigma_{\beta_r}{}^2$ is the range bias variance. All of these states will be estimated.

The "bias" will be modeled as an exponentially correlated random variable (first-order Markov process). From these assumptions, the dynamics for the two-way range system can be described as

$$\begin{aligned} \dot{\beta}_r &= -\frac{1}{\tau}\beta_r + q \\ \dot{\sigma_{\beta_r}{}^2} &= -\frac{1}{\tau}\sigma_{\beta_r}{}^2 - \frac{1}{\tau}\sigma_{\beta_r}{}^2 + Q \\ Q &= \frac{2\left(\sigma_{\beta_r}{}^2\right)_{\max}}{\tau} \end{aligned} \tag{2.28}$$

---

[12] Lear, W. M. , A Prototype, Real-Time Navigation Program For Multi-Phase Missions

where β_r is the range bias, q is the state noise, $\sigma_{\beta_r}^2$ is the variance of the range bias, Q is the covariance noise and τ is the time constant. From these dynamics it can be seen that the dynamics matrix block and the noise matrix block are

$$F_{2-wayrange} = \left[-\frac{1}{\tau}\right]$$
$$Q_{2-wayrange} = \left[\frac{2\left(\sigma_{\beta_r}^2\right)_{\max}}{\tau}\right] \tag{2.29}$$

One-Way Range

One-way ranging, like two-way ranging, measures the distance between the spacecraft and a NavSite or NavSat. Unlike two-way ranging, the beacon transmits a time tagged coded pulse sequence to the spacecraft and the transit time is used to measure the range between the two stations. The time tag is compared with the spacecraft clock in order to calculate the transfer time. The accuracy of this measurement is dependent on the stability of the onboard clocks and any inherent relative bias between the clocks. The relative clock bias and clock drift will be modeled as a range bias and a range rate bias.

The addition of one-way ranging will add two states per NavSite or NavSat to the state vector and covariance matrix. The covariance block for a one-way ranging system is of the form:

$$\begin{bmatrix} E_i & & \\ & \sigma_{\beta_r}^2 & \\ & & \sigma_{\beta_{rr}}^2 \end{bmatrix}$$

where the E_i is the NavSite or NavSat covariance block, $\sigma_{\beta_r}^2$ is the range bias variance and $\sigma_{\beta_{rr}}^2$ is the range rate bias variance. The NavSite or NavSat range bias will be estimated. The range rate bias will be considered but not estimated (consider state). It should be noted that to change a beacon from two-way to one-way ranging involves the addition of only one state, the range rate bias.

The range rate bias will be modeled by a Markov process and will drive the range bias state which thus becomes an integrated Markov process. From these assumptions, the dynamics for the one-way range system can be described as:

$$\begin{bmatrix} \dot{\beta}_r \\ \dot{\beta}_{rr} \end{bmatrix} = \begin{bmatrix} 0 & 1 \\ 0 & -\frac{1}{\tau} \end{bmatrix} \begin{bmatrix} \beta_r \\ \beta_{rr} \end{bmatrix} + \begin{bmatrix} 0 \\ q \end{bmatrix}$$

$$\begin{bmatrix} \dot{\sigma}_{\beta_r}^{\,2} \\ \dot{\sigma}_{\beta_{rr}}^{\,2} \end{bmatrix} = \begin{bmatrix} 0 & 1 \\ 0 & -\frac{2}{\tau} \end{bmatrix} \begin{bmatrix} \sigma_{\beta_r}^{\,2} \\ \sigma_{\beta_{rr}}^{\,2} \end{bmatrix} + \begin{bmatrix} 0 \\ Q \end{bmatrix} \tag{2.30}$$

$$Q = \frac{2\left(\sigma_{\beta_{rr}}^{\,2}\right)_{\max}}{\tau}$$

where β_r is the range bias, β_{rr} is the range rate bias, q is the state noise, $\sigma_{\beta_r}^{\,2}$ is the variance of the range bias, $\sigma_{\beta_{rr}}^{\,2}$ is the variance of the range rate bias, Q is the covariance noise and τ is the time constant. From these dynamics, it can be seen that the dynamics matrix block and the noise matrix block are

$$F_{1-way\,range} = \begin{bmatrix} 0 & 1 \\ 0 & -\frac{1}{\tau} \end{bmatrix}$$

$$Q_{1-way\,range} = \begin{bmatrix} 0 & 0 \\ 0 & \frac{2\left(\sigma_{\beta_r}^{\,2}\right)_{\max}}{\tau} \end{bmatrix} \tag{2.31}$$

Ranging Measurement Geometry Vectors

While one-way and two-way ranging have somewhat different dynamics, the measurement geometry of the two systems is the same. Therefore, the measurement geometry vector for one-way and two-way ranging is:

$$\vec{b} = \begin{bmatrix} \vec{u}_{LOS} \\ \vec{0} \\ \vdots \\ -\vec{u}_{LOS} \\ \vec{0} \\ 1 \\ 0 \end{bmatrix} \begin{matrix} \textit{Spacecraft Position} \\ \textit{Spacecraft Velocity} \\ \textit{Intermediate States} \\ \textit{NavSite/NavSat Position} \\ \textit{NavSat Velocity} \\ \textit{Range Bias} \\ \textit{Range Rate Bias} \end{matrix} \tag{2.32}$$

where $\vec{u}_{LOS}$ is the line-of-sight vector between the spacecraft and the NavSite or NavSat. It should be noted that the $\vec{u}_{LOS}$ must be in the proper coordinate frames for the spacecraft and NavSite or NavSat. The spacecraft and NavSat information are usually in inertial coordinates, and the NavSite information is usually in local vertical local horizontal (LVLH) coordinate system at the beacon (See Figure 4.1 for definition of LVLH frame).

Doppler

Doppler measures the relative velocity along the line-of-sight between the spacecraft and a NavSite or NavSat. The spacecraft transmits a tone to the NavSite/NavSat which retransmits it back to the spacecraft. The frequency shift is used to measure the relative velocity between the two stations. The accuracy of this measurement is dependent on the stability of the onboard frequency standards, and frequency bias due to environmental factors. Over the short transmit times for Lunar ranging, the frequency standard stability (drift) is not of concern, thus the frequency bias is the only state which must be modeled.

The addition of Doppler will add one state per NavSite/NavSat to the covariance matrix. The covariance block for a Doppler system is:

$$\begin{bmatrix} E_i & \\ & \sigma_{\beta_d}{}^2 \end{bmatrix}$$

where the E_i is the NavSite or NavSat covariance block and $\sigma_{\beta_d}{}^2$ is the Doppler bias variance. All of these states will be estimated. It should be noted that adding Doppler to a beacon that has one and two-way ranging capabilities involves the addition of only one

state, the Doppler bias. Although the Doppler bias is actually a frequency shift, it may be thought of as a relative velocity bias and is modeled as such.

The Doppler bias will be modeled as a Markov random process. The dynamics are the same as for the one-way range case (Equation 2.28) with the substitution of the Doppler bias β_d for the range bias β_r. The dynamics matrix and noise matrix blocks for the Doppler measurement are:

$$F_{Doppler} = \left[-\frac{1}{\tau}\right]$$
$$Q_{Doppler} = \left[\frac{\left(2\sigma_{\beta_d}{}^2\right)_{\max}}{\tau}\right] \tag{2.33}$$

Doppler Measurement Geometry Vectors

The measurement geometry vector for the Doppler measurement is quite a bit more complex than for ranging measurements. The measurement geometry vector for Doppler is:

$$\vec{b} = \begin{bmatrix} \frac{(\vec{R}_{REL}\times\vec{V}_{REL})\times\vec{R}_{REL}}{R_{REL}^{\,3}} \\ \vec{u}_{REL} \\ \vdots \\ -\frac{(\vec{R}_{REL}\times\vec{V}_{REL})\times\vec{R}_{REL}}{R_{REL}^{\,3}} - (\vec{\omega}_P \times \vec{R}_{REL}) \\ -\vec{u}_{REL} \\ 1 \end{bmatrix} \begin{matrix} \textit{Spacecraft Position} \\ \textit{Spacecraft Velocity} \\ \textit{Intermediate States} \\ \textit{NavSite/NavSat Position} \\ \textit{NavSat Velocity} \\ \textit{Doppler Bias} \end{matrix} \tag{2.34}$$

where $\vec{R}_{REL}$, $\vec{V}_{REL}$ and $\vec{u}_{REL}$ are the relative position, velocity and unit line-of-sight vectors of the spacecraft from the NavSite or NavSat. Again, it should be noted that the $\vec{u}_{REL}$ must be in the proper coordinate frames for the spacecraft and NavSite or NavSat. The spacecraft and NavSat states are usually in inertial coordinates, and the NavSite states are usually specified in local vertical local horizontal (LVLH) coordinates. Note that the term $(-\vec{\omega}_P \times \vec{R}_{REL})$ must be added for a NavSite case only where $\vec{\omega}_P$ is the rotation rate of the planet.

CHAPTER 3
Implementation

3.1 The Simulation

After obtaining the analytic equations for the propagation of the spacecraft state and covariance and the updating of the covariance through the taking of measurements, the next step was to implement the system in a simulation. Because of L1 and L2's proximity to the Moon, it was decided that the simulator would use Moon-centered coordinates for the analysis. The simulation integrates the spacecraft state and covariance using a sixth-order Runge-Kutta integrator. The measurements are taken at most once per time step of the integrator, and are incorporated into the covariance. Figure 3.1 shows a general block diagram of the simulation.

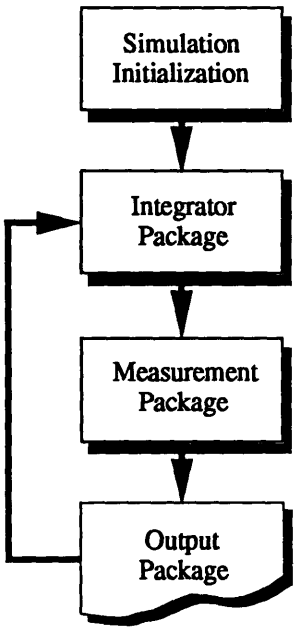

Figure 3.1 : Simulation Block Diagram

The simulation has many features which allow the user to model different environmental effects. The primary set of effects addressed in the design of the simulation are the perturbations discussed in Chapter 2.

3.1.1 Solar Effects

The simulation has the capability of modeling many solar effects. For simplicity due to the fact that we are using a Moon-centered system, the Sun is modeled as orbiting the Moon in a circular orbit of radius 1 a.u. In the model the inclination of the Sun to the Earth was specified to ensure proper Sun-Earth-Moon geometry by using Cassini's Law (Figure 3.2).

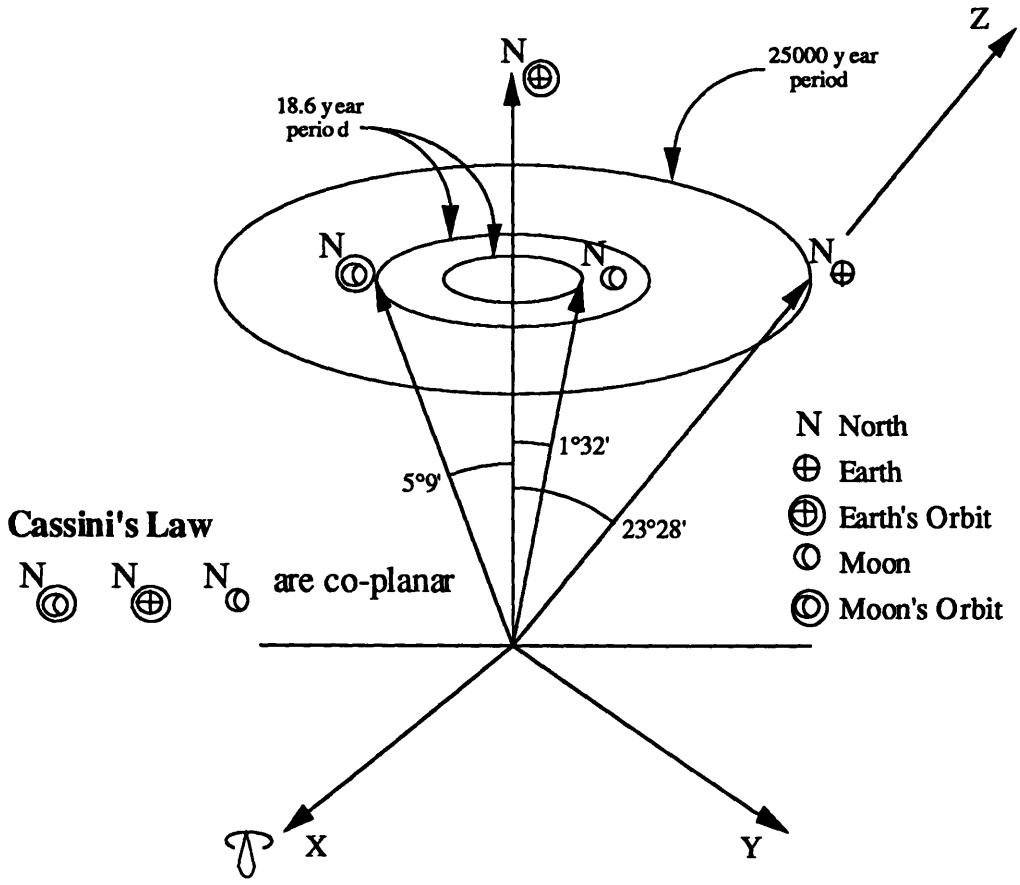

Figure 3.2 : Cassini's Law

There were three primary Sun perturbations modeled:

- Solar Gravity Gradient
- Solar Radiation Pressure
- Lunar Surface Illumination

For solar gravity gradient, the gravity gradient matrix of the Sun was added into the gravity gradient for the covariance propagation. This is done to account for any effect that the Sun's disturbing acceleration has on the navigation system. For solar radiation pressure, the model discussed in Section 2.4.2 was implemented. The force on the spacecraft was calculated using the reference mass and area input by the user. As will be seen, this effect is more of a station-keeping problem than a navigation one. The effects of solar radiation pressure on the navigation will be accounted for using increased process noise at a level of the solar radiation pressure. The solar illumination feature is used to determine whether the NavSites on the Moon are in direct sunlight. This will be used in one of the variations to show the effects of limited battery life during the long Lunar nights. Initially the modeling of the actual Solar gravity on the spacecraft was investigated. This involves not only modeling the effects on the spacecraft, but also on the Earth and Moon. The result is the modeling of the four-body problem which is somewhat more complex in it's implementation. This was deemed unnecessary after the analysis presented in Section 2.4.4 showed that the first-order disturbing acceleration would preserve the libration geometry. This allows simulation of the gravity gradient to account for the effects on the navigation, without being concerned with actual state perturbations.

3.1.2 Earth Effects

The last of the perturbations to be modeled from Chapter 2 is that of Earth-Moon eccentricity. Because we are using Moon-relative equations, the Earth must be initialized in an orbit about the Moon. This orbit can be either circular, which it is in the nominal cases, or eccentric in order to simulate the effects of eccentricity on the navigation.

Another feature in the simulation is the ability to place the NavSites on the rotating Earth. The Earth's face is not stationary in the rotating system like the Moon's is. Actually, the Earth is not only rotating, but it is also inclined with respect to the Earth-Moon line-of-sight coordinates. When placing NavSites on the Earth, all of these effects are accounted for in the simulation.

3.1.3 Burn Modeling

One area which must be investigated in the discussion of navigation is the effects of propulsive maneuvers on the system. The goal was to accurately model the effects, but also keep the model simple. We also wanted to avoid the modeling of actual burns, which would necessitate the inclusion of an Inertial Measurement Unit (IMU) model to measure sensed accelerations. The chosen model involved the periodic addition of velocity errors along the spacecraft velocity state diagonals in the covariance matrix. This allowed us to model the primary effect of propulsive maneuvers, which is the adding of velocity uncertainties into the system. Position and velocity errors on the order of 1000 m and 0.04 m/s were chosen as reasonable state uncertainties at the libration point post-insertion. To determine the optimal timing or periodicity of the burns, Monte Carlo runs were done using these uncertainties to observe the spacecraft's position and velocity relative to the libration point over time. Figure 3.3 shows the spacecraft position and velocity relative to L1 over a five day period given initial position and velocity dispersions of 1000 m and 0.04 m/s. After 5 days, the RSS position error is on the order of 40-150 km and velocity on the order of 0.3-1.2 m/s. The position error is not very large when considering it's relative size to the system geometry. The velocity error is significant, and is of the size which warrants station-keeping burns. The velocity has reached a level which is on the order of seven to thirty times the burn accuracy of the thrusters (0.04 m/s) which is the level at which a corrective burn begins to make sense. The behavior of the L2 dispersions were very similar, though the magnitudes of the position and velocity errors after five days were somewhat smaller. For these reasons, five days was chosen as the burn frequency to simulate the effects of station-keeping burns on the navigation. A case will also be run with a shorter frequency to characterize the navigation system performance under a more rigorous burn schedule.

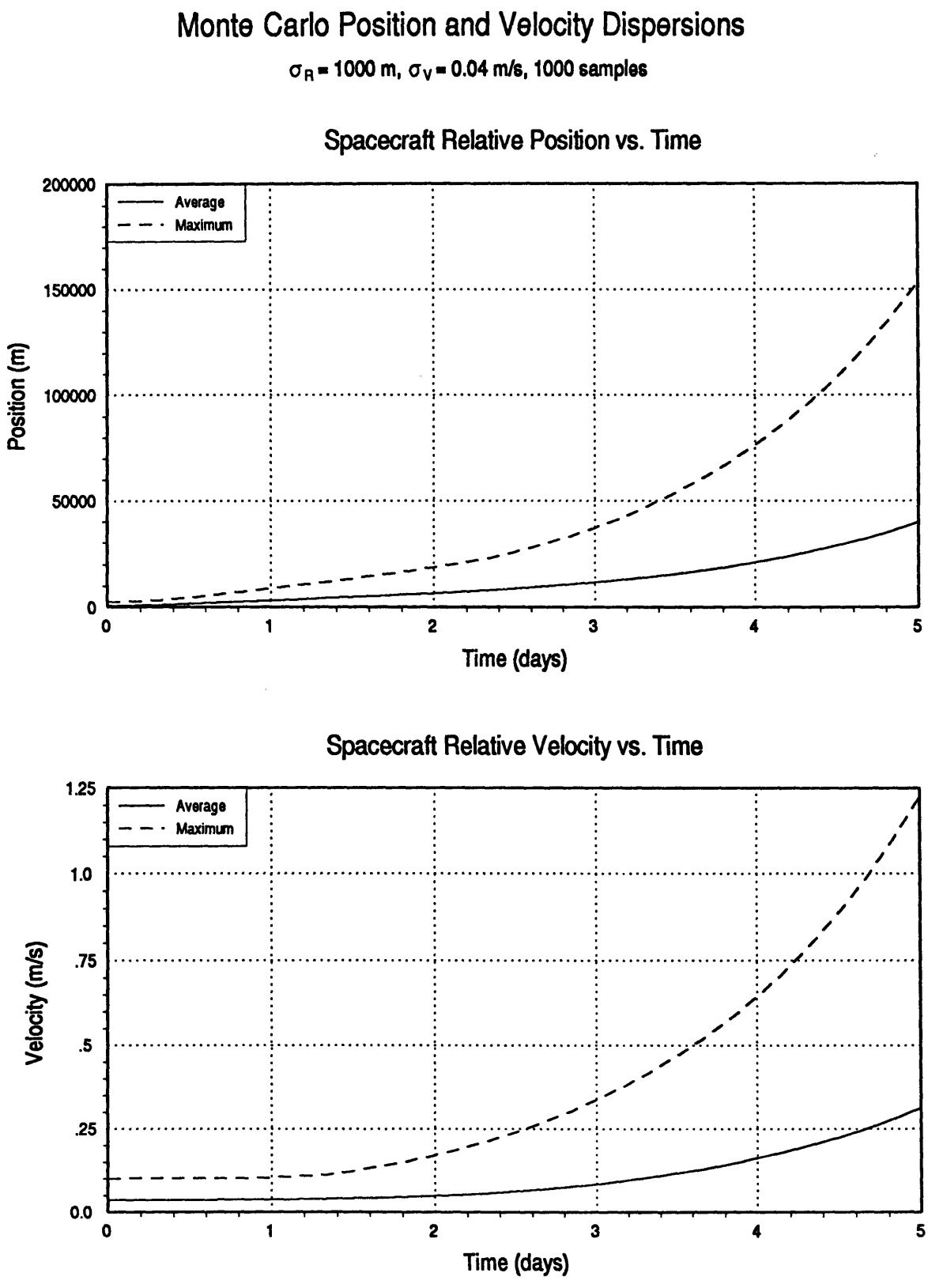

Figure 3.3 : Spacecraft Position and Velocity Error Growth Relative to L1

3.2 The Covariance

Each addition of a NavSite or NavSat adds states to the covariance. The initial decision was to include the capability to use up to 3 NavSites and 1 NavSat simultaneously. This results in a covariance with 33 states. The covariance was implemented in the form presented in Equation 3.1.

$$
E = \begin{bmatrix}
\underset{3x3}{\left[\vec{R}_{SC}\right]} & & & & & & \\
& \underset{3x3}{\left[\vec{V}_{SC}\right]} & & & & & \\
& & \underset{6x6}{\left[NavSite_1\right]} & & & & \\
& & & \underset{6x6}{\left[NavSite_2\right]} & & & \\
& & & & \underset{6x6}{\left[NavSite_3\right]} & & \\
& & & & & \underset{9x9}{\left[NavSat\right]}
\end{bmatrix}
$$

$$
[NavSite] = \begin{bmatrix}
\underset{3x3}{\left[\vec{R}_B\right]} & & \\
& \underset{2x2}{\begin{bmatrix} \beta_r & \\ & \beta_{rr} \end{bmatrix}} & \\
& & \underset{1x1}{\left[\beta_d\right]}
\end{bmatrix}
$$

$$
[NavSat] = \begin{bmatrix}
\underset{3x3}{\left[\vec{R}_{NS}\right]} & & \\
& \underset{3x3}{\left[\vec{V}_{NS}\right]} & \\
& & \underset{2x2}{\begin{bmatrix} \beta_r & \\ & \beta_{rr} \end{bmatrix}} \\
& & \underset{1x1}{\left[\beta_d\right]}
\end{bmatrix} \tag{3.1}
$$

Each NavSite and NavSat has two-way ranging, one-way ranging and Doppler measurement capabilities. The NavSites can be placed on the Earth or Moon and at any latitude/longitude location.

3.3 Measurement Specifications

To conclude the descriptions of the various measurement types from Section 2.6 we must define all of the measurement error modeling assumptions. The following tables contain the specifications for our nominal two-way ranging, one-way ranging and Doppler systems. The noise units for the one-way and two-way ranging systems are meters per 1000 kilometers of line-of-sight range.

Table 3.1 : Two-Way Ranging Specifications

Variable	Symbol	Value	Units
Range Bias	σ_{β_r}	20	m
Noise	α_{2WR}	7	m/1000 km
Time Constant	τ	1	day

Table 3.2 : One-Way Ranging Specifications

Variable	Symbol	Value	Units
Range Bias	σ_{β_r}	1000	m
Range Rate Bias	$\sigma_{\beta_{\dot{r}}}$	0.003	m/s
Noise	α_{1WR}	5	m/1000 km
Time Constant	τ	1	day

Table 3.3 : Doppler Specifications

Variable	Symbol	Value	Units
Doppler Bias	$\sigma_{\beta_{\dot{r}}}$	0.1	m/s
Noise	α_D	0.1	m/s
Time Constant	τ	1	day

When a system is referred to as one-way ranging, two-way ranging or Doppler with no additional description, the reference is being made to the systems described above. In the variational cases for the primary missions, some of the measurement specifications will be varied to determine the sensitivity of the navigation system to the specification.

3.4 Baseline Missions

The goal of this study is to determine which types of navigation systems will perform best for Earth-Moon libration point missions. As discussed in Section 2.6, Doppler and two-way and one-way range measurement types will be examined using NavSite and NavSat platforms. Four primary missions will be analyzed in an attempt to span the range of applications discussed in Section 1.4. To investigate the relative performance of the measurement systems, a baseline for each mission must be established. Table 3.4 presents the six primary missions, the duration over which they will be analyzed, measurement frequency and the Baseline measurement and platform types. The measurement frequency was chosen so as to result in 150+ measurements being taken over the time frame of the particular mission.

Table 3.4 : Primary Missions

Mission	Number	Duration	Measurement Frequency	Baseline Measurement System
L1 Station-keeping	1	28 days	4 hours	3 Lunar NavSites, two-way ranging
L2 Station-keeping	2	28 days	4 hours	3 Lunar NavSites, two-way ranging
L1 to Lunar Transfer	3	25 hours	10 minutes	3 Lunar NavSites, two-way ranging
Lunar to L1 Transfer	4	25 hours	10 minutes	3 Lunar NavSites, two-way ranging
L2 to Lunar Transfer	5	28 hours	10 minutes	3 Lunar NavSites, two-way ranging
Lunar to L2 Transfer	6	28 hours	10 minutes	3 Lunar NavSites, two-way ranging

The station-keeping missions consist of a spacecraft sitting at the libration points. Being that the Earth and Moon revolve around their common center of mass over a period of approximately 28 days, this period was chosen as the time frame over which the station-keeping missions were to be analyzed.

The LPoint to Lunar transfers consist of the spacecraft starting at either L1 or L2 and transferring down to the Moon. The spacecraft's velocity is initialized to the post-burn transfer velocity. Even a small burn at a libration point will result in the spacecraft "falling" toward the Earth or Moon after a sufficient period of time. However, the transfer time is proportional to the initial ΔV. When choosing the baseline missions, the target was a transfer time of about 1 day which resulted in ΔVs on the order of 550 m/s. All of the transfers are in the Moon's orbit plane. Table 3.5 contains the specifications of the libration-Lunar transfers. Periapse longitude assumes that 0° longitude is at the L1 sub-libration point. The ± for the periapse longitudes are due to the fact that the transfers to and from the Moon are symmetric about the Earth-Moon line of sight axis.

Table 3.5 : Libration-Lunar Transfer Specifications

Mission Numbers	Transfer	Time (dd:hh:mm)	ΔV_{LPoint} (m/s)	ΔV_{CIRC} (m/s)	Periapse Altitude (km)	Periapse Longitude (°)
3,4	L1-Lunar	1:00:56	553.2	666.3	200	±170.8
5,6	L2-Lunar	1:03:58	557.1	671.1	200	±7.7

Since the transfers to and from the Moon are symmetric, they require the same propulsive maneuvers and transfer time. ΔV_{Lpoint} is the burn to inject into the transfer orbit from the libration point, and to stop at the libration point after a transfer from the Moon. ΔV_{CIRC} is the burn to inject into a circular orbit from the transfer at periapse, and to inject into the transfer from periapse. Figures 3.4 and 3.5 show the Libration-Lunar transfers.

For each of the missions, initial position and velocity uncertainties must be chosen. For the station-keeping missions, initial position and velocity uncertainties were chosen to be 20 kilometers and 0.05 m/s. These were chosen because they are large and much above the desired levels of position and velocity uncertainties, and somewhat typical of trans-Earth uncertainties. For the transfers down to the Moon, 0.1% of the propulsive ΔV value was root-sum-squared (RSS) with the station-keeping initial position and velocity uncertainties. This is consistent with a burn direction error of about 200 arc seconds, which is a conservative number for a propulsion maneuver. For transfer up from the Moon, the initial position uncertainty was assumed to be 1 km, which is a conservative number for a Moon-orbiting craft. The velocity errors were again assumed to be 0.1% of the ΔV. Table 3.6 contains the initial position and velocity uncertainties for each of the primary mission scenarios.

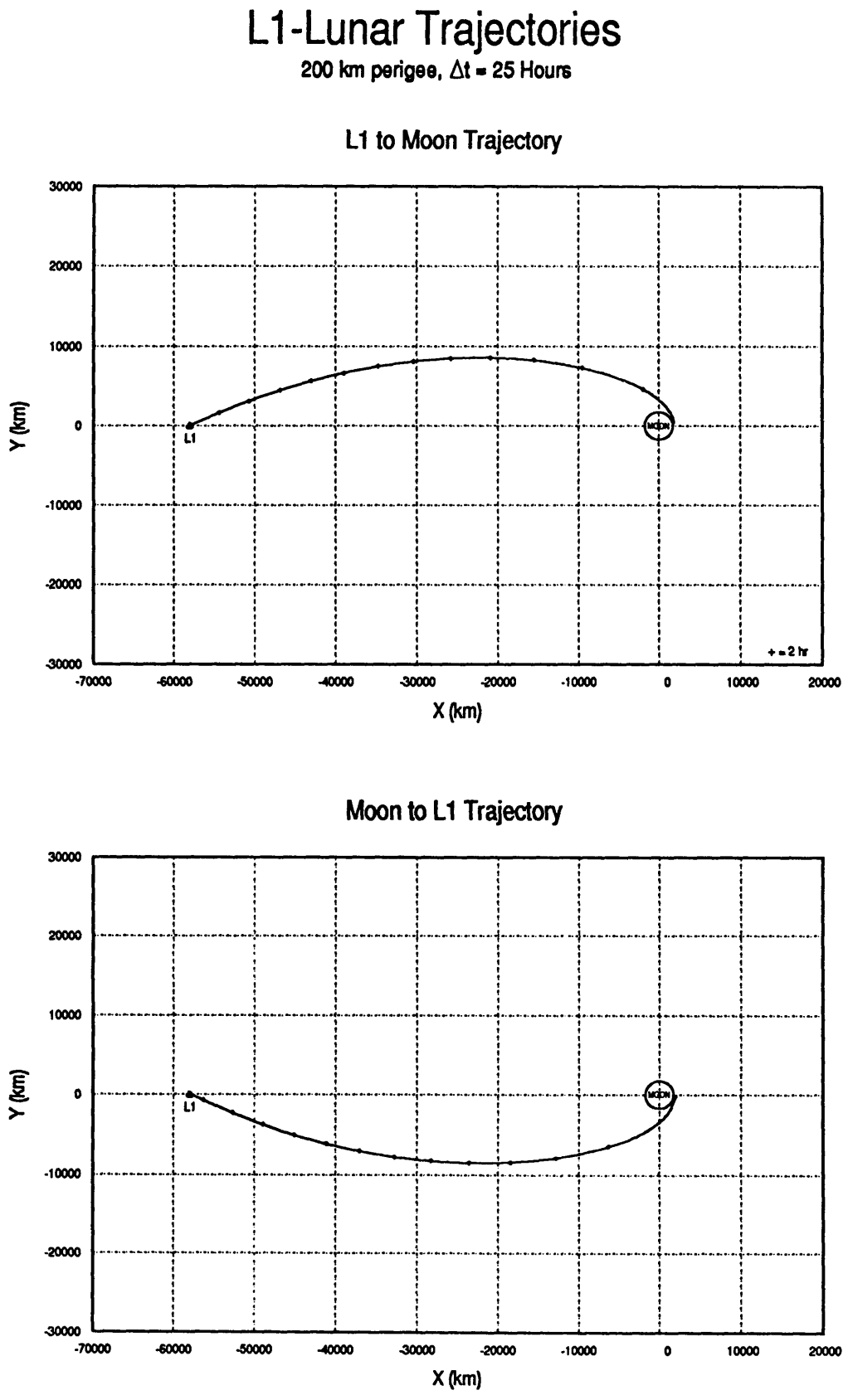

Figure 3.4 : L1-Lunar Trajectories

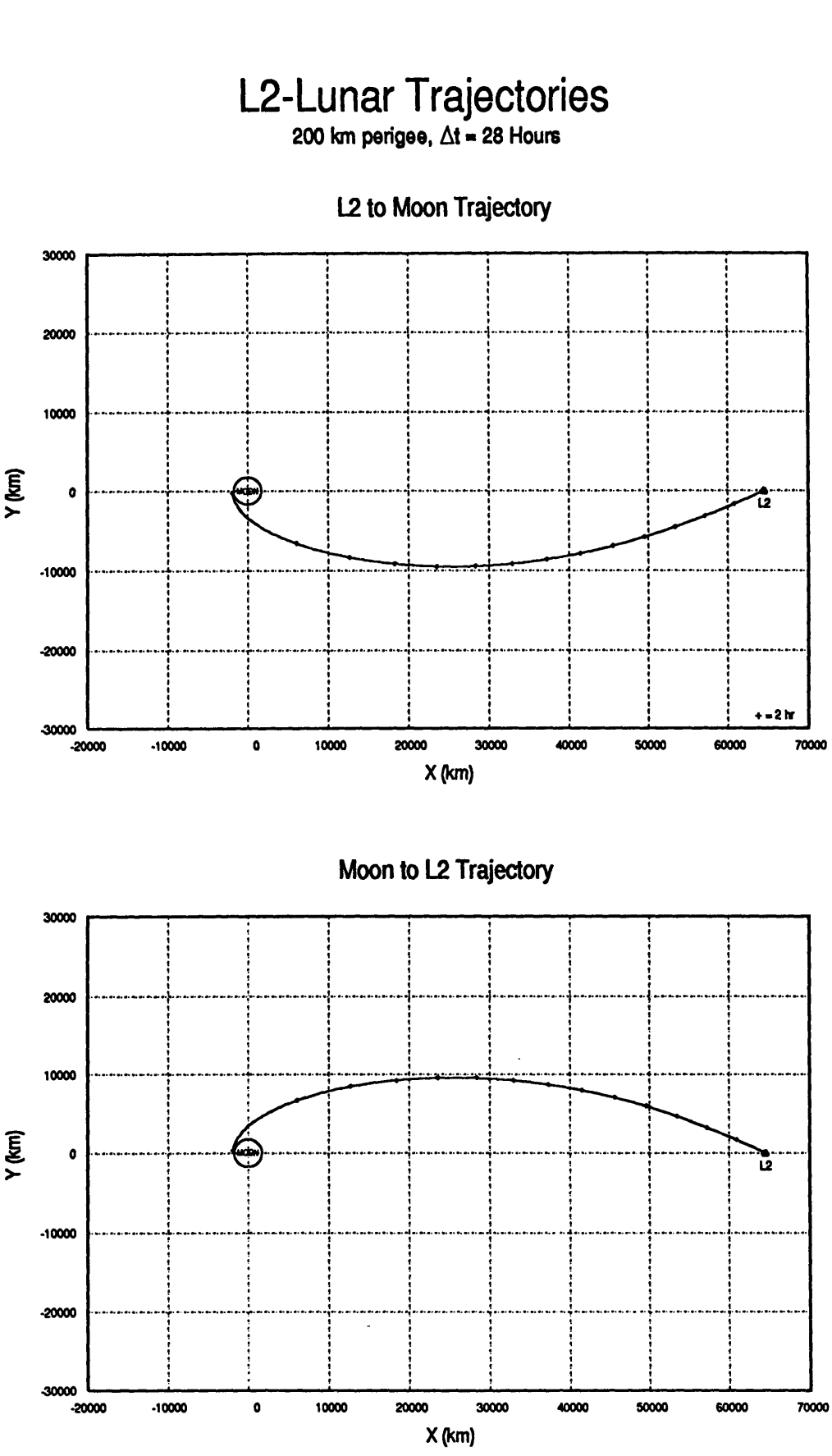

Figure 3.5 : L2-Lunar Trajectories

Table 3.6 : Initial Position and Velocity Uncertainties

Mission Number	Mission	Position Uncertainty (km)	Velocity Uncertainty (m/s)
1	L1 Station-keeping	20	0.05
2	L2 Station-keeping	20	0.05
3	L1 to Moon Transfer	20	0.55
4	Moon to L1 Transfer	1	0.67
5	L2 to Moon Transfer	20	0.56
6	Moon to L2 Transfer	1	0.67

Preliminary examination of the measurement types indicated that two-way ranging is superior to one-way ranging or Doppler in navigation performance. For this reason, two-way ranging was chosen as the baseline measurement type. Moon-based NavSites were chosen because of their proximity to the mission locations. Both ranging measurements degrade in performance with increasing distance from the target. Similarly, a Doppler system's performance should be degraded with increasing distance between the transmitter and the receiver (this was not modeled). Having NavSites requires only position uncertainties for each beacon in the covariance, whereas NavSats require position and velocity. An advantage of the NavSite navigation approach is that the beacon states have no dynamics. It is assumed that the angular velocity of the planet ($\vec{\omega}_p$) is known. The velocity of the beacon is therefore written as:

$$\vec{V}_b = \vec{\omega}_p \times \vec{R}_b \tag{3.2}$$

where $\vec{R}_b$ is the beacon position vector relative to the center of the planet. The beacon is not moving in the planet-fixed axes, and therefore has no dynamics. Table 3.7 contains the initial position uncertainties used for Earth-based and Moon-based NavSites. This assumes that the Moon NavSites have been surveyed. The Lunar NavSites on the front can be surveyed from the Earth, and those on the back can be surveyed from orbit using a NavSite on the front as a reference. These numbers are typical of the type of position uncertainties that are obtainable from Earth. The uncertainties are shown in downrange (DR), vertical

(VT) and crosstrack (CT) directions which correspond to East, altitude and North on the planets surface.

Table 3.7 : Initial Position Uncertainties for NavSite

	DR (m)	VT (m)	CT (m)
Moon	15	5	15
Earth	1	1	1

Table 3.8 contains the initial position and velocity uncertainties used for the Lunar NavSat. These numbers were calculated using initial downrange, vertical and crosstrack errors of 300, 100 and 200 meters and a period error of 0.1 seconds.[13] These numbers are thought to be typical of a Lunar satellite.

Table 3.8 : Initial Position and Velocity Uncertainties for NavSat

Position Errors (m)			Velocity Errors (m/s)		
DR	VT	CT	DR	VT	CT
300	100	200	.020	.049	.040

Navigation performance is dependent upon the measurement accuracy as well as the amount of measurement geometry that the spacecraft has relative to the navigation aids. The Moon's orbital period is the same as its rotational period which means that it maintains a fixed orientation with respect to the Earth (±1° about the orbital angular momentum axis). Therefore, Lunar NavSites will maintain a constant orientation relative to the libration point. A triad of beacons was chosen as the baseline under the assumption that the navigation system would need three dimensional information geometry to adequately bound the covariance. This did not take into consideration any coupling of the dynamics of the system, which will be examined in the variational cases. The baseline configuration of the beacons on the Moon is presented in Figure 3.6

[13] Shepperd, S.W., Constant Covariance in Local Vertical Coordinates for Near-Circular Orbits

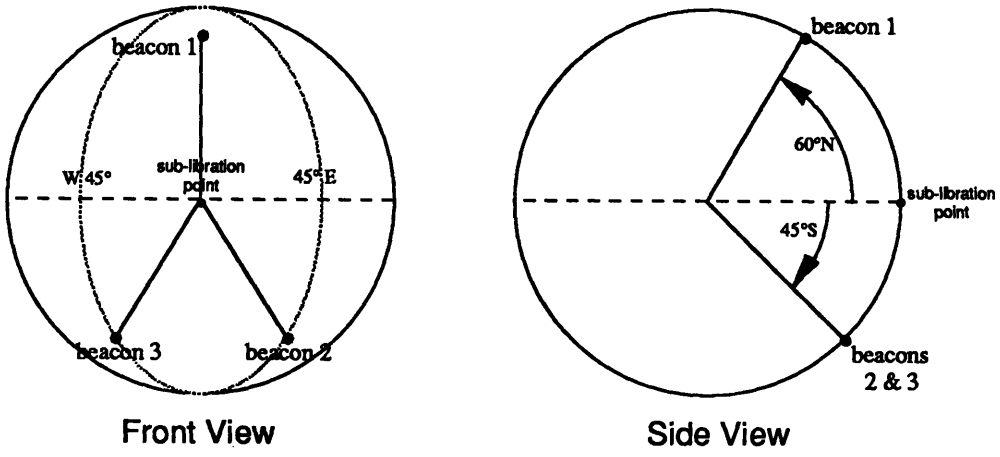

Figure 3.6 : Baseline Beacon Configuration

3.5 Summary of Case Variations

Many variations from the baseline were run to evaluate the navigation performance under various conditions. The following Tables (3.7-3.12) provide a list of all of the cases for each of the defined missions. Each case is coded with a two digit number. The first number refers to the mission, the second to the variation number where zero is the baseline. The results of these cases are presented in Chapter 4.

3.5.1 L1 Station-keeping

Table 3.9 : L1 Station-keeping Cases

Variation Type	Case Number	Description
Baseline	1.0	3 two-way range Lunar NavSites
Measurement Type	1.1	One-way ranging
	1.2	Doppler
Navigation Infrastructure	1.3	No NavSites, 1 Lunar NavSat in 5000 km, 45° inclination circular orbit
	1.4	3 Lunar NavSites and 1 Lunar NavSat in 5000 km, 45° inclination circular orbit
	1.5	2 Lunar NavSites - 1 at 75° N, 0° E - 1 at 75° N, 0° E
	1.6	1 Lunar NavSites - 60° N, 0° E
	1.7	1 Lunar NavSite - 0° N, 60° E
	1.8	1 Lunar NavSite - 0° N, 0° E
	1.9	3 Earth NavSites, 120° apart on equator 1.4 m/1000 km measurement noise
	1.10	3 Earth NavSites - 1 at 0° N, 0° E - 1 at 30° N, 120° E - 1 at 30° S, 120° W 1.4 m/1000 km measurement noise
Burn Modeling	1.11	0.04 m/s ΔV every 5 days
	1.12	0.04 m/s ΔV every 2 days
	1.13	One-way ranging, 0.4 m/s ΔV every 5 days
Environmental Perturbations	1.14	Earth-Moon eccentricity
	1.15	Solar gravity gradient
Measurement Specification	1.16	0.7 m/1000 km Measurement Noise
	1.17	2.0 m range bias
	1.18	One-way range with 0.03 m/s range rate bias
Miscellaneous	1.19	Process Noise 1×10^{-8} m^2/s^3
	1.20	NavSites lose power when not in sunlight

3.5.2 L2 Station-keeping

Table 3.10 : L2 Station-keeping Cases

Variation Type	Case Number	Description
Baseline	2.0	3 two-way range Lunar NavSites
Measurement Type	2.1	One-way ranging
	2.2	Doppler
Navigation Infrastructure	2.3	No NavSites, 1 Lunar NavSat in 5000 km, 45° inclination circular orbit
	2.4	L2 lissajous figure
Miscellaneous	2.5	L2 lissajous figure, Earth NavSites, 120° apart on equator

3.5.3 L1 to Moon Transfers

Table 3.11 : L1 to Moon Transfer Cases

Variation Type	Case Number	Description
Baseline	3.0	3 two-way range Lunar NavSites
Measurement Type	3.1	One-way ranging
	3.2	Doppler
Navigation Infrastructure	3.3	No NavSites, 1 Lunar NavSat in 5000 km, 45° inclination circular orbit Overhead when injecting into orbit at periapse
Miscellaneous	3.4	Initialize Covariance with steady-state covariance final conditions from 28 day station-keeping

3.5.4 Moon to L1 Transfers

Table 3.12 : Moon to L1 Transfer Cases

Variation Type	Case Number	Description
Baseline	4.0	3 two-way range Lunar NavSites
Measurement Type	4.1	One-way ranging
	4.2	Doppler
Navigation infrastructure	4.3	No NavSites, 1 Lunar NavSat in 5000 km, 45° inclination circular orbit Overhead when injecting into orbit at periapse

3.5.5 L2 to Moon Transfers

Table 3.13 : L2 to Moon Transfer Cases

Variation Type	Case Number	Description
Baseline	5.0	3 two-way range Lunar NavSites

3.5.6 Moon to L2 Transfers

Table 3.14 : Moon to L2 Transfer Cases

Variation Type	Case Number	Description
Baseline	6.0	3 two-way range Lunar NavSites

CHAPTER 4
Results

The following sections present the results for each of the nominal missions. Some of the time histories of the position and velocity uncertainties will be presented in the Chapter. All of them can be found in Appendix A for further reference. Most of the results are presented in the local vertical - local horizontal frame which consists of the downrange (DR), vertical (VT) and crosstrack (CT) directions. Figure 4.1 shows the LVLH frame geometry. It should be noted that for Moon-centered coordinates, the vertical axis is in the radial direction, and the crosstrack is in the opposite direction of the Earth-Moon rotation axis, and represents the out-of-plane component. The system is a standard right handed system with DR x VT = CT.

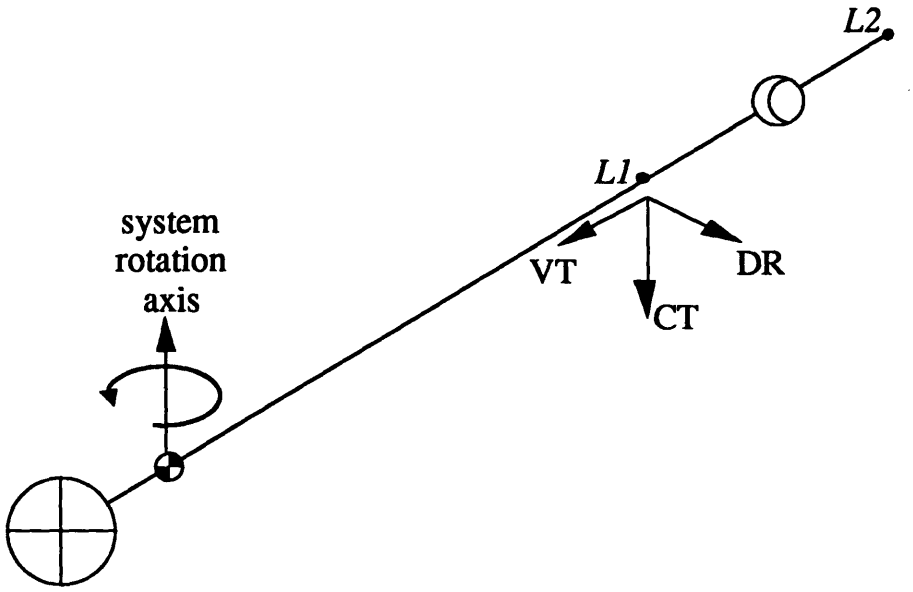

Figure 4.1 : LVLH Frame Geometry

4.1 L1 Station-keeping

The results of the baseline and variational runs for the L1 station-keeping mission are presented in Table 4.1. The case definitions can be found in Table 3.7.

Table 4.1 : L1 Station-keeping Results after 28 days
Initial σ_R=20000 m, σ_V=.05 m/s

Run	Position Errors (1σ) (m)			Velocity Errors (1σ) (m/s)		
	DR	VT	CT	DR	VT	CT
1.0	815	144	1487	0.0050	0.0036	0.0091
1.1	1241	462	4360	0.0058	0.0055	0.0280
1.2	11097§	9143	8463-19908*	0.0467§	0.0825	0.0510-0.1203*
1.3	879	301	1438	0.0053	0.0048	0.0092
1.4	792	134	1190	0.0049	0.0035	0.0076
1.5	835	172	1443	0.0051	0.0038	0.0089
1.6	1818	375	8409-19002*	0.0084	0.0046	0.0508-0.1147*
1.7	834	235	8477-20065*	0.0052	0.0041	0.0511-0.1214*
1.8	861	226	8477-20065*	0.0053	0.0041	0.0511-0.1214*
1.9	867	227	6653§	0.0053	0.0041	0.0467§
1.10	859	221	4674§	0.0053	0.0040	0.0299§
1.11 £	1018	149	1974	0.0056	0.0040	0.0110
1.12 £	2803	165	3695	0.0107	0.0080	0.0247
1.13 £	1484	478	5199	0.0064	0.0059	0.0297
1.14	727	139	1402	0.0049	0.0036	0.0094
1.15	815	144	1487	0.0049	0.0036	0.0091
1.16	659	24	546	0.0042	0.0022	0.0044
1.17	815	143	1477	0.0050	0.0036	0.009
1.18	4078	2757	8367-15977*	0.0194	0.0253	0.0507-0.0963*
1.19	4958	198	3823	0.0376	0.0181	0.0369
1.20 †	18816,820	40102,144	2080	0.0414,0.0051	0.3613,0.0036	0.0122

* - Oscillatory: range is indicated
§ - Damped oscillatory: final value indicated
£ - Propulsive maneuvers: lower bound indicated
† - Other: maximum, steady state indicated

The Baseline (1.0)

Figure 4.2 is the time history of the position and velocity errors over the 28 day period. As we can see from this figure, the position and velocity errors are reduced to the near steady state values after about five days. After examining the baseline case (1.0) we see that after one lunar cycle, the position errors are in the 200-1500 meter range. These represent more than an order of magnitude reduction from the initial errors of 20 kilometers. Likewise for the velocity errors, we have about an order of magnitude reduction from 0.05 m/s to the 0.004-0.01 m/s range. The vertical uncertainties are so small due to the fact that we are taking range measurements, and are getting mostly vertical information. The downrange motion is coupled to the vertical which results in it having the next to smallest uncertainties. The crosstrack is the out-of-plane component and is mostly uncoupled from the vertical and downrange directions. The crosstrack has the largest uncertainties due to this lack of coupling and measurement information. This demonstrates significant system performance over a relatively short time frame.

4.1.1 Measurement Type Variations

The first set of variations involved the measurement system type. Cases 1.1 and 1.2 are the cases for the one-way range and Doppler systems respectively.

One-Way Ranging (1.1)

Figure A.2 in Appendix A shows the time history of this case. When compared to the baseline, the one-way ranging system did rather well. After five days of station-keeping, one-way ranging reduced the position errors to within a few hundred meters of the baseline, in the downrange and vertical channels. Likewise the velocity errors were reduced to within a few hundredths of a meter per second of the baseline in the same two channels. The one-way range system did not fair as well as the baseline in the crosstrack error components. The crosstrack components represent the out-of-plane direction in the Earth-Moon-Lpoint system. In the equations of motion, there is little coupling between the in-plane and out-of-plane components (none for the linear analysis), but the two in-plane components are significantly coupled. All of the measurement types considered here provide information primarily to the vertical direction. Through the in-plane dynamic coupling, we can infer downrange information from this abundance of vertical information, as the correlations build up, . The downrange and crosstrack channels get information on their own due to the geometry of the navigation aids.

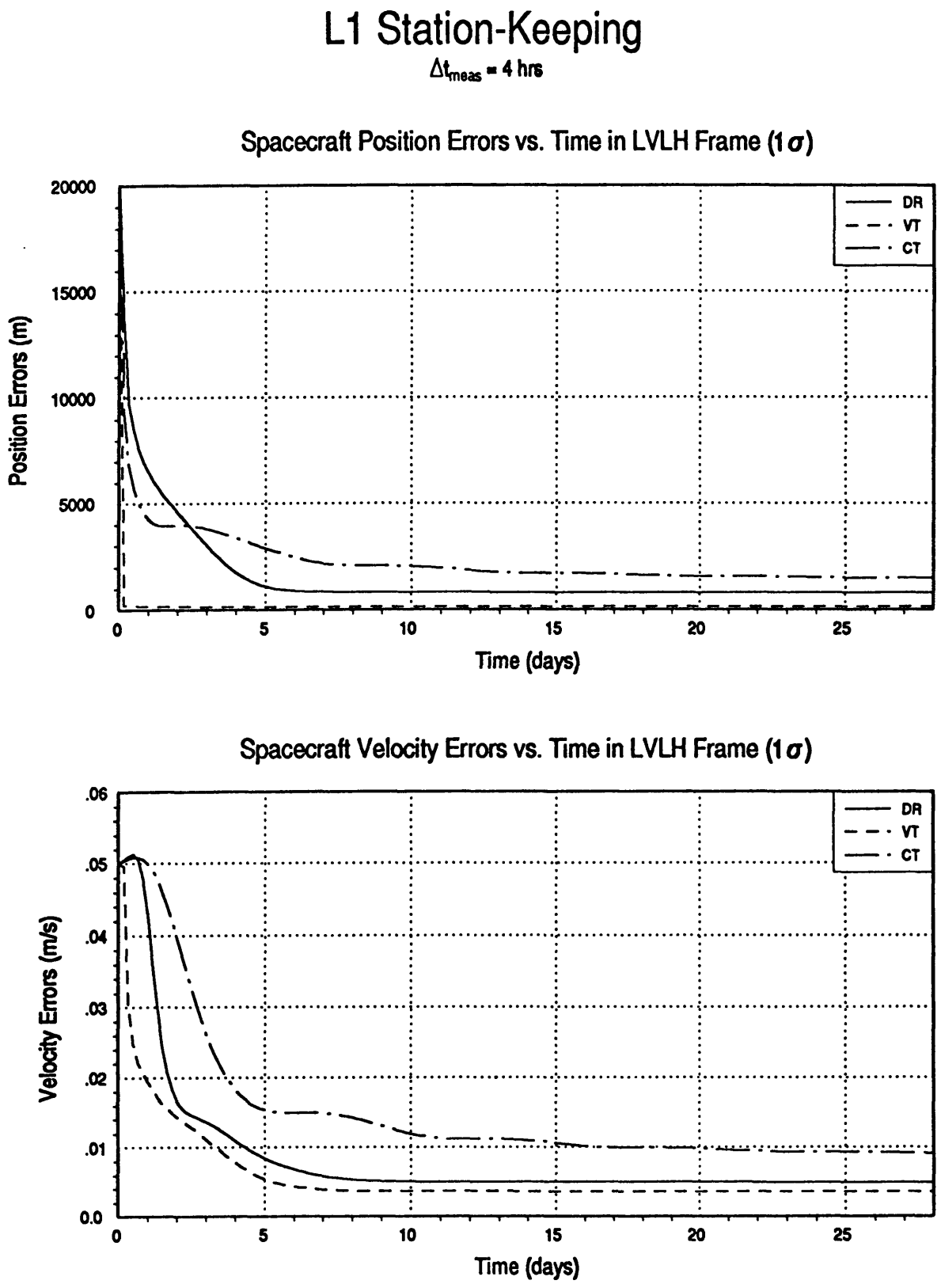

Figure 4.2 : L1 Station-keeping Baseline (Case 1.0)

For the baseline two-way ranging case, the crosstrack channel is getting sufficient information on its own to reduce the errors. For the one-way ranging case, although the measurement geometry is the same, the measurement accuracy is less resulting in a significant degradation in the crosstrack channel navigation performance. After 28 days, the resulting errors in the crosstrack direction are thousands of meters off the baseline in position and tenths of meters per second off in velocity. In spite of the decreased performance, these are still quite adequate position and velocity uncertainties for many applications.

Doppler (1.2)

Doppler measurement systems have a much more difficult time than the one or two-way ranging systems in reducing the position and velocity errors. Figure A.3 in Appendix A shows the time history of this case. Again as with the one-way range system, the Doppler system had difficulty in estimating the crosstrack position and velocity. The value for the crosstrack position oscillates in the 8 to 20 kilometer range with no signs of damping. The crosstrack velocity oscillates in the 0.05-0.12 m/s range also with no signs of damping. The downrange position and velocity components do oscillate, but seem to diminish toward a steady state of about 11 km over the 28 day period. The vertical channel, which is getting most of the information does considerably better. The position uncertainties decrease to a steady state of about 9 kilometers although the velocity uncertainties increase to a steady state of about 0.08 m/s. The Doppler system, although certainly not a replacement for one or two-way ranging, does provides a marginal level of performance.

4.1.2 Navigation Infrastructure Variations

The next set of variations involved changing the configuration of the navigation infrastructure. There variations in the system configuration involve changing the number of NavSites and/or NavSat, their locations, etc. Several variations were run to analyze the significance of the platform geometry, and the advantages of NavSats vs. NavSites.

The NavSat (1.3)

The first variation on the navigation infrastructure involved replacing the three NavSite system with a single NavSat. Figure A.4 in Appendix A shows the time history of this case. The NavSat was placed in a 5000 kilometer circular orbit, which resulting in an orbital period of about 8.8 hours. The orbit was inclined at 45° to accomplish the

maximum measurement geometry for the in-plane and out-of-plane components. The NavSat performance was almost equal to that of the baseline system. There is only nominal difference in the downrange and crosstrack channels, and the vertical channel performs marginally poorer than the baseline. Although the steady state values at 28 days vary little, the baseline system does converge to the steady state values somewhat faster in some channels. The NavSat provides excellent geometry with its large orbital radius and 45° inclination. In addition the orbit plane of the NavSat is inertially fixed and rotates once per 28 days in the Earth-Moon-Lpoint coordinate system. Due to the high orbital altitude, there is also very little occultation of the NavSat by the Moon. The NavSat provides nearly continuous coverage over the 28 day period. Clearly, the NavSat is a very viable alternative to Moon-based NavSites.

Three NavSites and a NavSat (1.4)

This case was run to confirm the performance of the baseline. Figure A.5 in Appendix A shows the time history of this case. Essentially, two systems with equal performance were combined to form a presumably "better" system. As can bee seen from the data in Table 4.1 the system performance was only slightly better than the nominal. By studying Figures A.1 and A.5 in Appendix A, we can also see that the time histories are almost identical.

Two Lunar NavSites (1.5)

Noting that adding to the baseline didn't improve the system performance appreciably, the next logical step was subtracting from it. Relying on the coupling of the downrange and vertical channels, the decision was to go with a system comprised of two NavSites along a single line of longitude. Figure A.6 in Appendix A shows the time history of this case. The NavSites were placed at ± 75° along the 0° line of relative longitude from the sub-libration point. Figure 4.3 Shows the NavSite configuration. Representing a larger North to South footprint than the nominal, this system produced slightly increased navigation performance (about 50 m) in the crosstrack direction. There were marginal increases in the downrange and vertical uncertainties on the order of 15-30 meters, but these are insignificant. The only significant variation from the baseline was the convergence rate of the downrange components. This is due to the fact that the downrange is being inferred from the vertical rather than being directly measured, being that there is no component of the measurement geometry vector in the downrange direction.

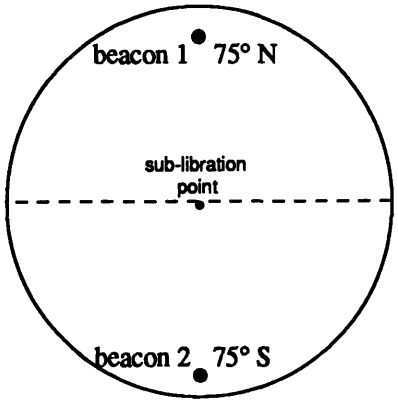

Figure 4.3 : Two NavSite Configuration (Case 1.5)

Single Lunar NavSites (1.6-1.8)

With the success of the two NavSite systems, single NavSite systems were next in line to be studied. Three single NavSite configurations were analyzed in Cases 1.6-1.8. Figures A.7-A.9 in Appendix A shows the time histories of these cases. The NavSite configuration for each are presented in Figure 4.4 below.

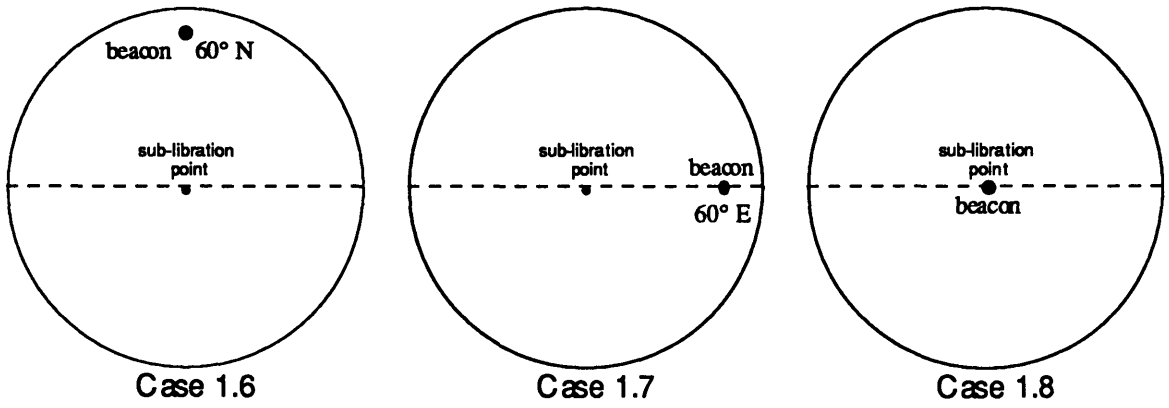

Figure 4.4 : Single NavSite Configurations (Cases 1.6-1.8)

The configurations with the NavSite 60°E of and directly at the sub-libration (1.7 and 1.8) resulted in uncertainties within 100 meters of baseline in the downrange and vertical directions. The configuration with the NavSite 60°N of the sub-libration point (1.6) did not do as well, with these two channels having uncertainties about double the baseline. All three of the configurations had no success in reducing the crosstrack (out-of-plane) position and velocity uncertainties. Although the crosstrack components oscillated and did not shrink, they did not appear to grow either. This indicates that should you be

able to reduce the crosstrack uncertainties initially, they will not grow again. This is consistent with linear analysis of the equations of motion which indicates that the out-of-plane component is oscillatory and "stable". Single NavSite configurations do estimate the in-plane uncertainties reasonably well, but may need augmentation in the out-of-plane components depending on the mission requirements.

Earth NavSites (1.9-1.10)

The last variation of the navigation infrastructure concerns the location of the NavSites. Because of the power availability, easy maintenance and low emplacement costs, the idea of using Earth-based NavSites to perform libration point navigation is appealing. Two cases with three Earth based NavSites were run.

The first case consisted of three NavSites on the equator, 120° apart (Case 1.9). Due to the fact that the Earth is inclined between 18.28-28.58° to the Moon's orbital plane, and the fact that the Earth rotates relative to the Earth-Moon-Lpoint frame, this configuration does supply some geometry in all directions. Although the relative locations of the NavSites change as the Earth rotates providing better measurement geometry, the spacecraft also loses sight of the NavSites as the Earth rotates them out of view.

The second case consisted of one NavSite 30° North, one on the equator, and one 30° South, all 120° apart (Case 1.10). Figures A.10-A.11 in Appendix A shows the time histories of these cases. Both of these configurations reduced the downrange and vertical position and velocity errors to levels slightly worse than the baseline. In the crosstrack direction, they both showed results similar to the one-way ranging case (1.1) with Case 1.10 performing slightly better because of its superior geometry.

4.1.3 Burn Modeling Variations

Another very important effect to understand is that of propulsive maneuvers on the navigation system. In Chapter 3 we concluded that a burn magnitude of about 0.04 m/s at 5 day intervals would adequately model station-keeping burns. This model was implemented for both baseline (two-way ranging) and one-way ranging systems (Cases 1.11,1.13). A case was also run for an increased burn frequency to evaluate the effects on the navigation (1.12). Figure 4.5 shows the time history for the two-way range 5 day frequency case (1.11). Figures A.13-A.14 in Appendix A shows the time histories for the other two cases. Both Case 1.11 and 1.13 have position and velocity uncertainties approaching the baseline in the downrange and vertical channels.

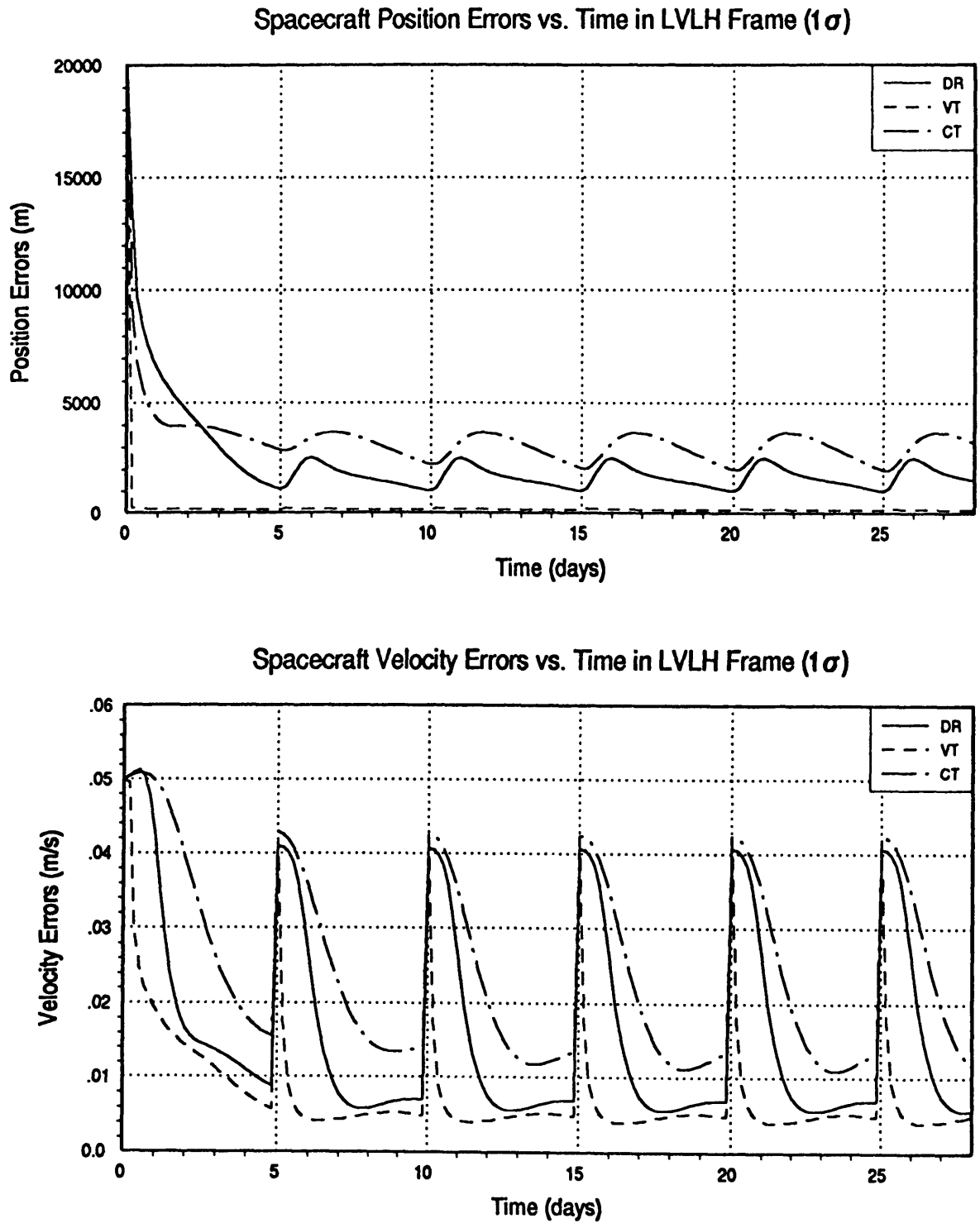

Figure 4.5 : L1 Station-keeping with Burns (Case 1.11)

The crosstrack components are somewhat larger than the baseline numbers primarily because of the slower dynamics in this component. The crosstrack channel does not respond as quickly as the other two, and does not have time to decrease sufficiently between burns. When the burn frequency is increased, all of the downrange and the crosstrack components remain significantly higher than the nominal. The vertical channel seems to respond quickly enough to the burns, but the other two axes' uncertainties remain elevated, not having enough time to decrease significantly between burns.

4.1.4 Environmental Perturbation Variations

From the analysis of environmental perturbations in Section 2.4, three perturbations warranted further study. Earth-Moon eccentricity effects, Solar disturbing forces and Solar radiation pressure. Two of these, eccentricity and Solar effects can be modeled directly by either reflecting the changing gravity gradient as in the eccentric case (Case 1.14), or by adding to the gravity gradient as with the Solar perturbation case (Case 1.15).

Earth-Moon Eccentricity (1.14)

For the Earth-Moon eccentricity case, almost no change in either the time history of the steady state values of the position and velocity uncertainties was evident. Figure A.15 in Appendix A shows the time histories for this case. There was a slight increase in navigation performance in the downrange channel (about 90 m steady state position) and even less in the other two channels. Over all, the eccentricity has very little effect on the navigation. For the eccentric case, the geometry angles have not changed, but the range to the NavSites has. This range change is about ±5% of the nominal circular range and therefore does not affect the measurement accuracy significantly.

Solar Disturbing Effects (1.15)

Even more so than the eccentric case, the addition of the Solar gravity gradient to the navigation is almost unnoticeable except for a 0.00001 m/s variation in the downrange velocity uncertainty. This is totally insignificant and indicates that the Solar gravity gradient has no appreciable effect on the navigation. Figures A.16 in Appendix A shows the time histories for this case.

4.1.5 Measurement Specification Variations

Certain instrument specifications were varied to test the sensitivity of the navigation to them.

Decreased 2-way Ranging Measurement Noise (1.16)

Case 1.16 represents a two-way ranging system with a measurement noise of 0.7 meters per 1000 kilometers. Figure A.17 in Appendix A shows the time histories for this case. This represents an order of magnitude accuracy improvement from the nominal instrument specifications, but still within reason[14]. All three components showed significant reduction in position and velocity uncertainties from the baseline. The rate of convergence of the system was much quicker, converging to steady state values in about 2 days as opposed to 5 for the baseline. This is not particularly surprising since measurement noise is usually a significant driver in the navigation system.

Decreased 2-way Range Bias (1.17)

Case 1.17 represents a two-way ranging system with a range bias of 2 meters. Figures A.18 in Appendix A shows the time histories for this case. This is an order of magnitude below the nominal instrument specifications. This reduction in the range bias produced very little effect. All values were within the 1% of the baseline. This would support the conclusion that the measurement noise is the system driver and outweighs the effects of the range bias.

Increased 1-way Range Rate Bias (1.18)

Case 1.18 represented a one-way ranging system with a range rate bias of 0.03 meters per second. Figure A.19 in Appendix A shows the time histories for this case. This is an order of magnitude above the nominal instrument range rate bias and implies a much less accurate spacecraft clock. This decrease in clock accuracy results in much higher steady state position and velocity uncertainties in the downrange and vertical directions (300%+ increase). The crosstrack position and velocity exhibited the same oscillation which was prevalent in the single NavSite cases. This demonstrates that the clock accuracy is a crucial system driver for the one-way ranging case.

---

[14] Konop, P., Range Measurement Accuracy

4.1.6 Miscellaneous Variations

There were two remaining cases for the L1 station-keeping mission which were of interest.

Increased Process Noise (1.19)

The third environmental perturbation unaccounted for above is Solar radiation pressure. A case was run with increased process noise to account for unmodeled Solar radiation pressure, unmodeled second-order disturbing accelerations and other unmodeled effects. The process noise was increased to $1x10^{-8}$ m^2/sec^3. This results in an effective "acceleration" due to noise of about $8x10^{-7}$ m/sec^2 (see Section 2.4.2 for more explanation of effective acceleration due to noise). This is on the order of the largest perturbations of the system (see figure 2.9). Figure A.20 in Appendix A shows the time histories for this case. This resulted in higher steady state values for all of the position and velocity uncertainties. The position uncertainties were still reasonable however with the downrange and vertical on the order of 4-5 kilometers. The vertical components seemed little effected by the increase in process noise with values still close to the baseline. The convergence to steady ate for this case was somewhat quicker than the baseline case.

NavSite Illumination(1.20)

The last case of interest involved consideration of the illumination of the NavSites by the Sun. For Lunar NavSites, battery reserves would not last for long in the 14 day Lunar night. For this case the NavSites were assumed to have no power when not directly illuminated by the Sun. Figure A.21 in Appendix A shows the time histories for this case. The 3 NavSites starts out fully "lit" and around 14 days begins to experience a period of about 5-6 days of total blackout. As expected the downrange and vertical errors grow during this time. As discussed before, once the crosstrack errors are driven down, they do not grow even during complete blackout of the system. The downrange and vertical position errors peak at about 19 and 40 km respectively and the velocities peak at about 0.36 and 0.04 m/s. After regaining even a single beacon, the errors are driven down to near steady state values almost instantaneously. These steady state values are fairly close to the nominal baseline values.

4.2 L2 Station-keeping

The results of the baseline and variational runs for the L2 Station-keeping mission are presented in Table 4.2. Results from the L1 station-keeping cases should be applicable to the L2 point. Although the dynamics of L2 are not the same as those for L1, they are similar and should produce similar results. For these reasons fewer L2 station-keeping cases were run. A select few were chosen to establish the level of difference between L1 and L2 and to point out the particular applications for the L2 point.

Table 4.2 : L2 Station-keeping Results after 28 days
Initial σ_R=20000 m, σ_V=.05 m/s

Run	Position Errors (1σ) (m)			Velocity Errors (1σ) (m/s)		
	DR	VT	CT	DR	VT	CT
2.0	1057	155	1858	0.0050	0.0041	0.0090
2.1	1735	578	6091§	0.0056	0.0064	0.0308§
2.2	14407§	11571§	10739-20031*	0.0387§	0.0881§	0.0510-0.0954*
2.3	1164	316	1907	0.0052	0.0051	0.0103
2.4	1007	152	1764	0.0045	0.0044	0.0092
2.5	1235	391	6510§	0.0056	0.0060	0.0265-0.0487*

* - Oscillatory: range is indicated
§ - Damped oscillatory: final value indicated

The Baseline (2.0)

After examining the baseline case we see that over the 28 day period, the L2 station-keeping performance is very similar to the L1 station-keeping performance. Figure 4.6 is the time history of the position and velocity errors over the 28 day period. The steady state DR, VT and CT position uncertainties for the L1 and L2 baselines are shown in Table 4.3 below.

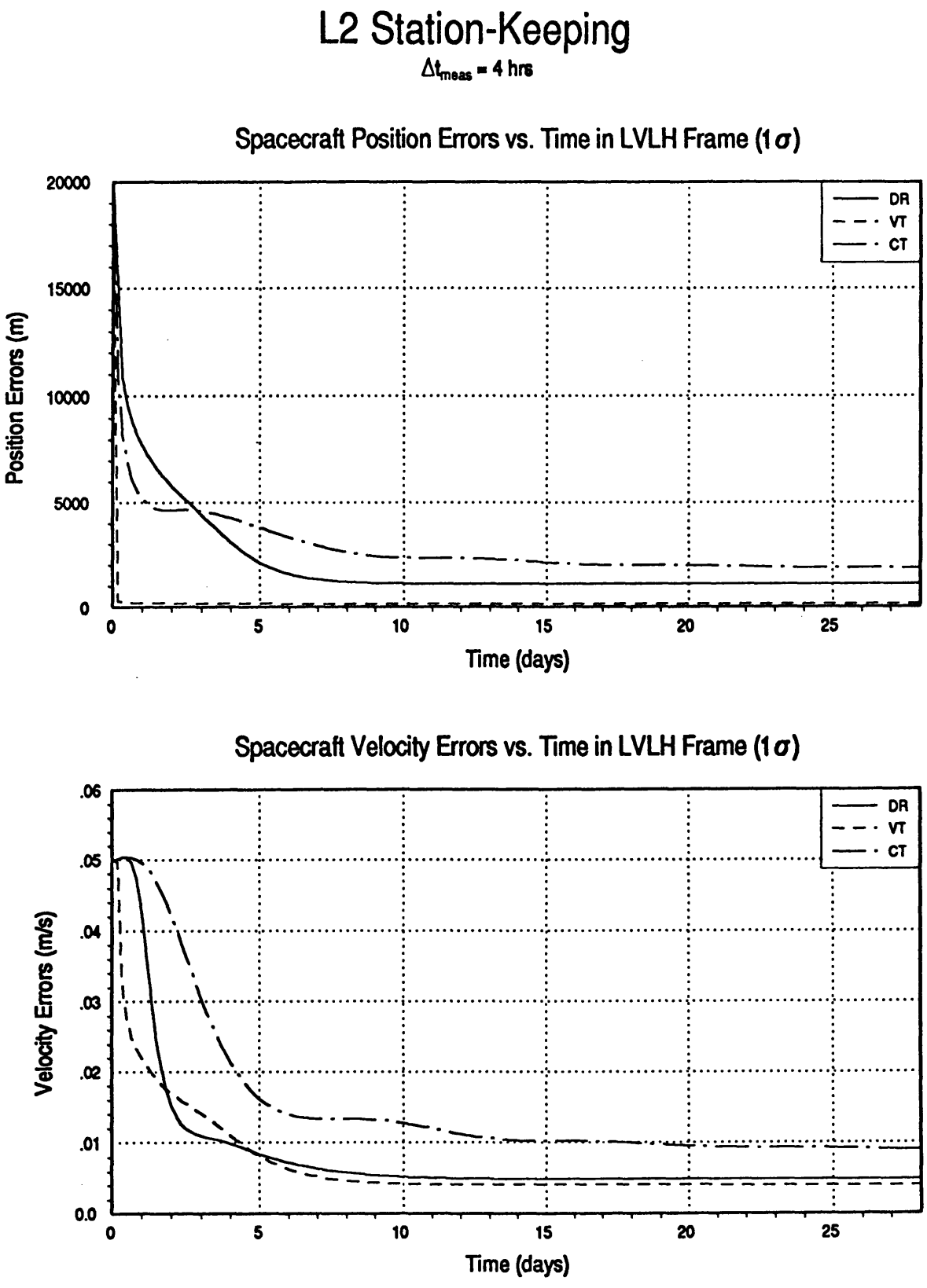

Figure 4.6 : L2 Station-keeping Baseline (Case 2.0)

Table 4.3 : L1 & L2 Baseline Station-keeping Results after 28 days
Initial σ_R=20000 m, σ_V=.05 m/s

Run	Position Errors (1σ) (m)			Velocity Errors (1σ) (m/s)		
	DR	VT	CT	DR	VT	CT
1.0	815	144	1487	0.0050	0.0036	0.0091
2.0	1057	155	1858	0.0050	0.0041	0.0090

While these do differ, they are still very close when considering that both systems started from the initial position and velocity uncertainties of 20 kilometers and 0.05 meters/second. When comparing the time histories (Figures 4.1 and 4.6) , we see that the behavior of the systems is very comparable. The difference in the magnitudes of the uncertainties is due to differences in the dynamics of the two points. Although the L2 point results in larger position uncertainties than L1, the velocity uncertainties are somewhat smaller. Again this indicates a slightly different dynamic characteristic.

4.2.1 Navigation Infrastructure Variations

Cases 2.1-2.3 involve varying the navigation infrastructure to one-way ranging, Doppler, and a two-way range NavSat respectively. Again these give similar results when compared to the analogous L1 variations (1.1-1.3). Figures A.23 - A.25 in Appendix A shows the time histories for these cases. One case which more clearly demonstrates the dynamic differences between the two points is the Doppler case (2.2). Figure 4.7 shows the time histories for the Doppler systems at L1 (Case 1.2) and L2 (Case 2.2). Although the dynamics are similar, it is evident that they have different periods. The L1 Doppler results exhibits a period of about 5 days whereas the L2 results exhibit a near 7 day period.

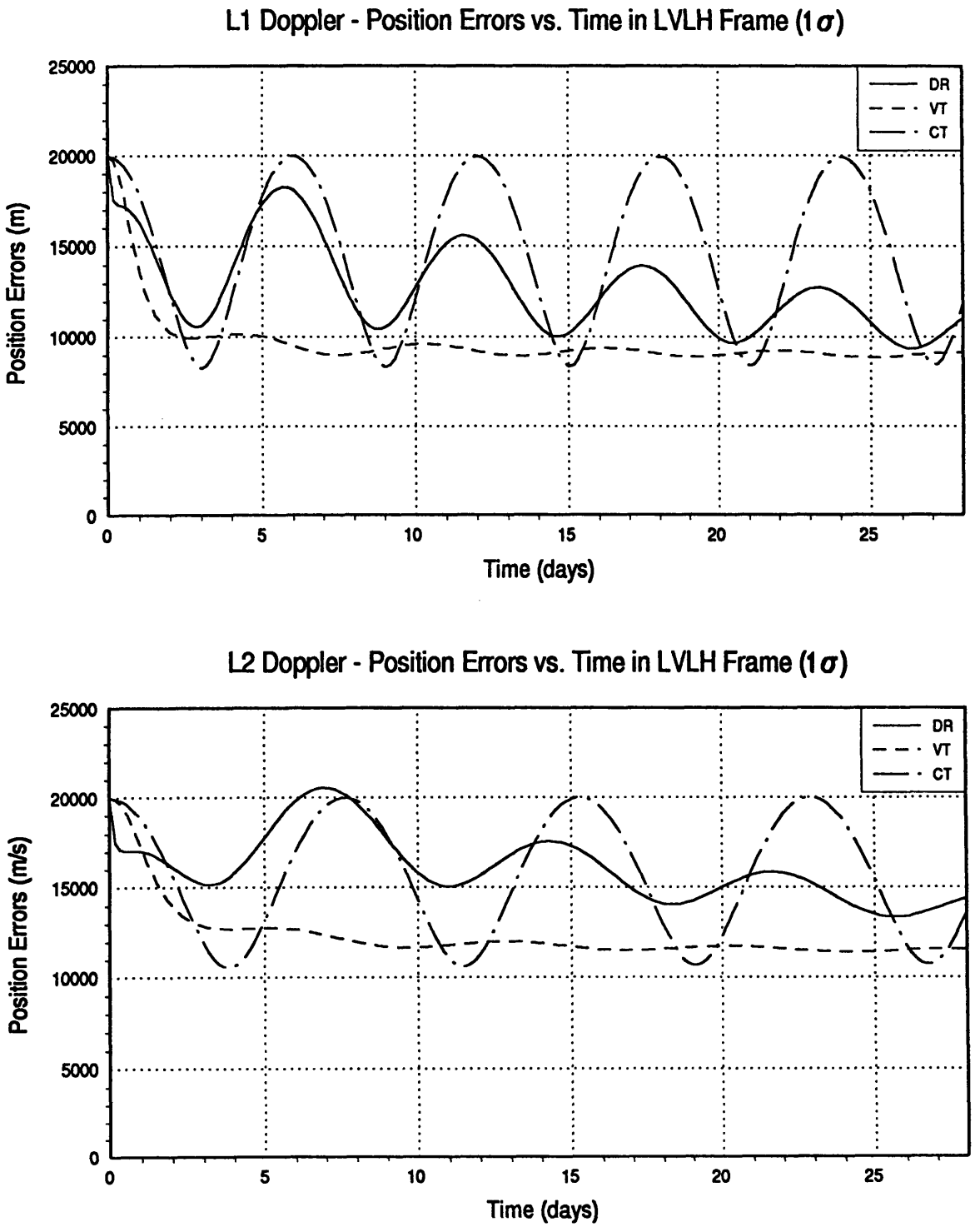

Figure 4.7 : L1 & L2 Doppler System Comparison (Cases 1.2, 2.2)

4.2.2 Lissajous Variations

Cases 2.4 and 2.5 are variations of particular interest for the L2 point. In both of these variations, the spacecraft is in a lissajous figure with an in-plane amplitude of around 9000 km and an out-of-plane amplitude of around 3000 kilometers. Figure 4.8 shows the lissajous figure used for both of these cases. Figures A.25 - A.27 in Appendix A shows the time histories for these cases.

Lissajous vs. Libration Point

Case 2.4 was done to analyze the differences between navigation performance in a lissajous or halo orbit versus sitting at the libration point. The results of this case were very similar to the baseline case. The time histories showed the same trends, and the position and velocity uncertainties were within several hundred meters and several hundredths of meters per second respectively. The lissajous navigation did not do quite as well as the baseline which is somewhat surprising considering the much larger geometry it has. This may be due to variations in the dynamics as we move further from the nominal libration point.

Earth NavSites from the Lissajous

Case 2.5 was run to investigate the use of Earth-based navigation aids at L2. Since the L2 point is on the far side of the Moon, it is never visible from the Earth. When we are in the lissajous figure, the Earth is visible at all times, allowing us to use Earth-based NavSites. This case is analogous to Case 1.9 which is the L1 Earth NavSite case. The NavSites are placed 120° apart on the Earth's equator. When comparing the L1 and L2 lissajous results we again see close correlation. The L2 uncertainties are slightly larger which can be explained due to an increase of about 120,000 kilometers in the range to the Earth which decreases the measurement geometry. The range measurement noise is about the same for Earth-based and Moon-based NavSites and is basically the same at any range if the NavSite can be acquired. Some of the performance differences between L1 and L2 is the result of the libration point dynamics differences.

L2 Lissajous Figure

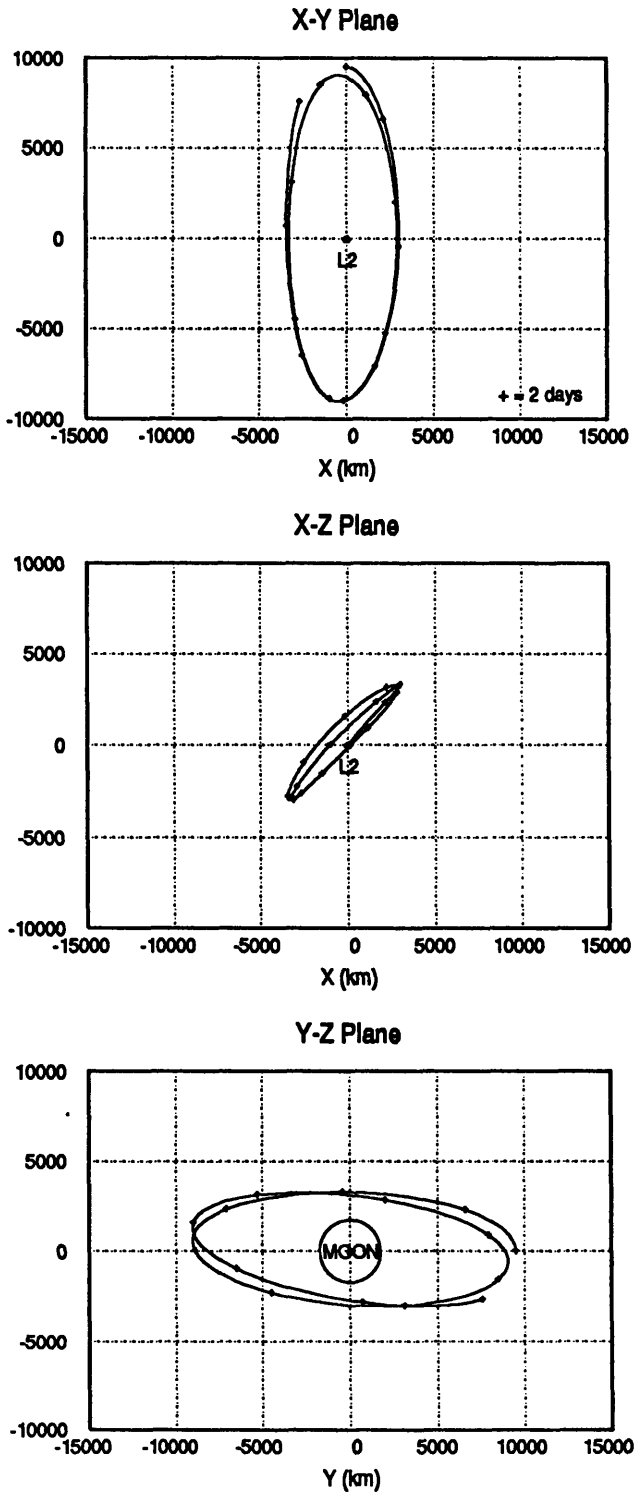

Figure 4.8 : L2 Lissajous Figure (Cases 2.4-2.5)

4.3 L1 & L2 to Lunar Transfers

The results of the baseline and variational runs for the L1 and L2 to Lunar transfer missions are presented in Table 4.4. For the transfer to the Moon the results are presented somewhat differently. The covariance is propagated to periapse at each time step using a two body transformation matrix[15]. At periapse, the periapse altitude (H_p) and crosstrack position and velocity are the components we are interested in. For all of the cases with the exception of the NavSat case, the beacon triad is on the half of the Moon facing the initial Lpoint, just as in the station-keeping baselines. The spacecraft will lose sight of the beacons as it passes around the Moon, injecting at periapse on the other side.

Table 4.4 : L1 & L2 to Lunar Transfer Results

Run	Position Errors (1σ) (m)		Velocity Errors (1σ) (m/s)
	H_p	CT	CT
3.0	95.1	85.8	0.118
3.1	182.2	375.9	0.420
3.2	667.8	770.7	1.815
3.3	142.7	92.9	0.119
3.4	53.4	45.3	0.066
5.0	60.4	51.9	0.071

The Baselines (3.0,5.0)

As can be seen from the data in Table 4.4 the performance for the transfers down to the Moon from both libration points results in very small altitude and crosstrack position and velocity errors at periapse. Figure 4.9 is the time history of the uncertainties for the L1 to Moon baseline from 10 hours prior to periapse. You will note some discontinuities in the curves around 18.5 and 23 hours. These occur as the spacecraft loses each beacon as it passes around the far side.

---

[15] Shepperd, S.W. , Universal Keplarian State Transition Matrix

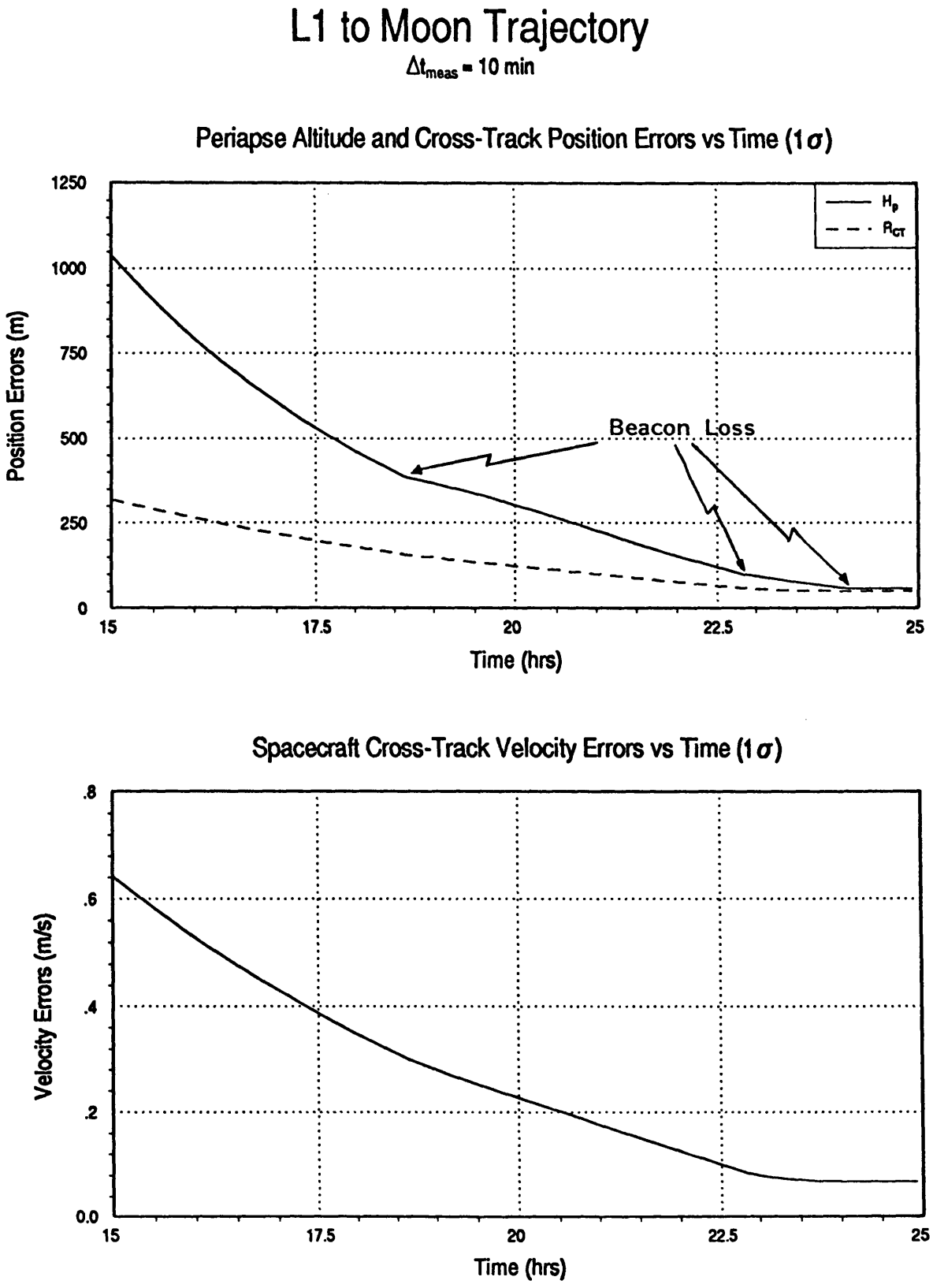

Figure 4.9 : L1 to Moon Transfer Baseline (Case 3.0)

The result is a more shallow slope due to the decrease in measurement information. Figure A.37 in Appendix A shows the time histories for the L2 to Moon case.

The most important consideration in all of the transfers down to the Moon is the level of periapse altitude uncertainty. In other words, at what point is the uncertainty down to a sufficient level such that corrective maneuvers become feasible.

4.3.1 Measurement Type Variations

One-way Range (3.1)

The one-way range case produces somewhat degraded performance relative to the baseline. The periapse altitude uncertainty doubles and the crosstrack uncertainty more than triples. Even taking this into consideration, the uncertainties are still very reasonable for orbital insertion at periapse. This system would still be more than adequate for most applications. Figure A.29 in Appendix A shows the uncertainties' time histories for this case.

Doppler (3.2)

The results for the Doppler case represent an appreciable step down from the baseline. The periapse altitude uncertainty and the crosstrack uncertainties increase by an order of magnitude. As seen from the time histories (Figure A.30 in Appendix A), the convergence rate for the periapse altitude decrease quite significantly after each beacon is lost. The performance does improve as the craft approaches periapse. The uncertainties at periapse that the Doppler system provides would be adequate for injection, but as mentioned, we are concerned with the smallest uncertainties as early as possible. The Doppler system does not provide the small uncertainties as early on as the ranging systems and is therefore at a disadvantage.

4.3.2 Navigation Infrastructure Variations

NavSat (3.3)

For Variation 3.3, a single NavSat is placed in a 5000 km circular polar orbit such that it is overhead when the spacecraft arrives at periapse. Figure 4.10 shows the time history of the uncertainties for this case. The NavSat system suffers in performance when the Moon occults the spacecraft view of the satellite. This occurrence shows up as the plateau in Figure 4.10.

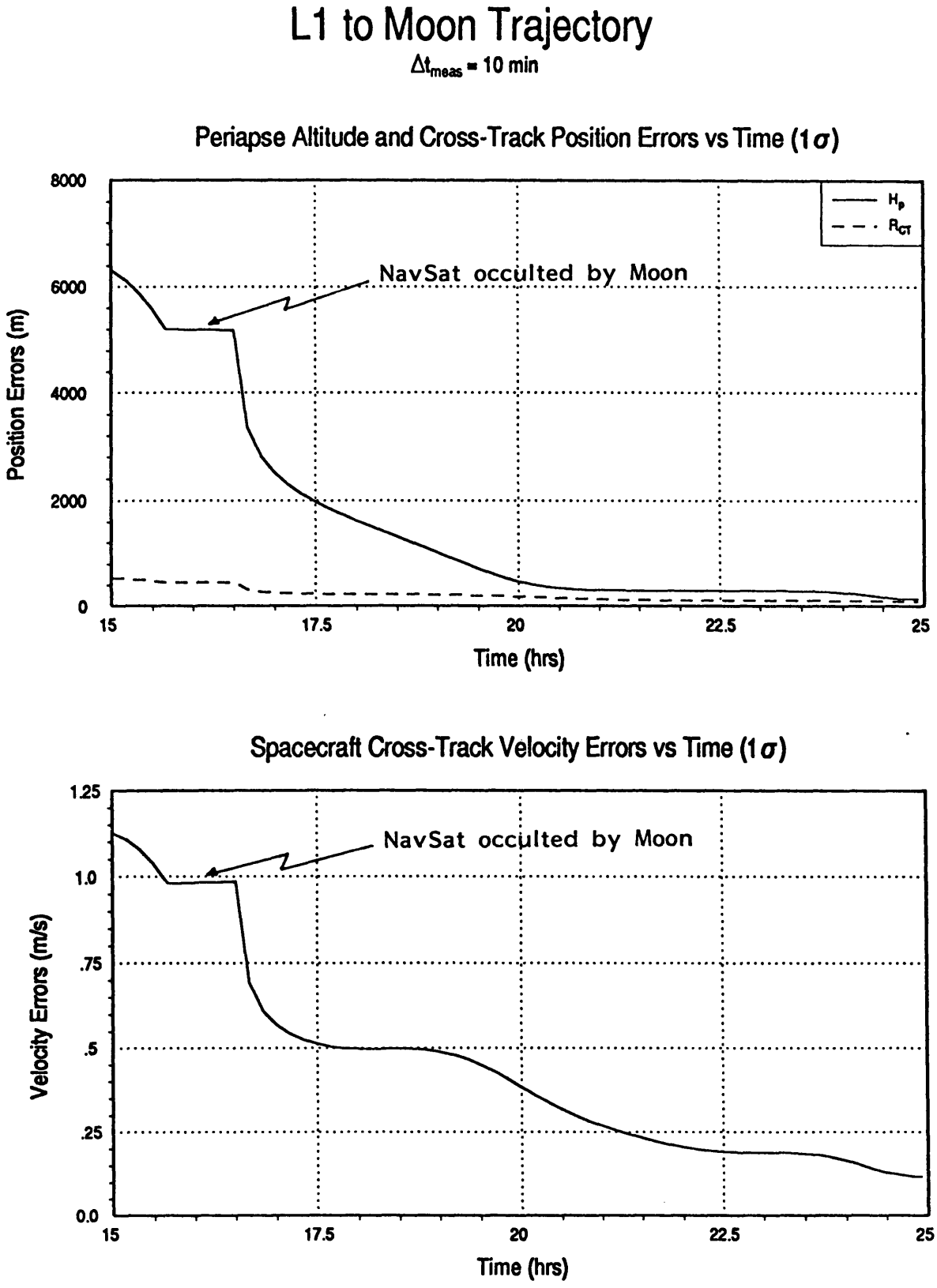

Figure 4.10 : L1 to Moon Transfer - NavSat Case (3.3)

The final uncertainties are quite respectable, outperforming the one-way range system. The rate of convergence is not as good as the one-way range system until the satellite is about 5 hours from periapse at which point the performance surpasses the one-way range system. The NavSat performance is overall quite good, with a somewhat slow convergence rate.

Initializing with Steady State Station-keeping Covariance(3.4)

For Variation 3.4, the baseline configuration was used with the covariance being initialized with the steady state station-keeping covariance. Figure A.32 in Appendix A is the time history of the state uncertainties for this case. This case simulates a spacecraft making the transfer after remaining at the libration point long enough to reach the steady state uncertainties achieved in the L1 station-keeping case (Case 1.0). The velocity error of the propulsive maneuver at the libration point (0.1% of the burn magnitude) is RSS into the steady state covariance which results in approximately the same velocity uncertainty as the baseline. The position uncertainties are less, which results in the system outperforming the baseline overall. The uncertainties at periapse are less, but the convergence rate is roughly the same since the measurement type is the same as the baseline. The system does provide better navigation performance than the baseline. However, the additional time and/or fuel spent station-keeping at the libration point may not be feasible for all missions.

4.4 Lunar to L1 & L2 Transfers

The last set of missions involve the transfers from the Moon. The results of the baseline and variational runs for the Lunar to L1 and L2 transfer missions are presented in Table 4.5. All of the results are presented in the LVLH frame. The NavSites are on the opposite side of the Moon from the spacecraft's initial location. The craft will acquire the beacons as it passes around the other side moving toward the target Lpoint.

Table 4.5 : Lunar to L1 & L2 Transfer Results

Run	Position Errors (1σ) (m)			Velocity Errors (1σ) (m/s)		
	DR	VT	CT	DR	VT	CT
4.0	1479	47	953	0.0107	0.0026	0.0086
4.1	10746	319	13286	0.0754	0.0140	0.0844
4.2	24723	4277	23946	0.1694	0.0664	0.1664
4.3	2591	94	3110	0.0179	0.0038	0.0233
6.0	1590	47	1004	0.0120	0.0026	0.0094

Baselines (4.0, 6.0)

Figure 4.11 is the time history of the Moon to L1 baseline transfer. Figure A.38 in Appendix A is the time history of the Moon to L2 baseline transfer. As seen from the figures, there is large initial growth of all of the uncertainties as the burn errors propagate, unchanged by external updates. The uncertainties are quickly reduced as the spacecraft picks up the beacons as it passes around the other side of the Moon. The beacon acquisitions are evident as shown by the sudden decreases in the uncertainties. Upon comparing the final position and velocity uncertainties on Lpoint approach, we see that the vertical and crosstrack uncertainties are slightly lower than the steady state station-keeping values. The downrange uncertainties were somewhat larger than the station-keeping values, but still quite respectable. It should be noted that the uncertainties grow steadily with increasing distance from the Moon. Although they might initially overshoot the station-keeping uncertainties, the uncertainties will reach the steady state station-keeping values once the spacecraft has injected into the libration point location. The L1 and L2 baselines had nearly identical performance characteristics over the transfer. This indicates that the libration point dynamics have a much smaller role in the transfers from the Moon than to the Moon as would be expected.

4.4.1 Measurement Type Variations

One-way Range and Doppler (4.1, 4.2)

For both the one-way range and Doppler cases, the results were significantly poorer than the baseline. Figures A.34 - A.35 in Appendix A are the time histories for these two cases. The one-way range case had small vertical uncertainties (~300 m) at L1 injection, but the downrange and crosstrack were an order of magnitude worse than the baseline with position uncertainties in the 11-13 kilometer range. The Doppler system was even less successful with the position errors being on the order of 24-25 kilometers in the downrange and crosstrack directions. Although both of these systems represent a significant decrease in performance from the baseline, the uncertainties were of the same relative size as the initial conditions used for the station-keeping cases.

4.4.2 Navigation Infrastructure Variations

NavSat (4.3)

For this case, the NavSat was placed in a 500 kilometer 45° inclined circular orbit. Figure A.36 in Appendix A is the time history for this case. The overall system performance when compared to the baseline was quite good. The uncertainties at L1 injection were around twice the baseline values. These are very viable and demonstrate the NavSat as a viable alternative to ground-based ranging.

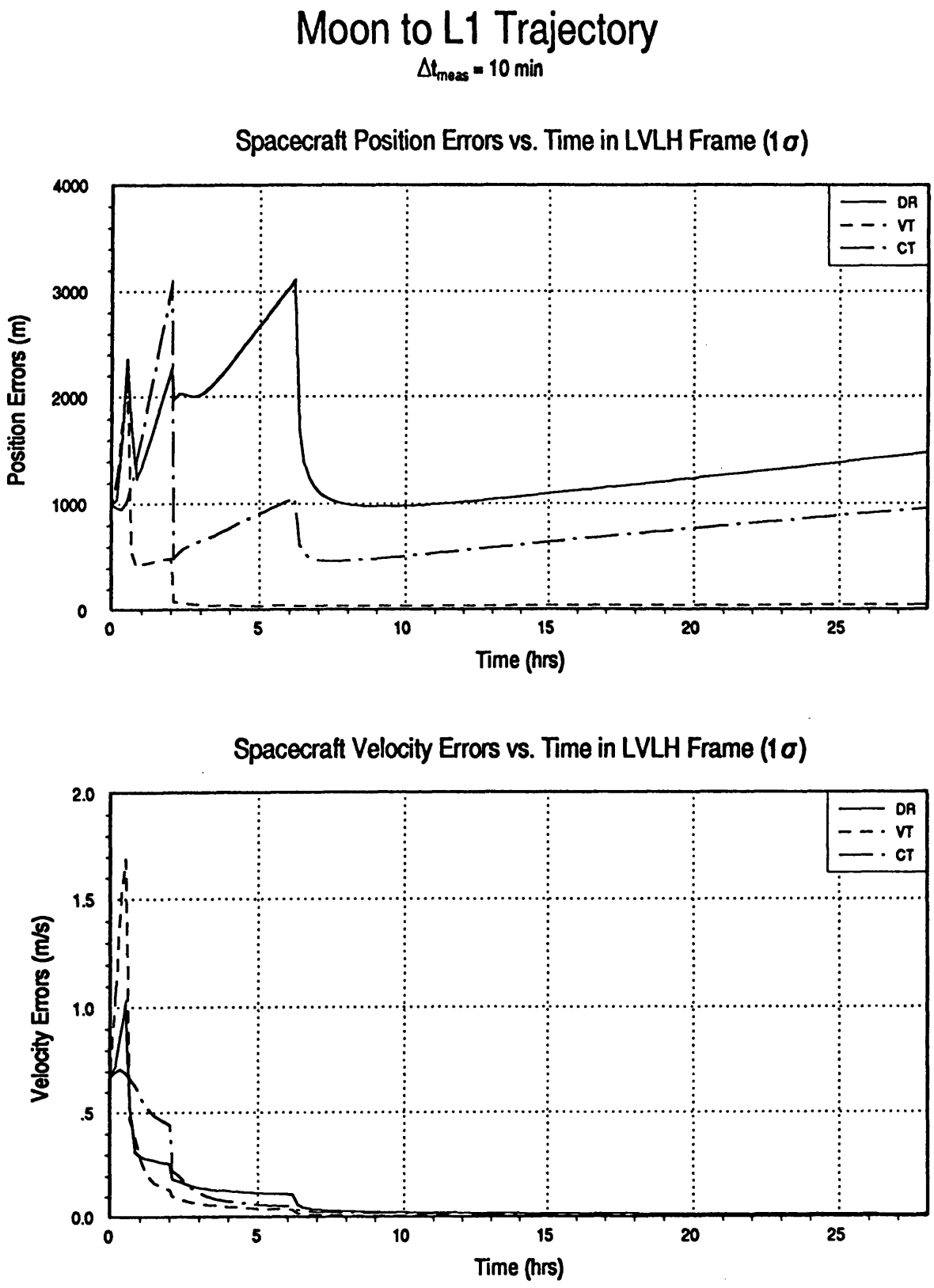

Figure 4.11 : Moon to L1 Transfer Baseline (Case 4.0)

CHAPTER 5
Conclusion

5.1 Summary

The goal of this thesis was to investigate the feasibility of using current radiometric techniques for the navigation of a spacecraft to, from or at Earth-Moon libration points using a local infrastructure. The principle measurement types analyzed were: two-way range, one-way range and Doppler. The navigation infrastructures consisted of Earth and Lunar beacons (NavSites) and a Lunar navigation satellite (NavSat). The effects of the most important perturbations on the satellite's navigation system were investigated including, Earth-Moon eccentricity, Solar radiation pressure and the disturbing effects due to the Sun and the other planets. Three missions were investigated for both the L1 and L2 points: Libration point station-keeping, transfers to the Moon and transfer from the Moon. The baseline for all the missions consisted of three Lunar NavSites using a two-way ranging system. The baseline stationkeeping and Lunar to libration point transfer cases achieved accuracies on the order of 0.2-1.5 km and 0.005-0.01 m/s (LVLH coordinates) for the cases studied. The libration point to Lunar transfer baseline case achieved accuracies on the order of 90 m in periapse altitude and crosstrack directions and 0.1 m/s in crosstrack velocity.

When analyzing the effects of environmental perturbations on the navigation, it was discovered that there were two primary types of effect:

1) Relative Geometry Preserving

2) Relative Geometry Destroying

The Earth-Moon eccentricity and the first-order Sun and planet gravitational perturbing accelerations fall into the first category. Though the absolute system geometry changes, the relative ratios of the Primary-Lpoint and Primary-Primary distances remain the same. If the spacecraft is inserted into "orbit" with initial conditions which take these effects into account, the spacecraft will track the nominal libration point.

Solar radiation pressure and second-order Sun and planet gravitational perturbing accelerations fall into the second category. These effects do not preserve the relative geometry of the system, and therefore force the spacecraft off the nominal libration point.

Again, these effects should be modeled, but proper modeling will not eliminate the need for station-keeping burns. A case was run to approximate the unmodeled effects due to solar radiation pressure. The navigation performance did degrade to the 0.2-4.0 km and 0.02-0.04 m/s uncertainty range, but this is still quite acceptable. Another case was run to ascertain the effects of the second-order gravitational perturbations due to the Sun. This perturbation had no net affect on the navigation performance.

When comparing the measurement types, two-way ranging seems to be the best candidate followed by one-way ranging and Doppler. One-way and two-way ranging have similar performance characteristics with two-way ranging performing somewhat better, particularly in the crosstrack (out-of-plane) component. Doppler is significantly worse than ranging with accuracies in the 10 km and 0.1 m/s range. Both one-way range and Doppler had noticeable trouble in determining the out-of-plane components.

Both double and single NavSite configurations were found to give reasonable navigation performance. For the two NavSite configuration one in-plane component does not converge to the steady state value as fast as the nominal. This is due to the planar geometry of the two NavSite infrastructure. The overall performance is however, very similar to the three NavSite configuration. For the single NavSite configurations the principle degradation of the performance from the two and three NavSite configurations concerned the out-of-plane components which oscillated in the 10-20 km range. The out-of-plane components are typically the first to show loss in performance when the system geometry is diluted. Even so, with additional caution concerning the out-of-plane uncertainties, the single NavSite systems provides very good performance.

In all the missions, the navigation performance was very similar for the L1 and L2 points with slight variation due to the slightly different dynamic nature of each point. Two-way ranging was the clear performer followed by one-way ranging and Doppler. Concerning infrastructure variations, both the NavSat and NavSite configurations produced similar results when using the same measurement type.

The results clearly show that libration point navigation using a real-time autonomous Moon-based infrastructure is viable. No major advances in instrument accuracy are required to achieve reasonable state uncertainties for these missions. Missions requiring high accuracy position and velocity knowledge (i.e., halo orbit stationkeeping) may need higher accuracy measurement systems than those presented here. These levels of navigation performance should be attainable given the results of this study.

5.2 Future Work

This study represents only a preliminary look at the problem. There were no specific requirements for the systems being tested, making evaluation of the performance somewhat difficult. The next step in this research should be an integrated Guidance & Navigation analysis. This would allow the integration of the results presented here with the more widely researched areas of libration point station-keeping and orbit determination. With an integrated G&N system, specific requirements can be formulated to evaluate the system performance. In addition, an integrated system would allow the issues of perturbation modeling and burn handling to be handled in a more thorough way. Other types of measurements should also be investigated (i.e. Optical navigation for libration to LLO missions) to provide a more complete spectrum of navigation alternatives.

APPENDIX A
Graphical Results

L1 Station-Keeping

Δt_{meas} = 4 hrs

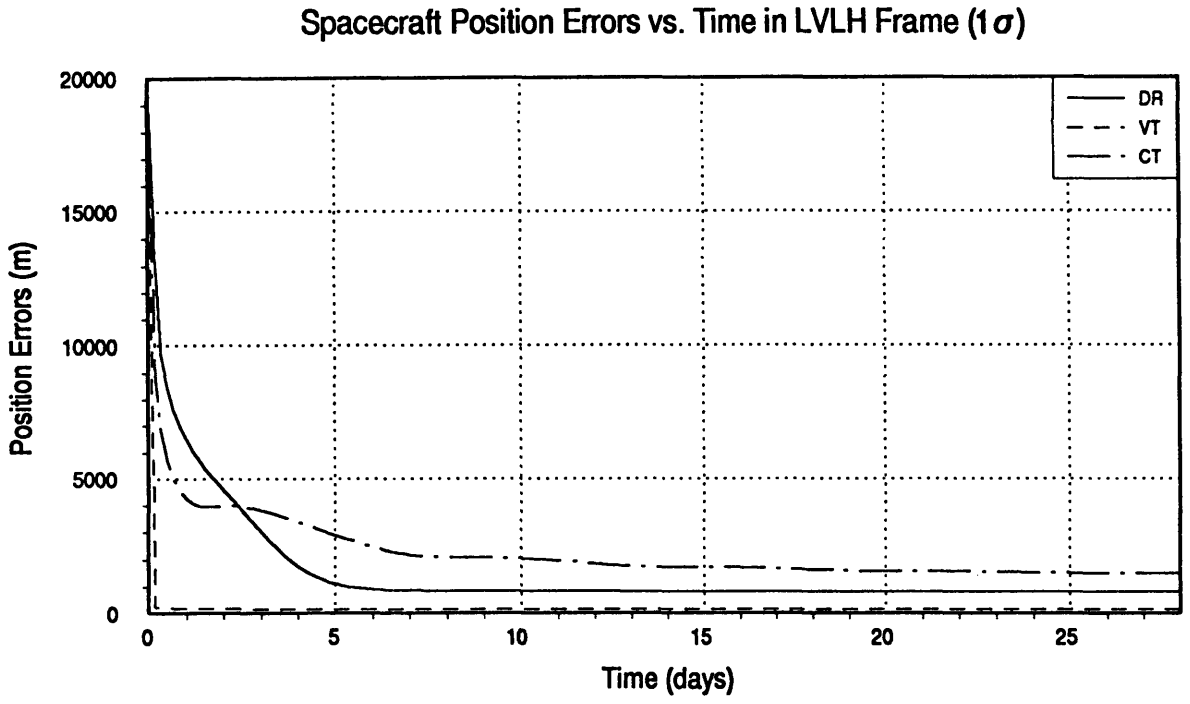

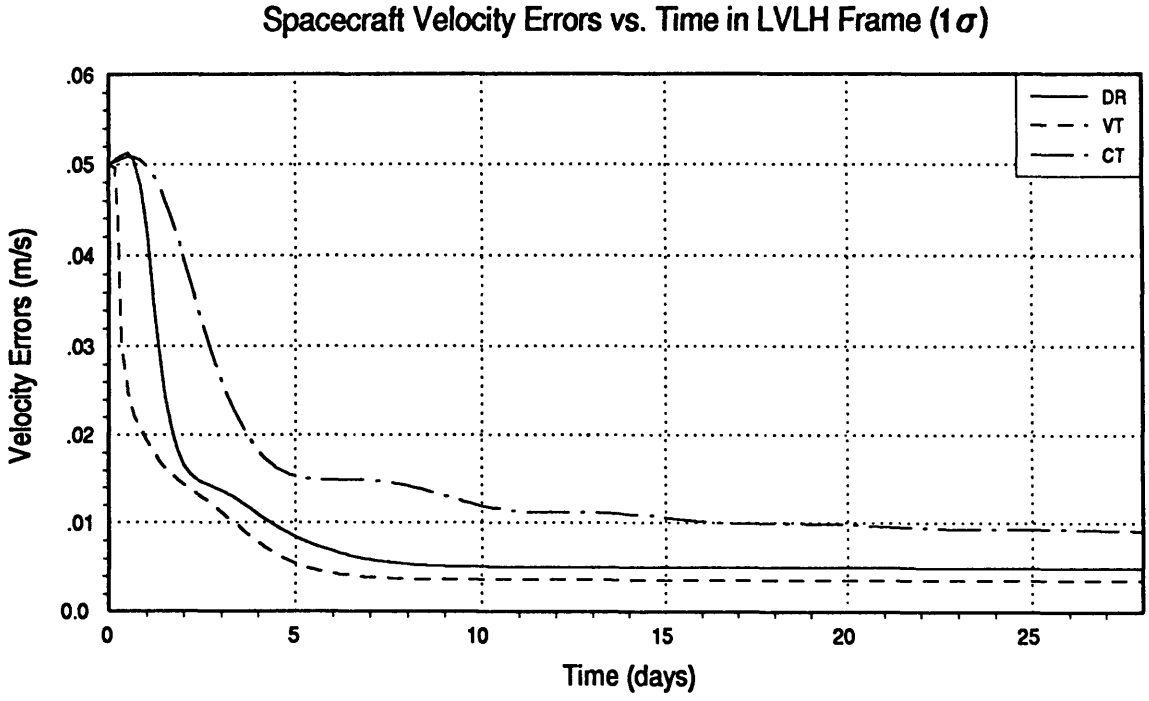

Figure A.1 : Case 1.0

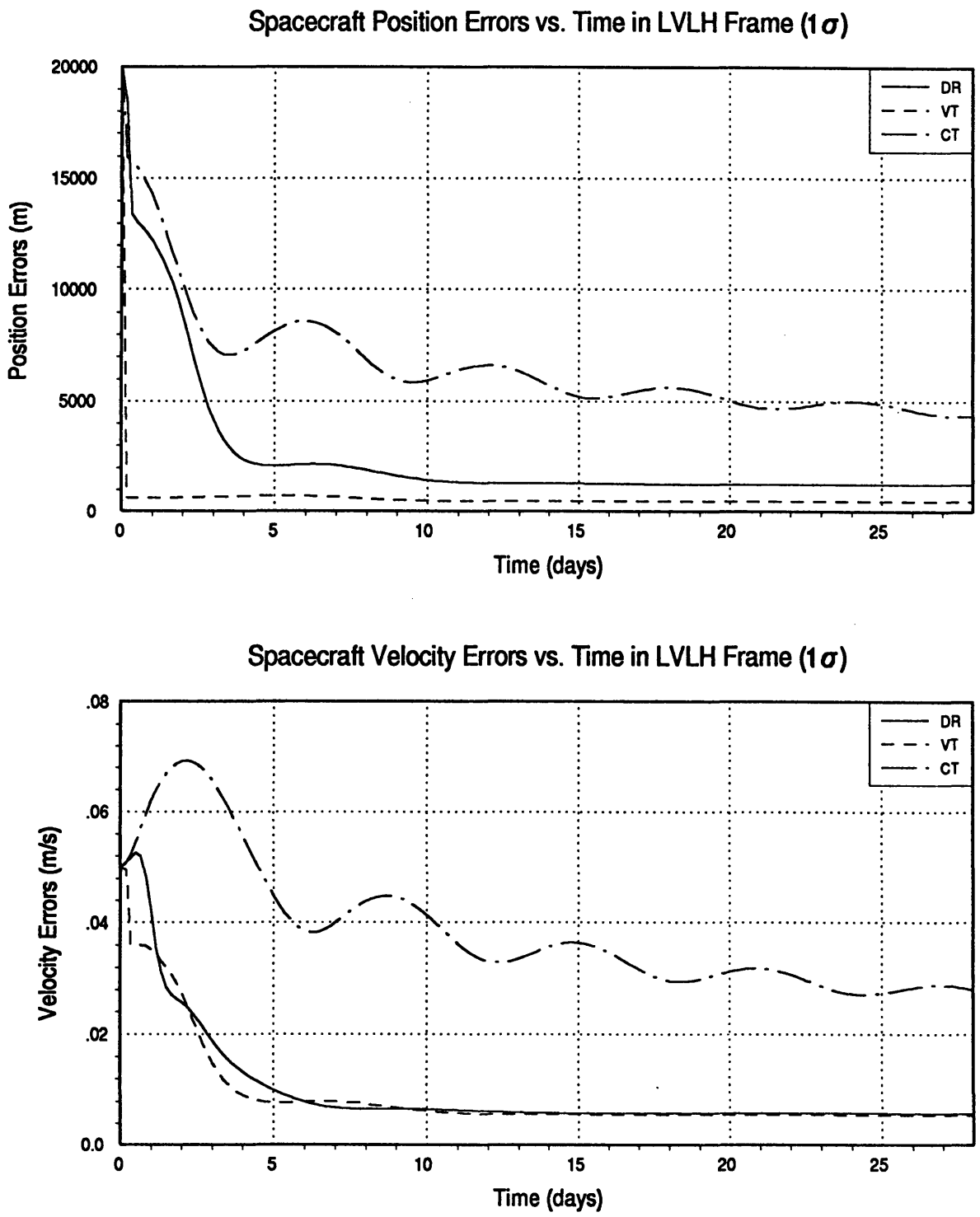

Figure A.2 : Case 1.1

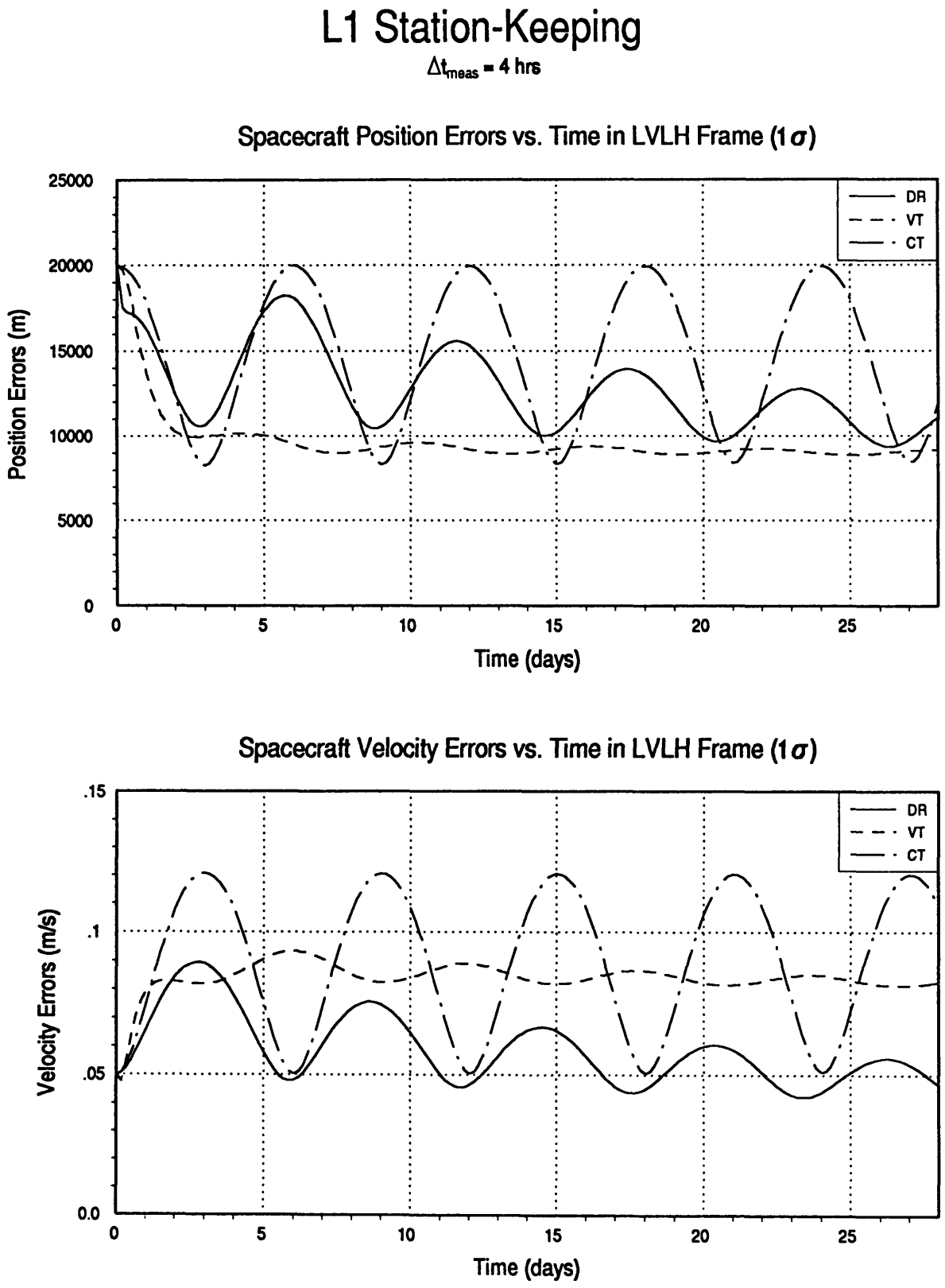

Figure A.3 : Case 1.2

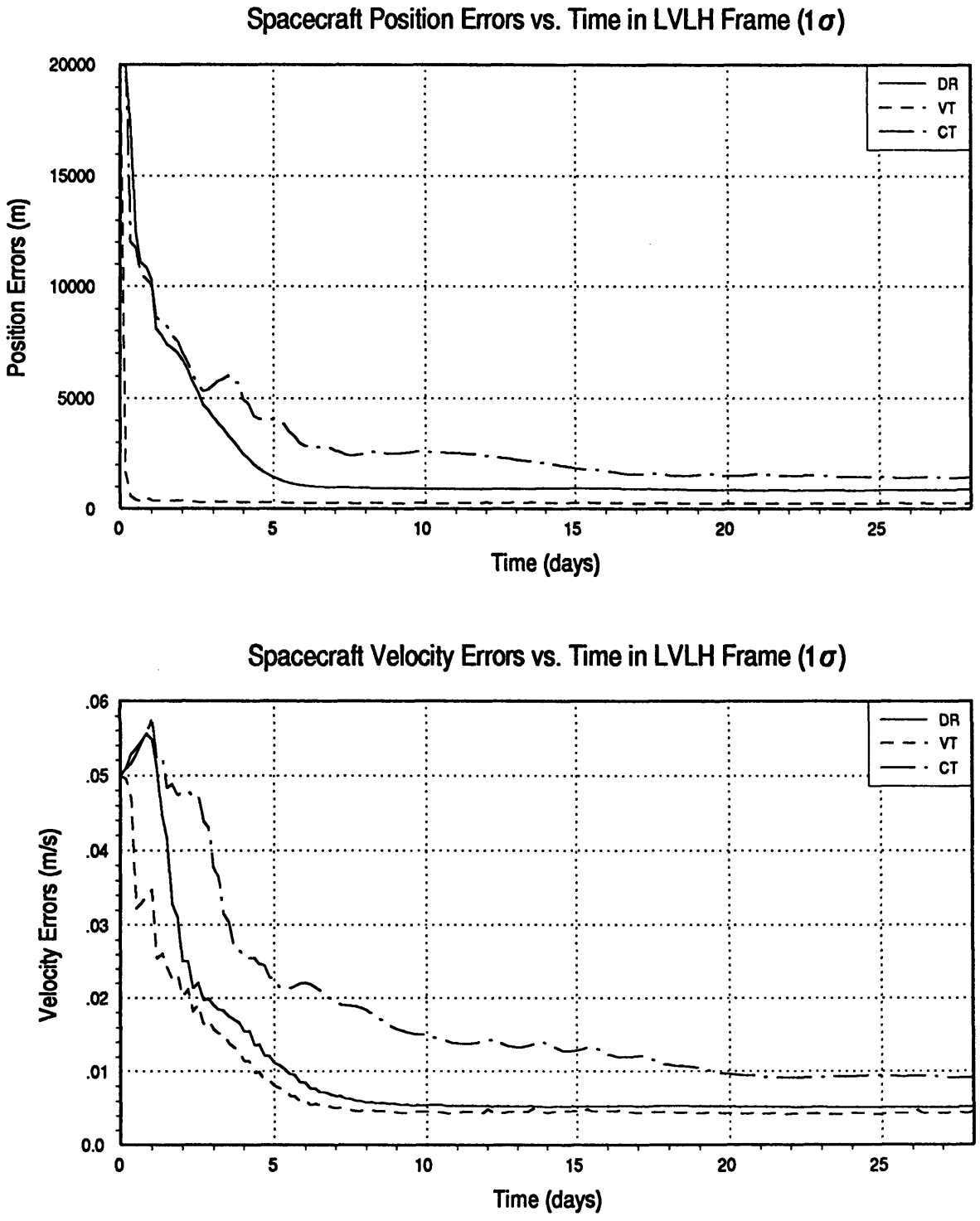

Figure A.4 : Case 1.3

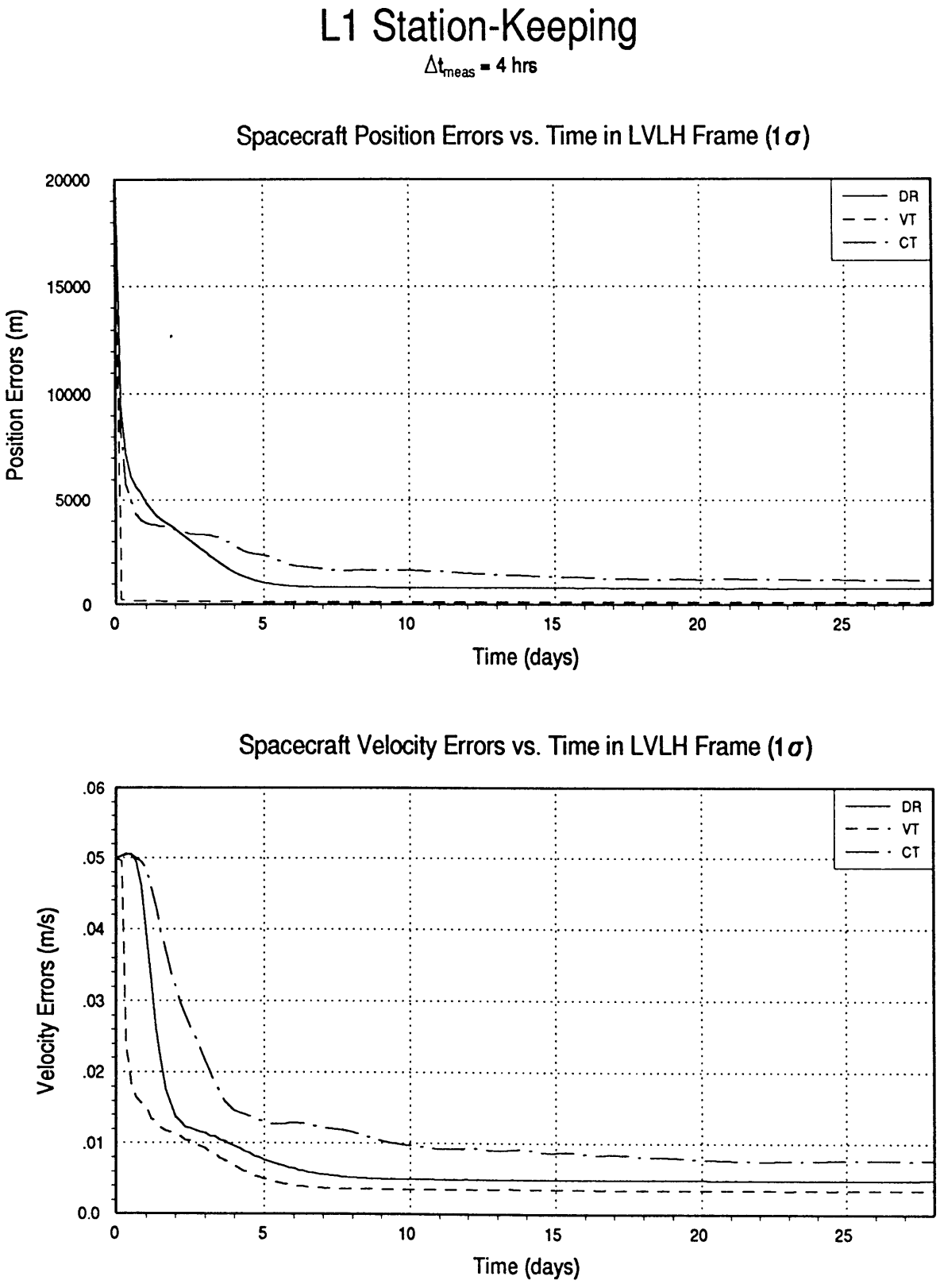

Figure A.5 : Case 1.4

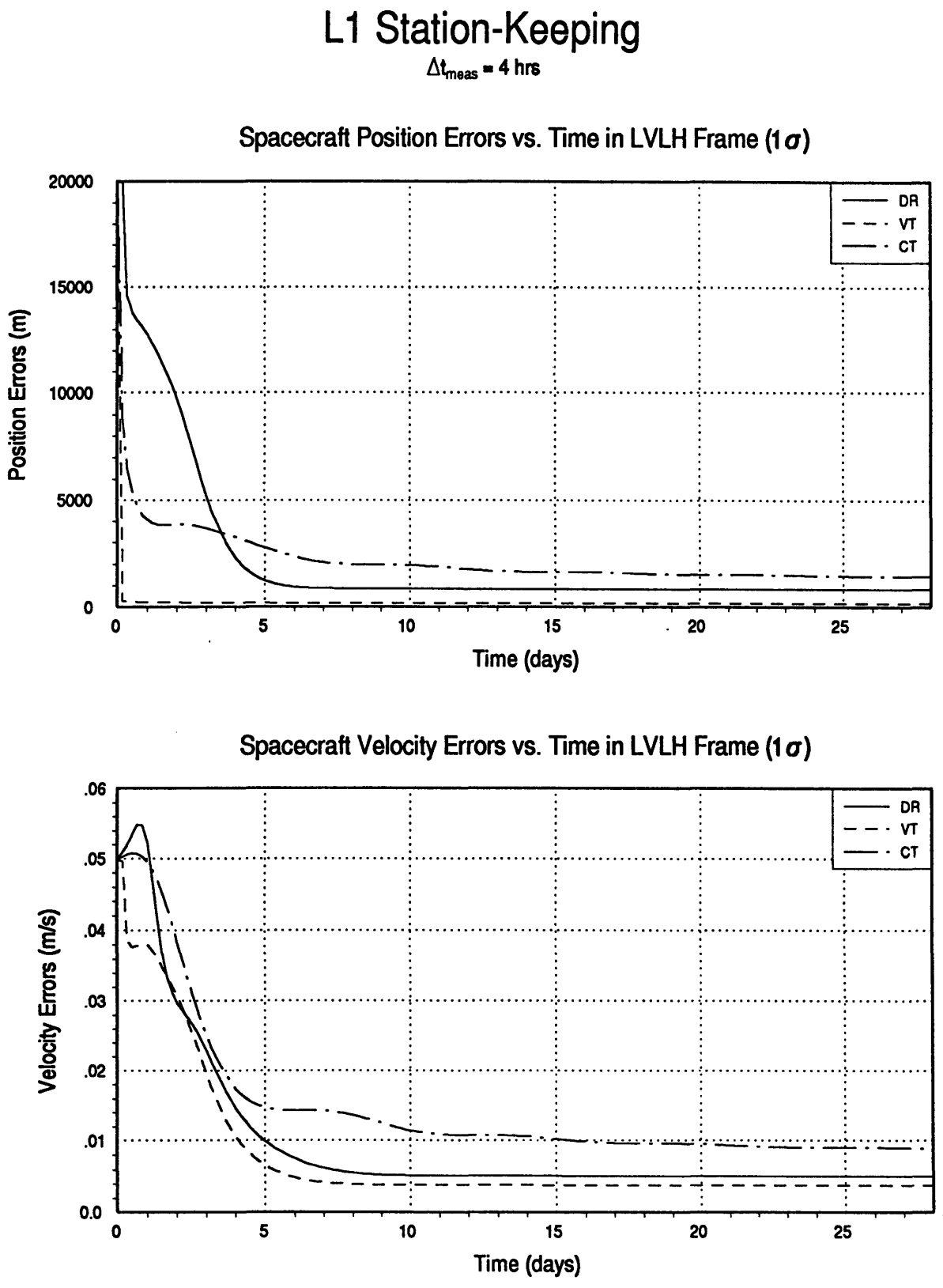

Figure A.6 : Case 1.5

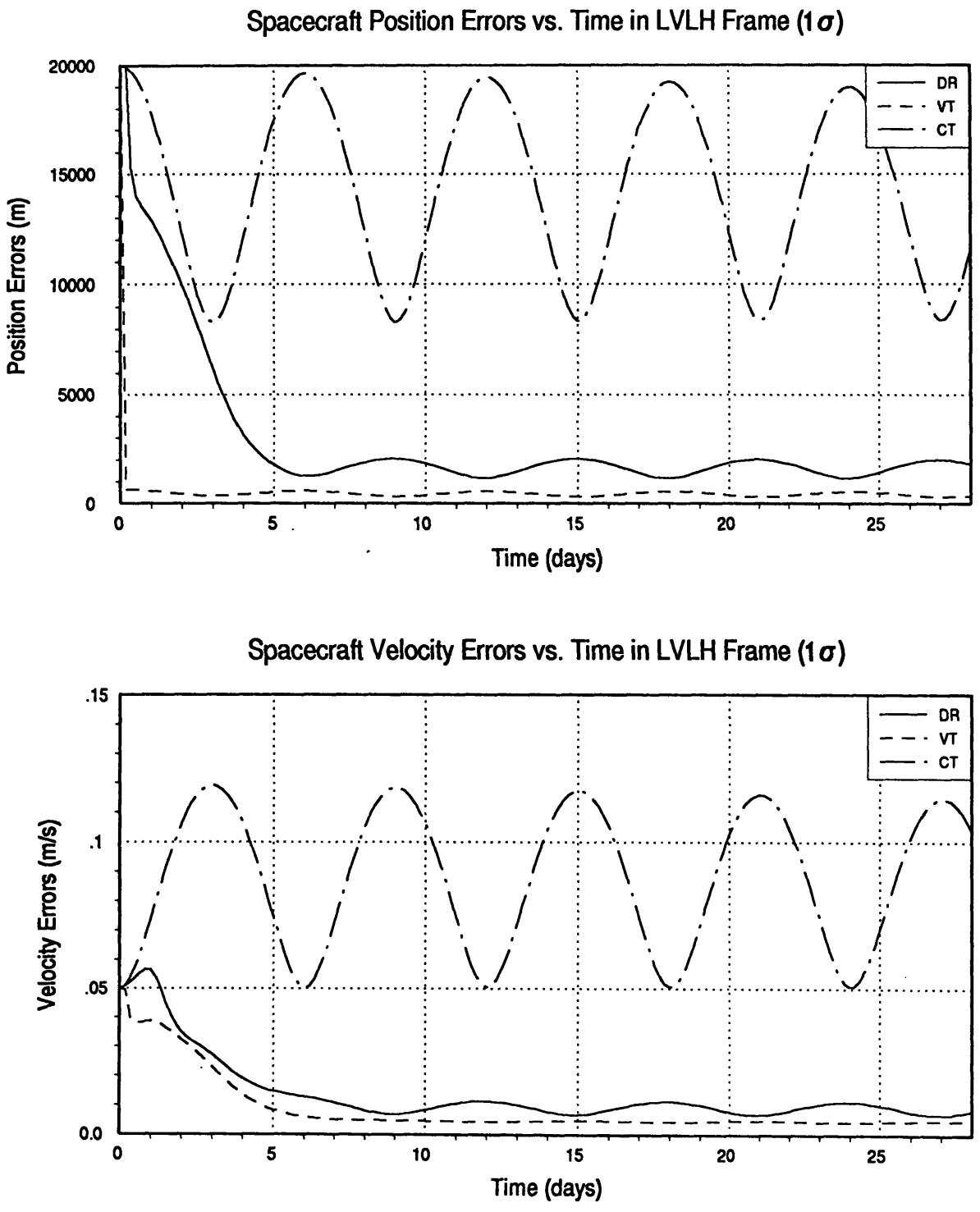

Figure A.7 : Case 1.6

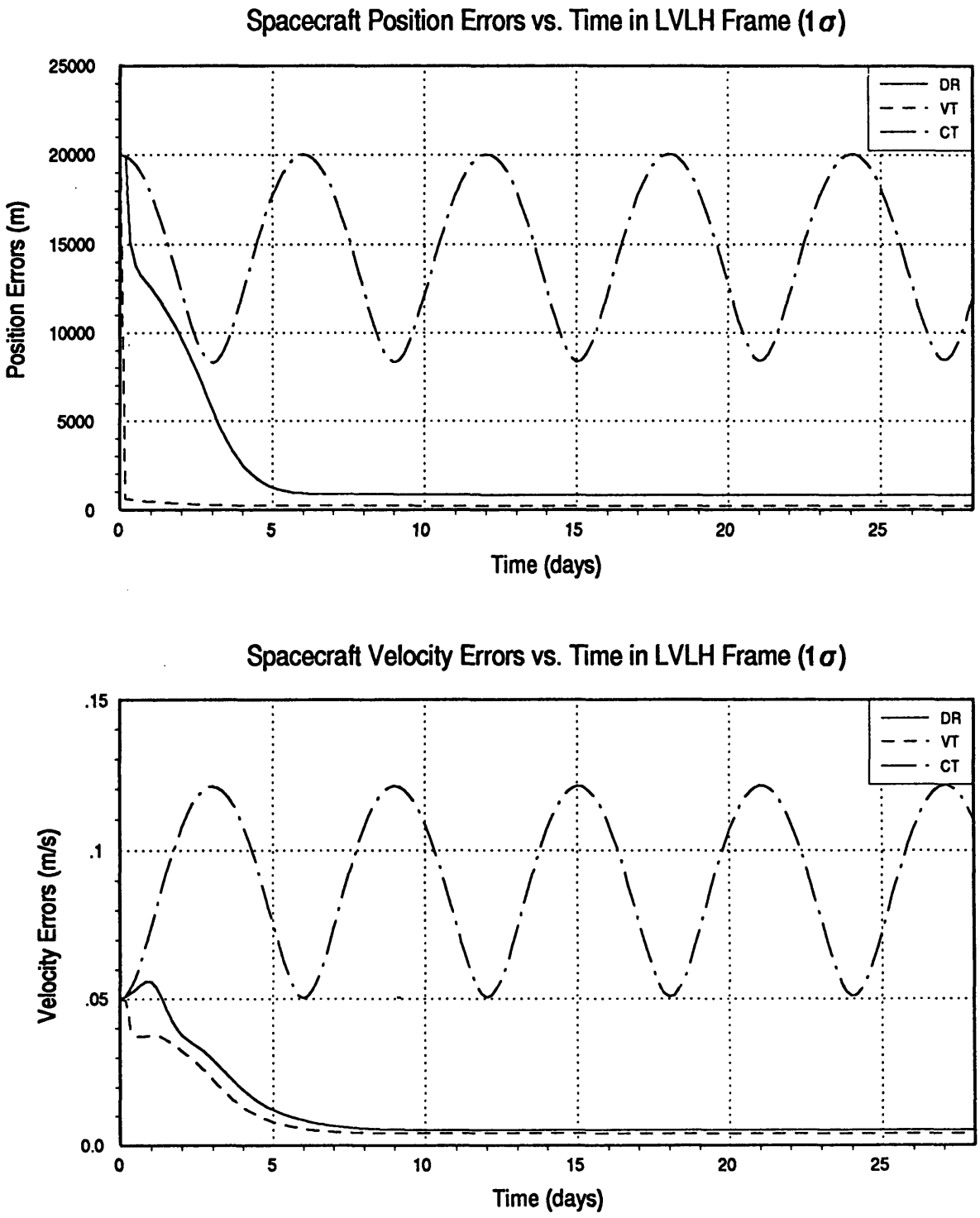

Figure A.8 : Case 1.7

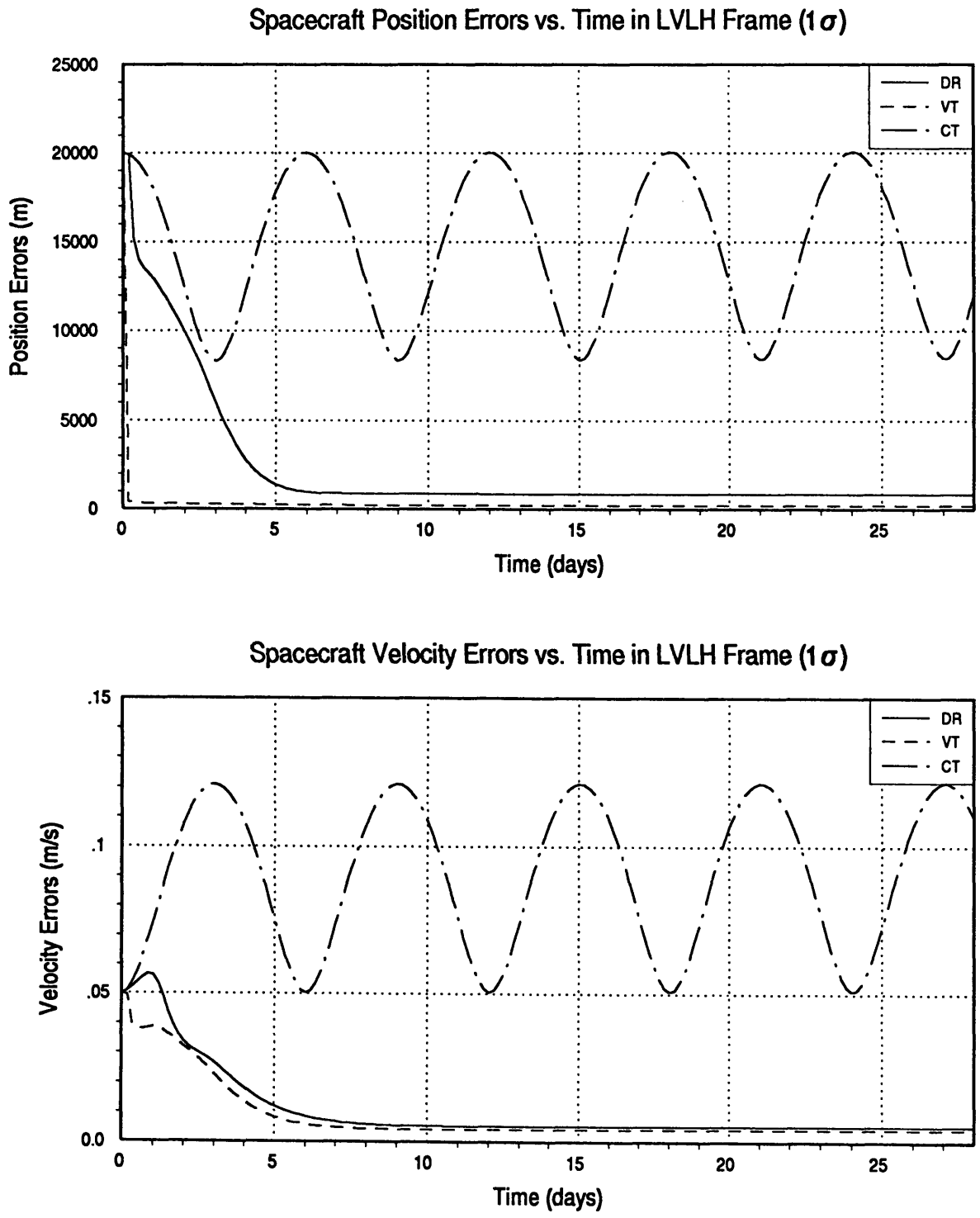

Figure A.9 : Case 1.8

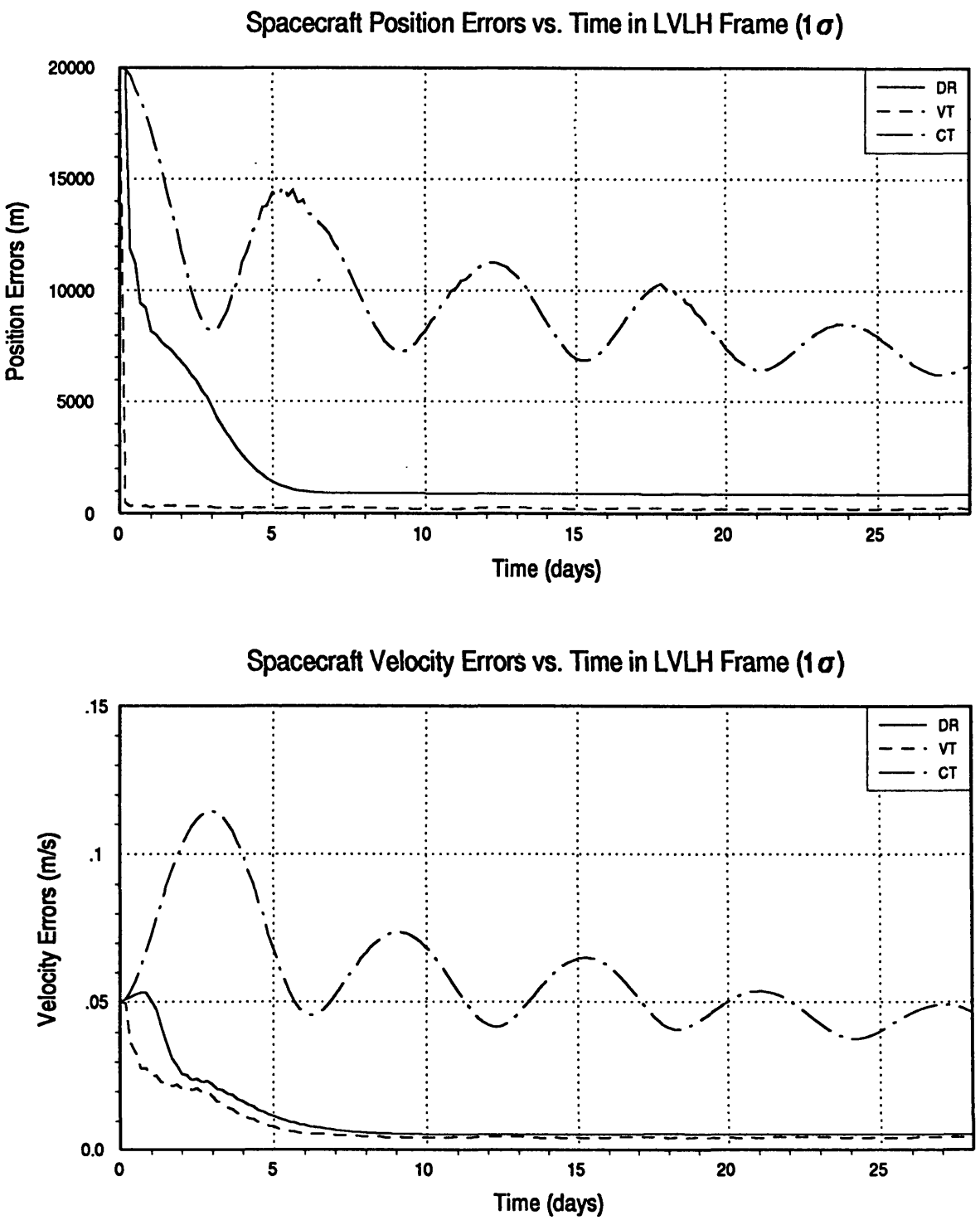

Figure A.10 : Case 1.9

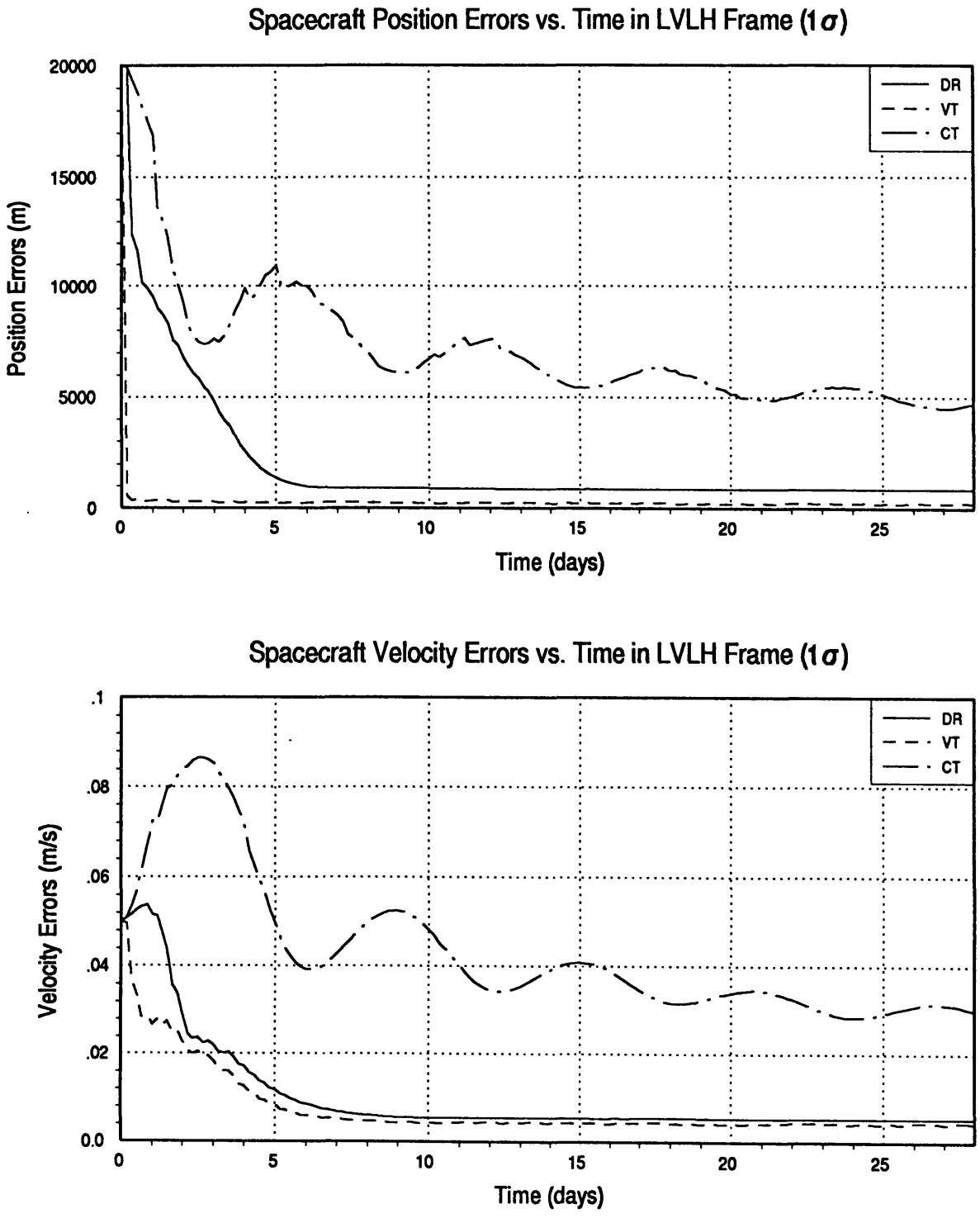

Figure A.11 : Case 1.10

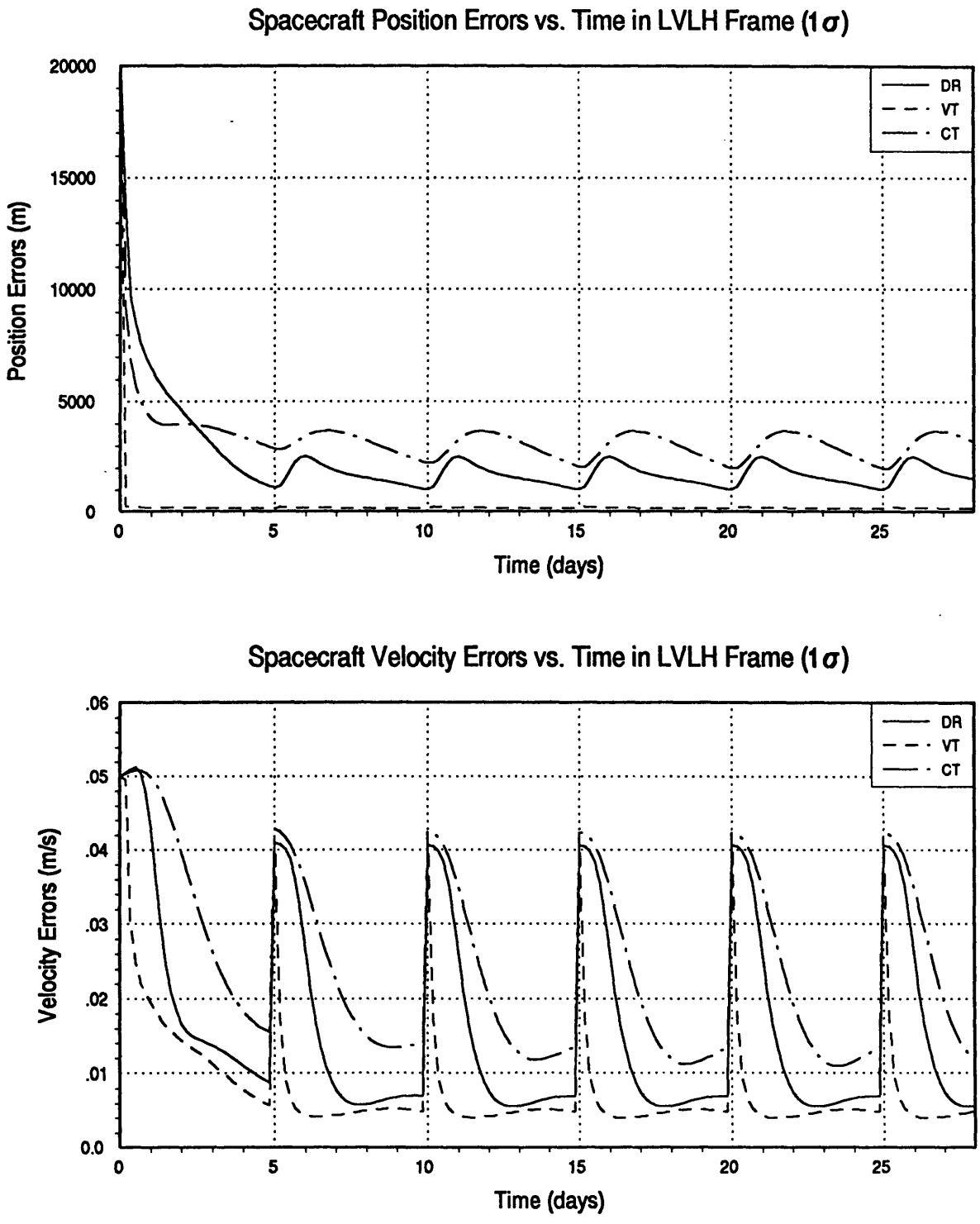

Figure A.12 : Case 1.11

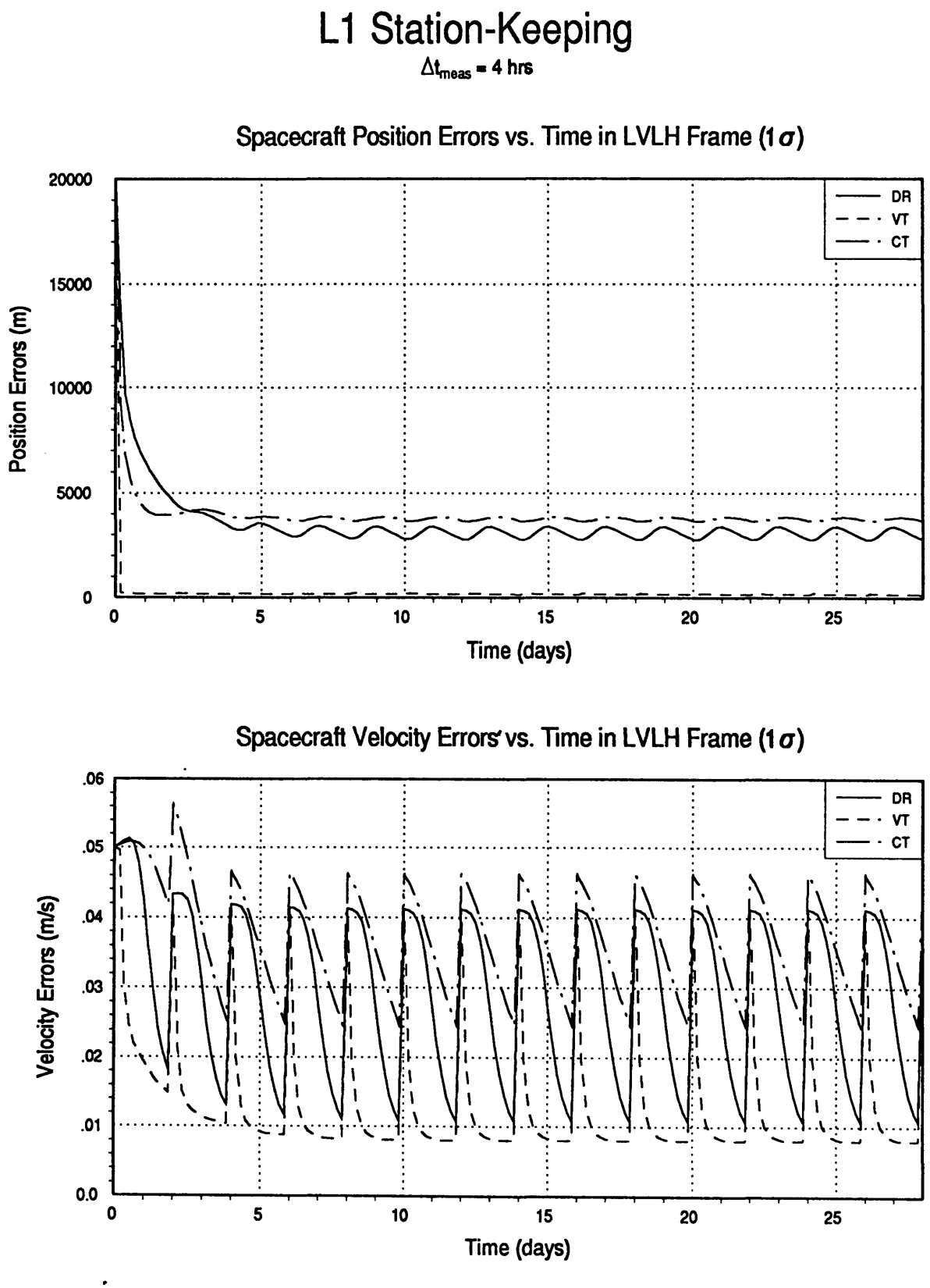

Figure A.13 : Case 1.12

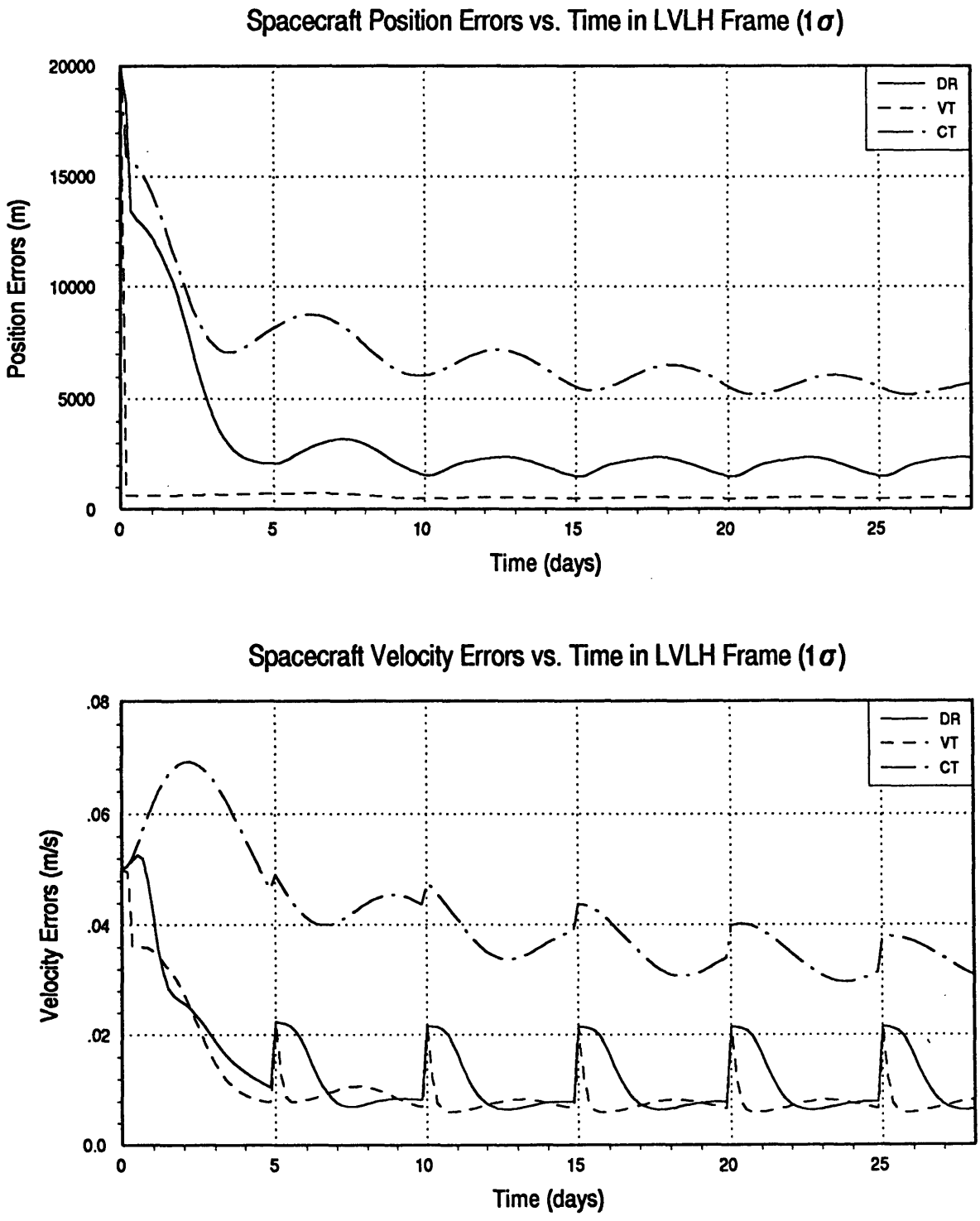

Figure A.14 : Case 1.13

L1 Station-Keeping

Δt_{meas} = 4 hrs

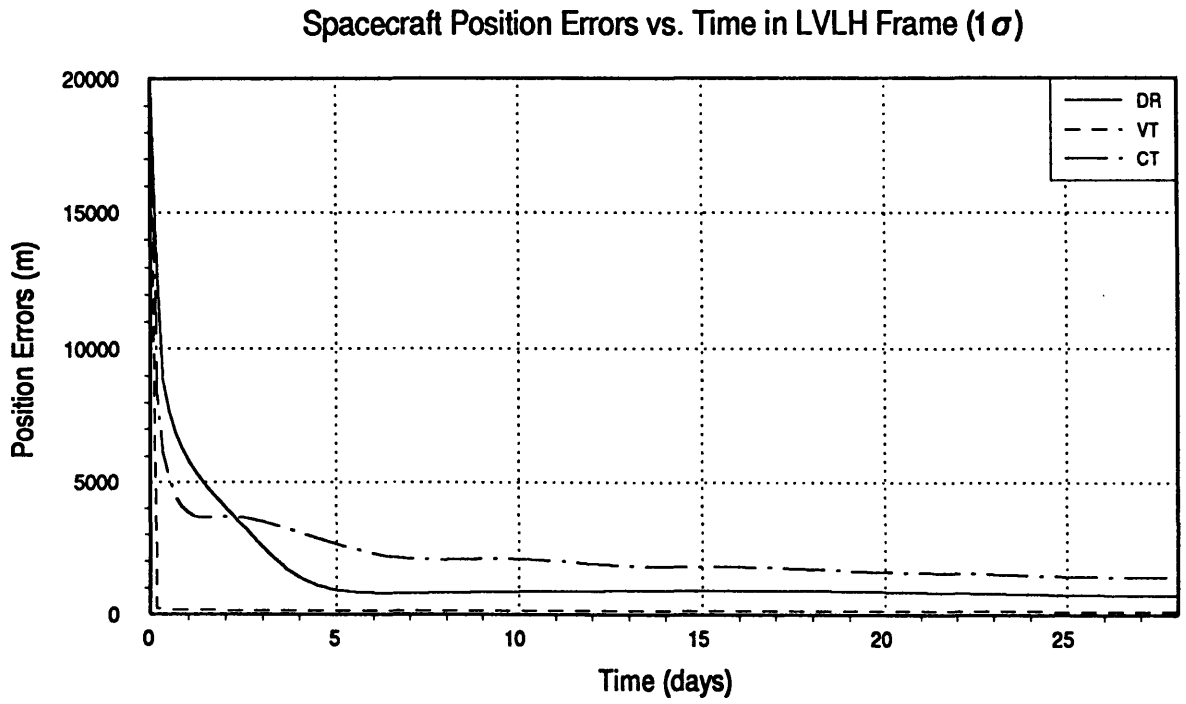

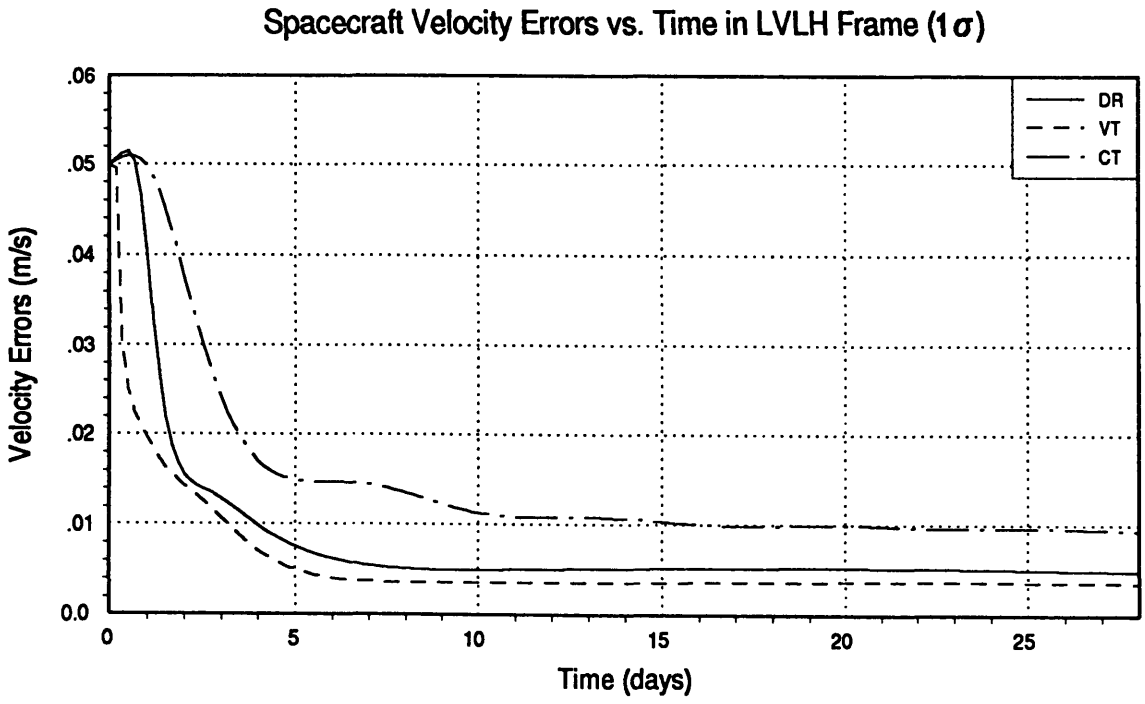

Figure A.15 : Case 1.14

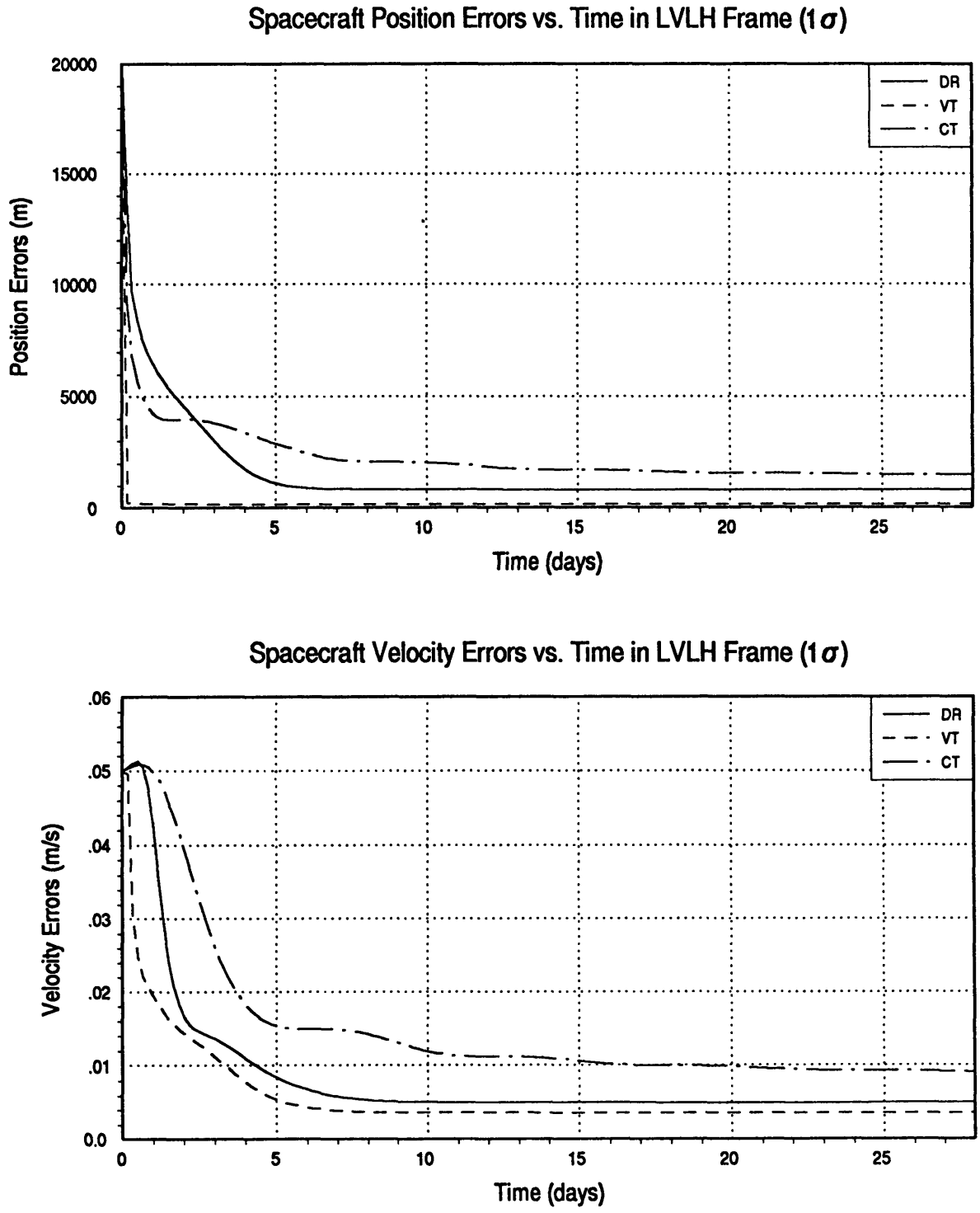

Figure A.16 : Case 1.15

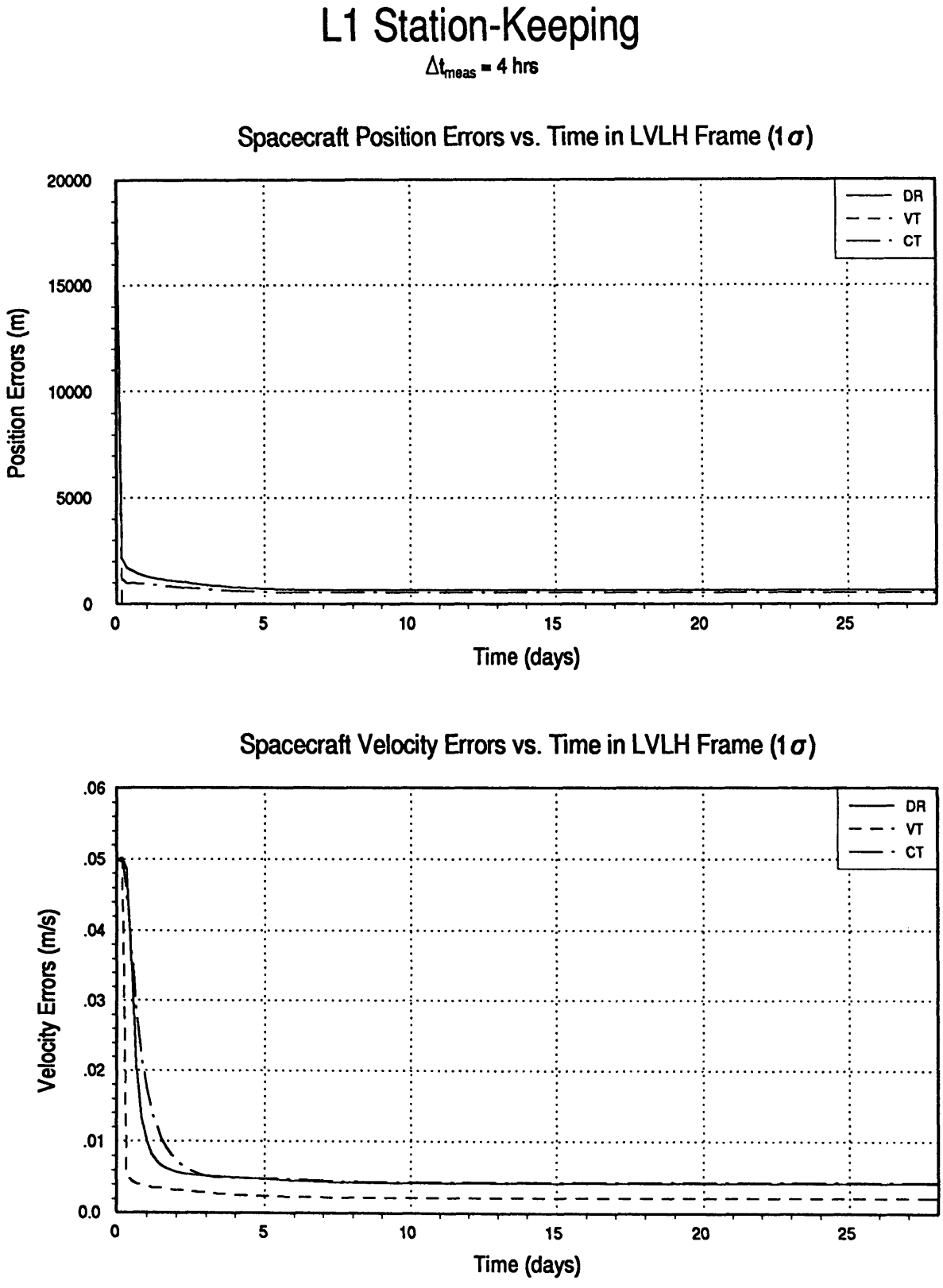

Figure A.17 : Case 1.16

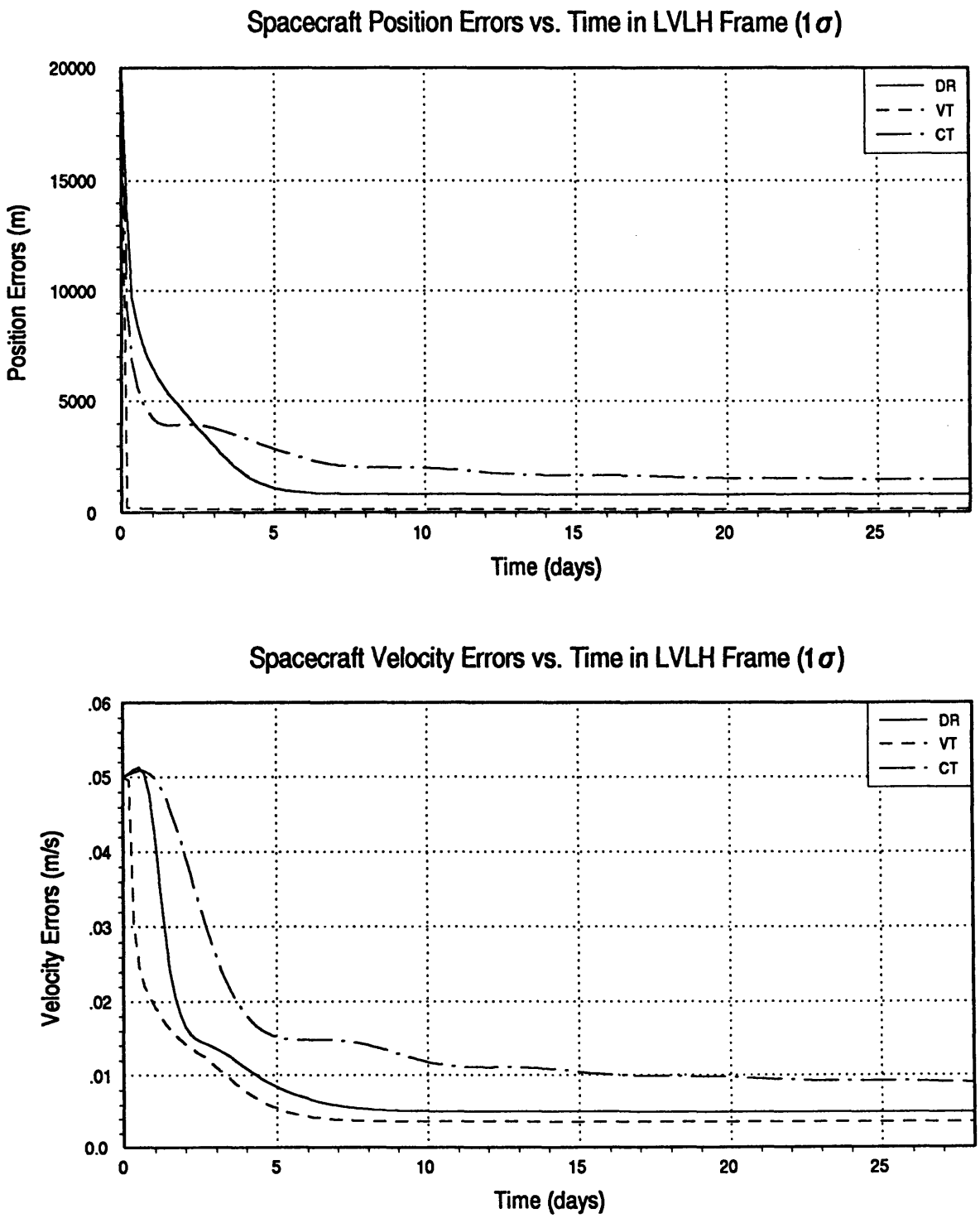

Figure A.18 : Case 1.17

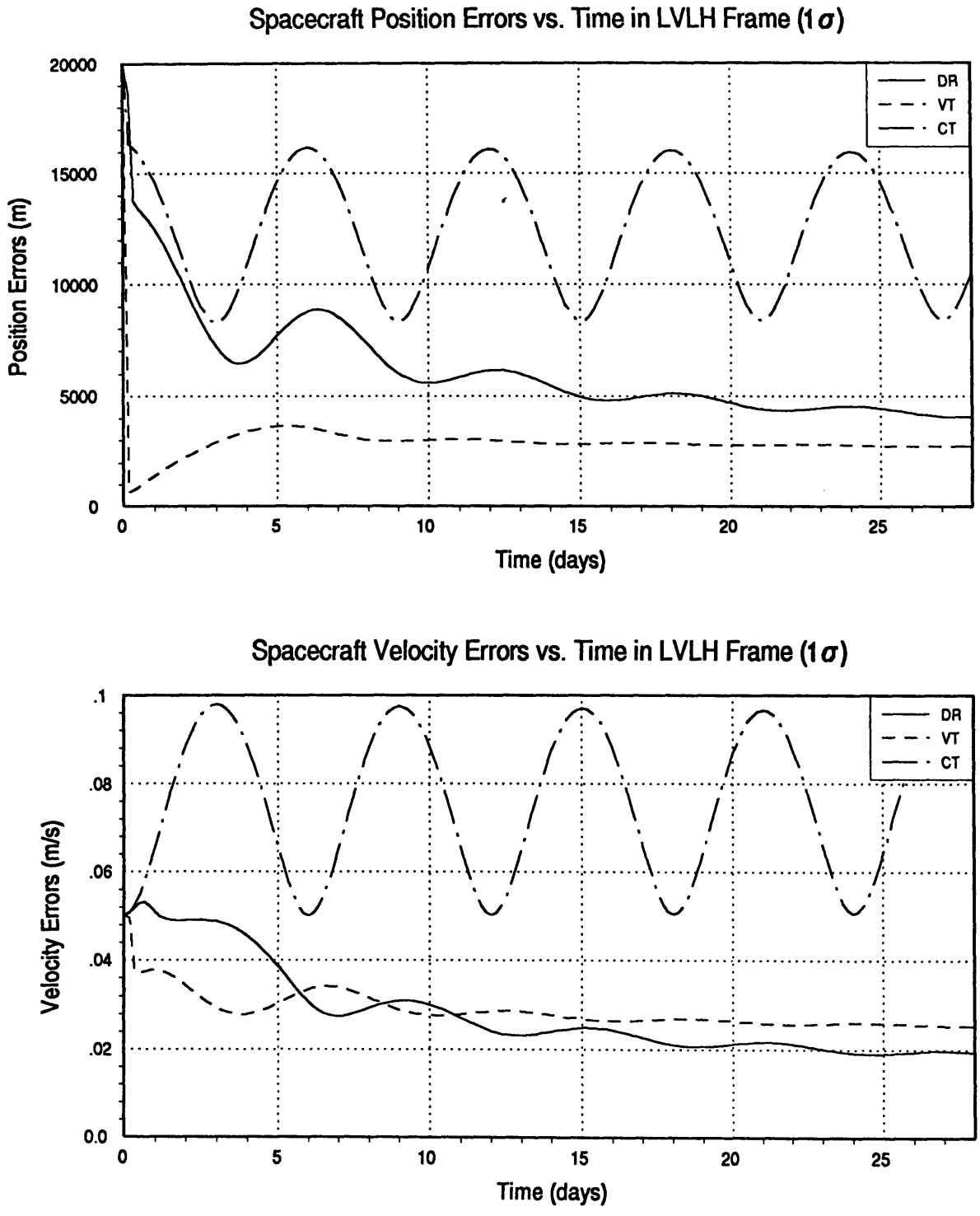

Figure A.19 : Case 1.18

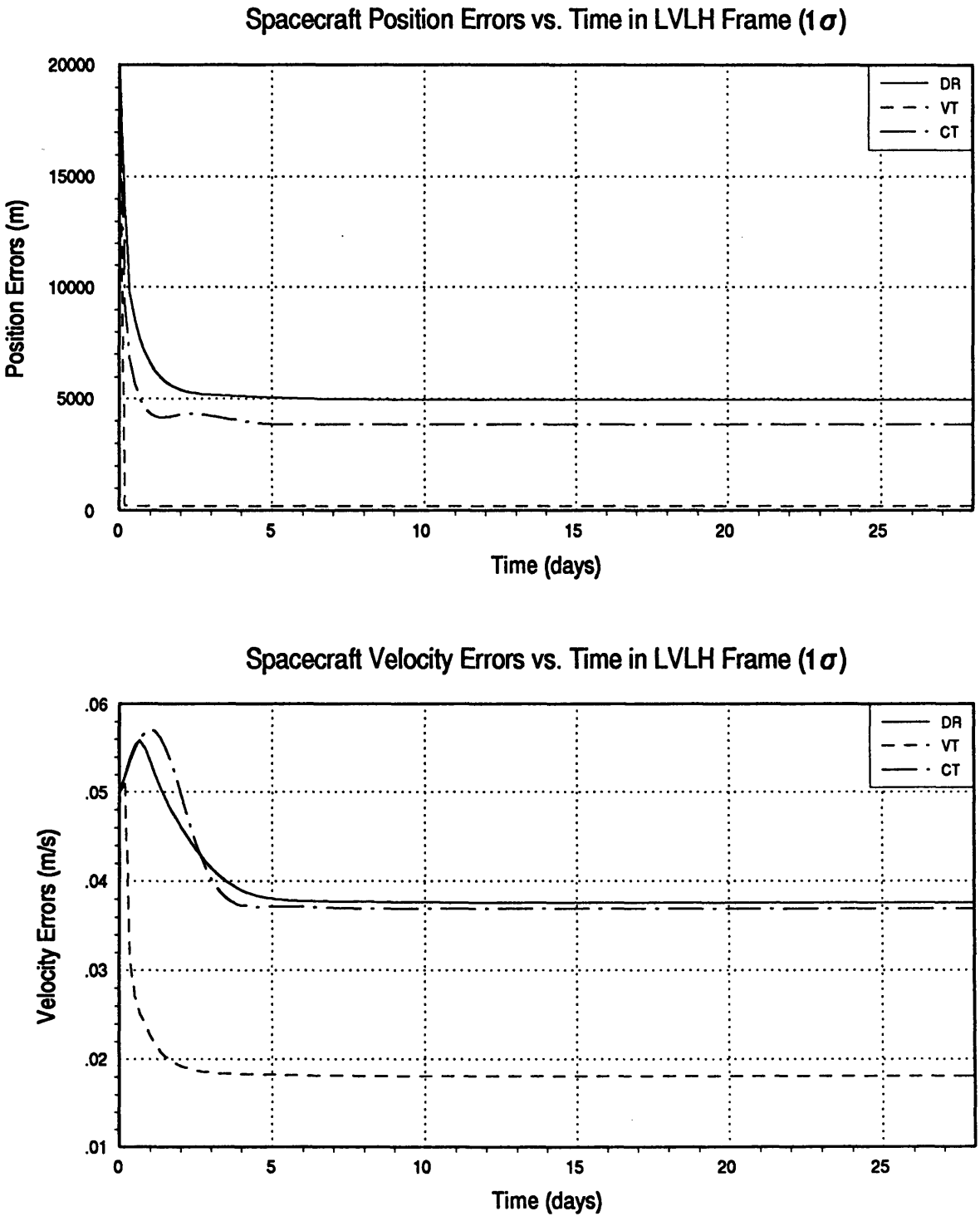

Figure A.20 : Case 1.19

L1 Station-Keeping

Δt_{meas} = 4 hrs

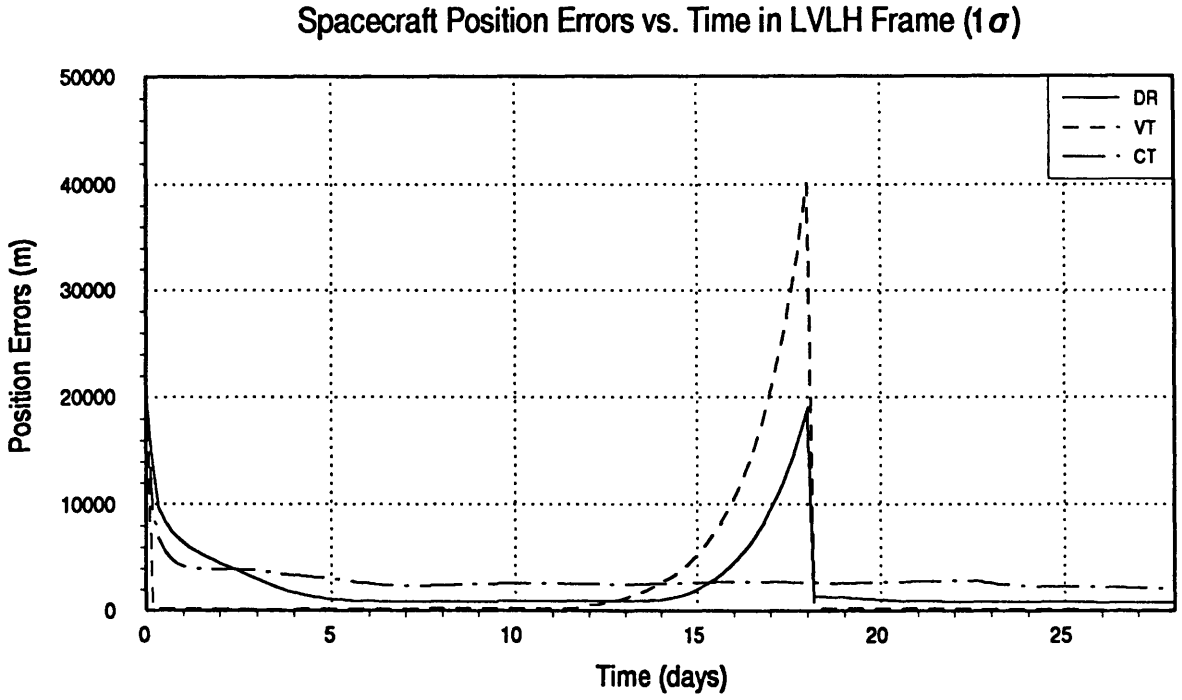

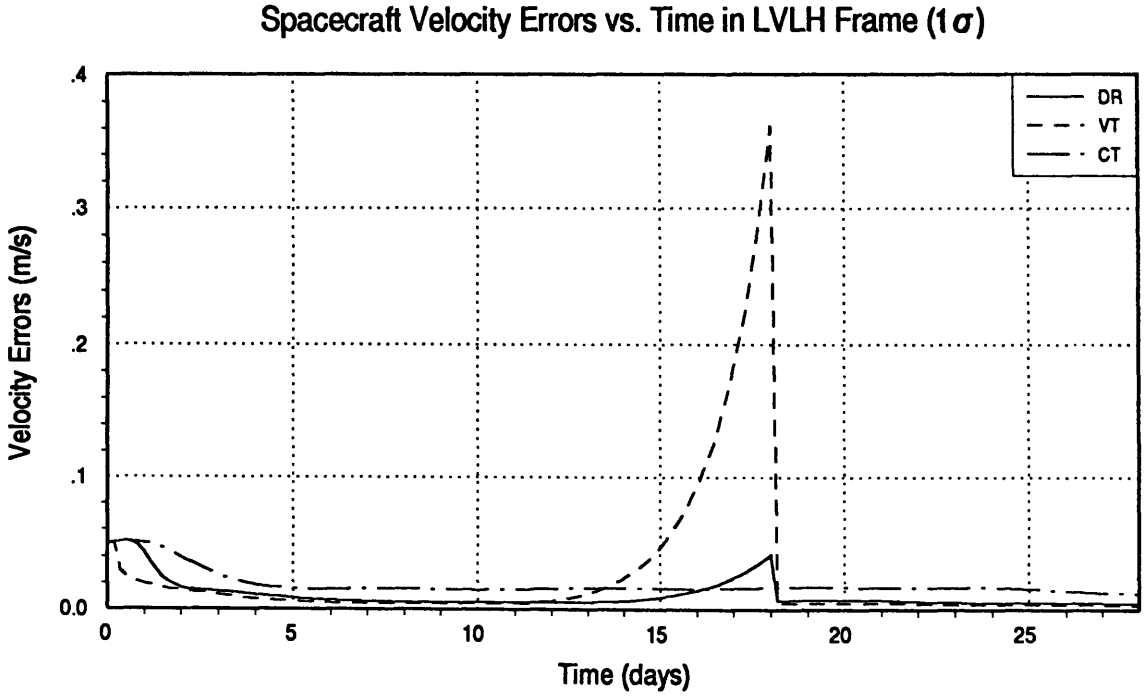

Figure A.21 : Case 1.20

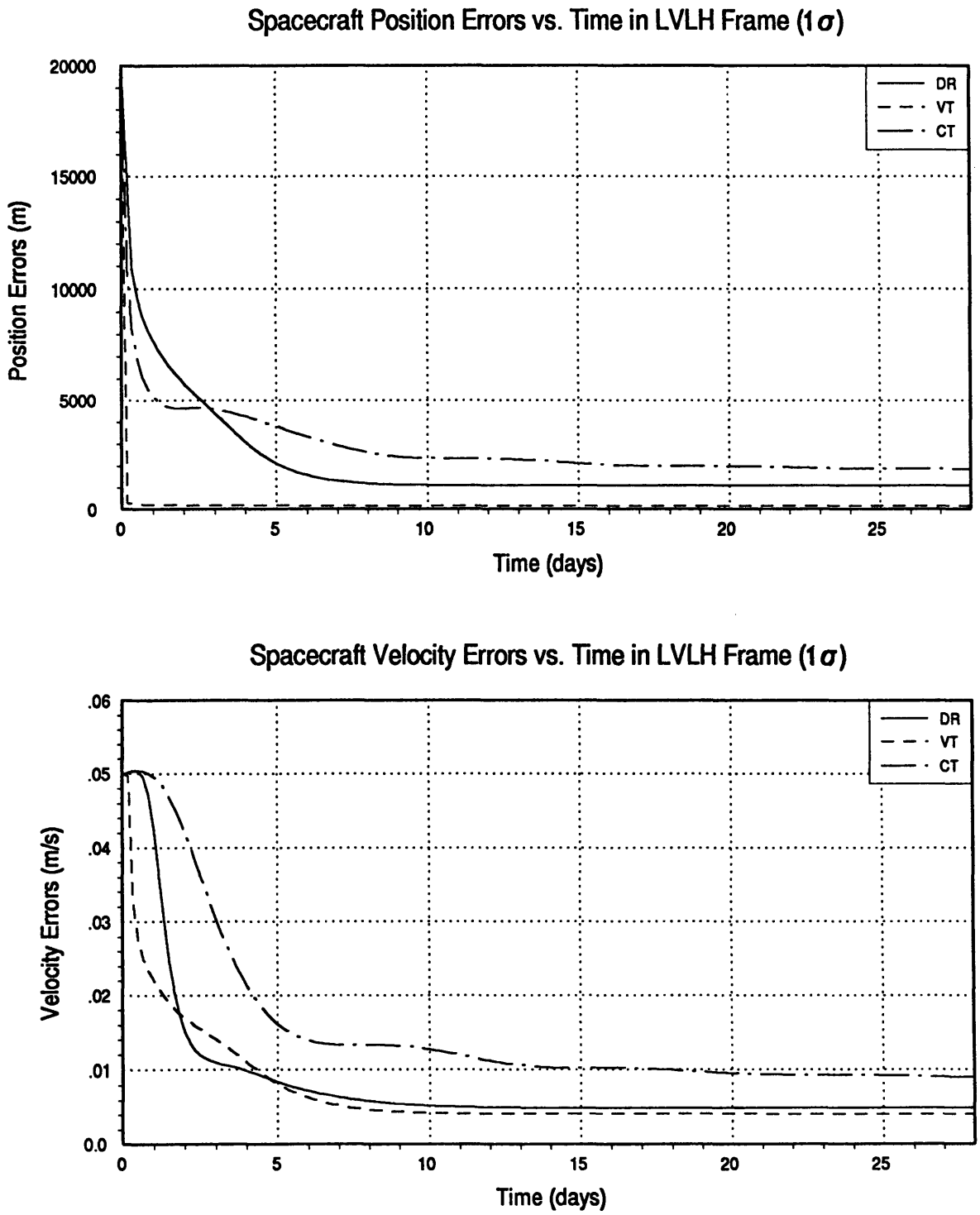

Figure A.22 : Case 2.0

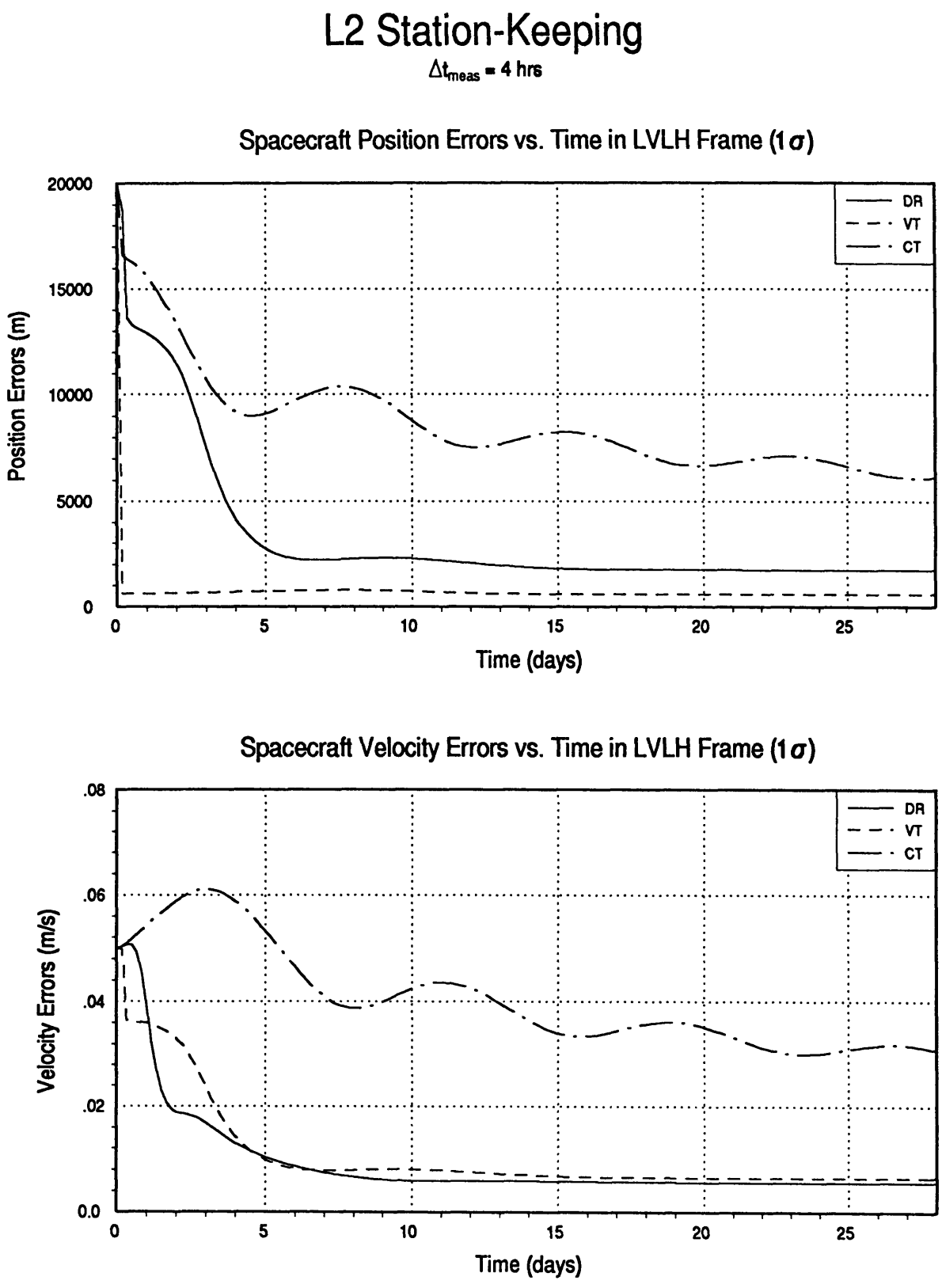

Figure A.23 : Case 2.1

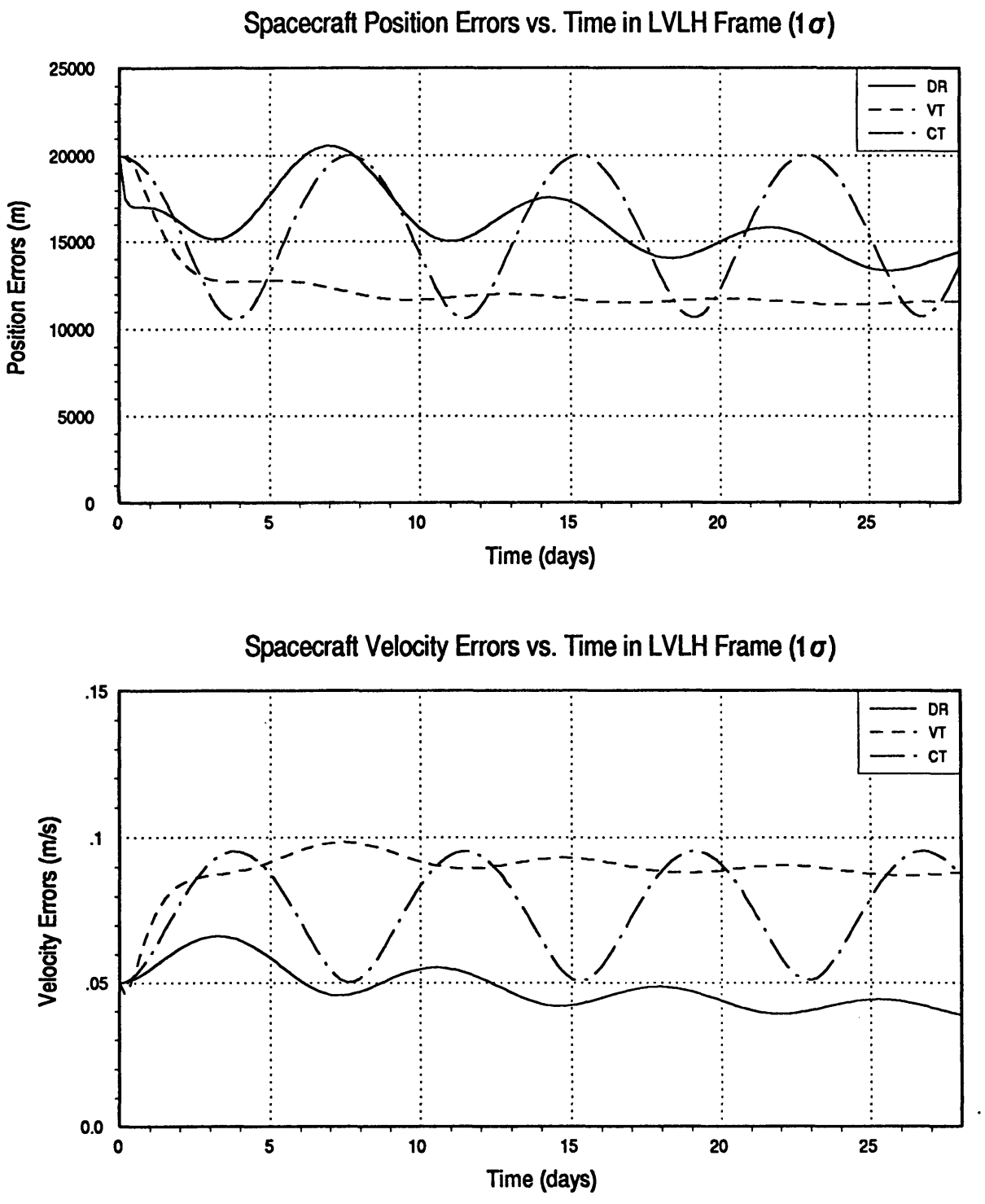

Figure A.24 : Case 2.2

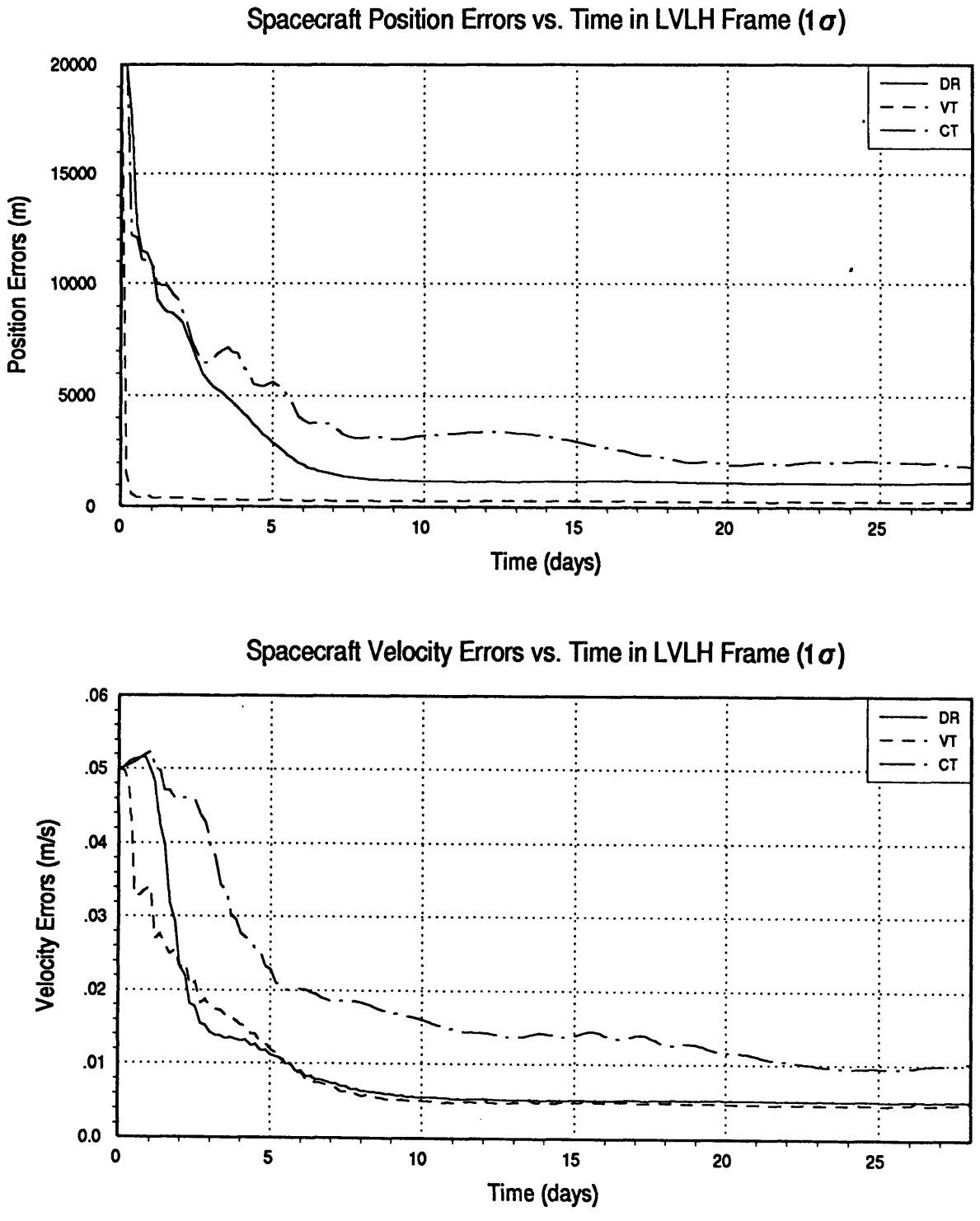

Figure A.25 : Case 2.3

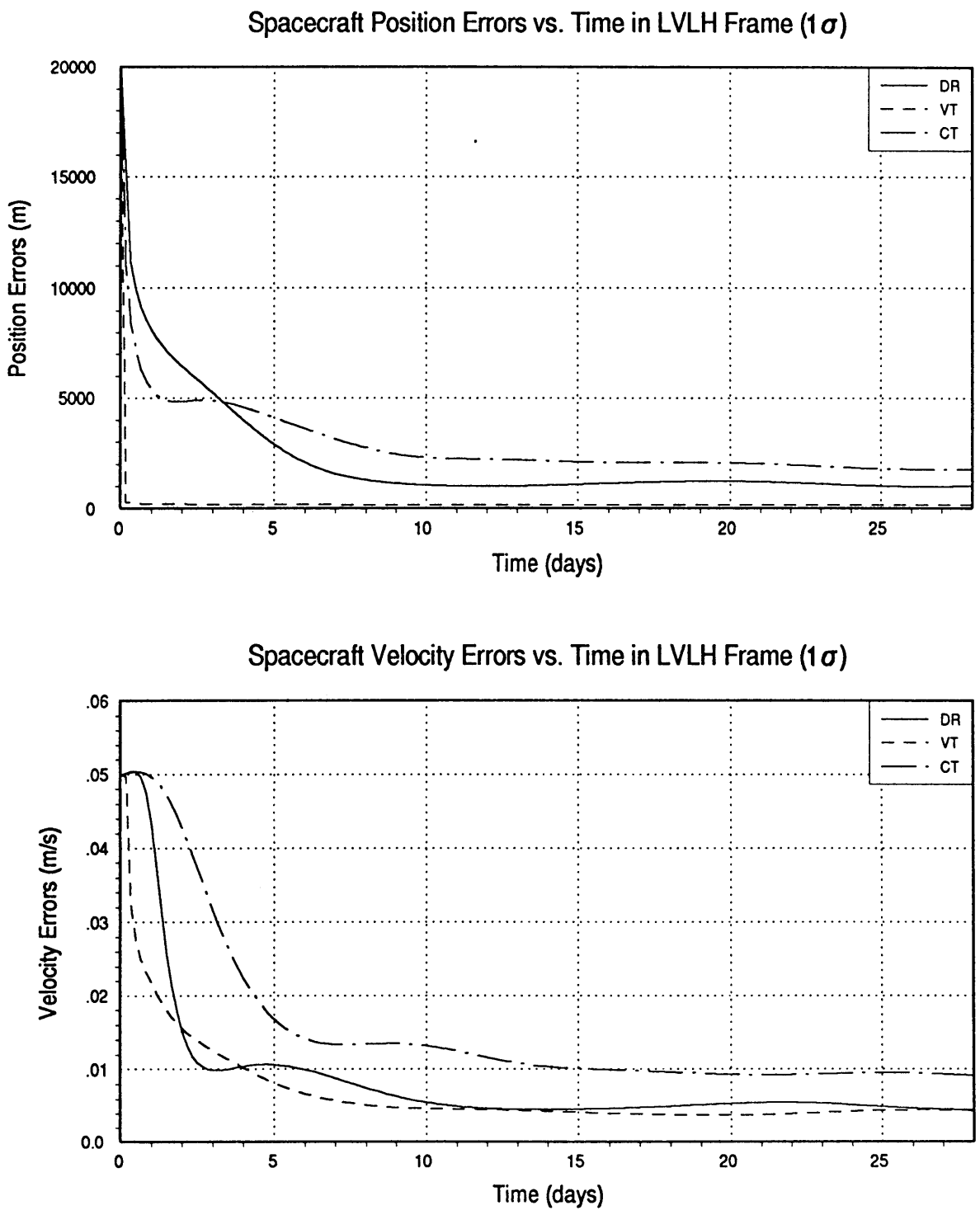

Figure A.26 : Case 2.4

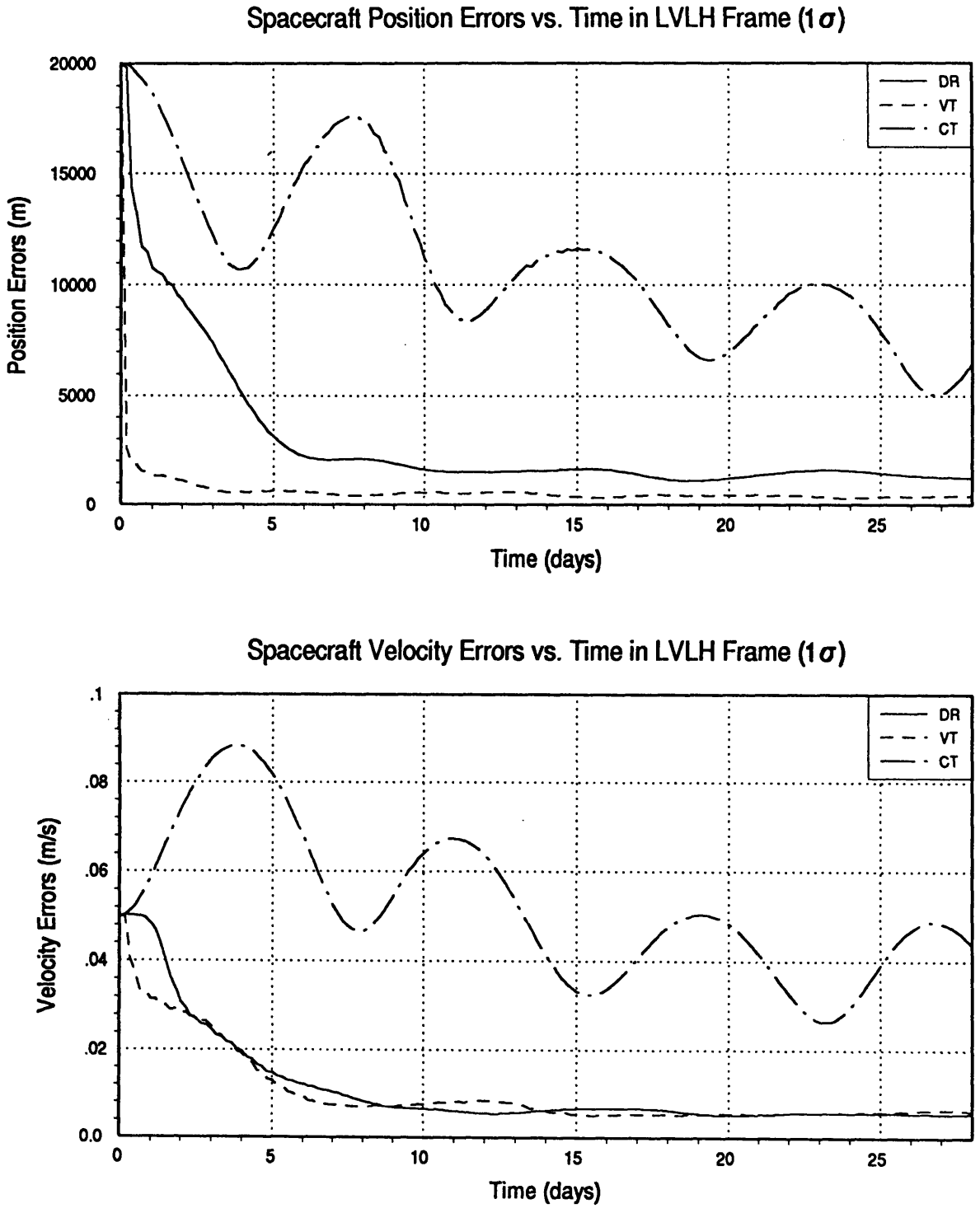

Figure A.27 : Case 2.5

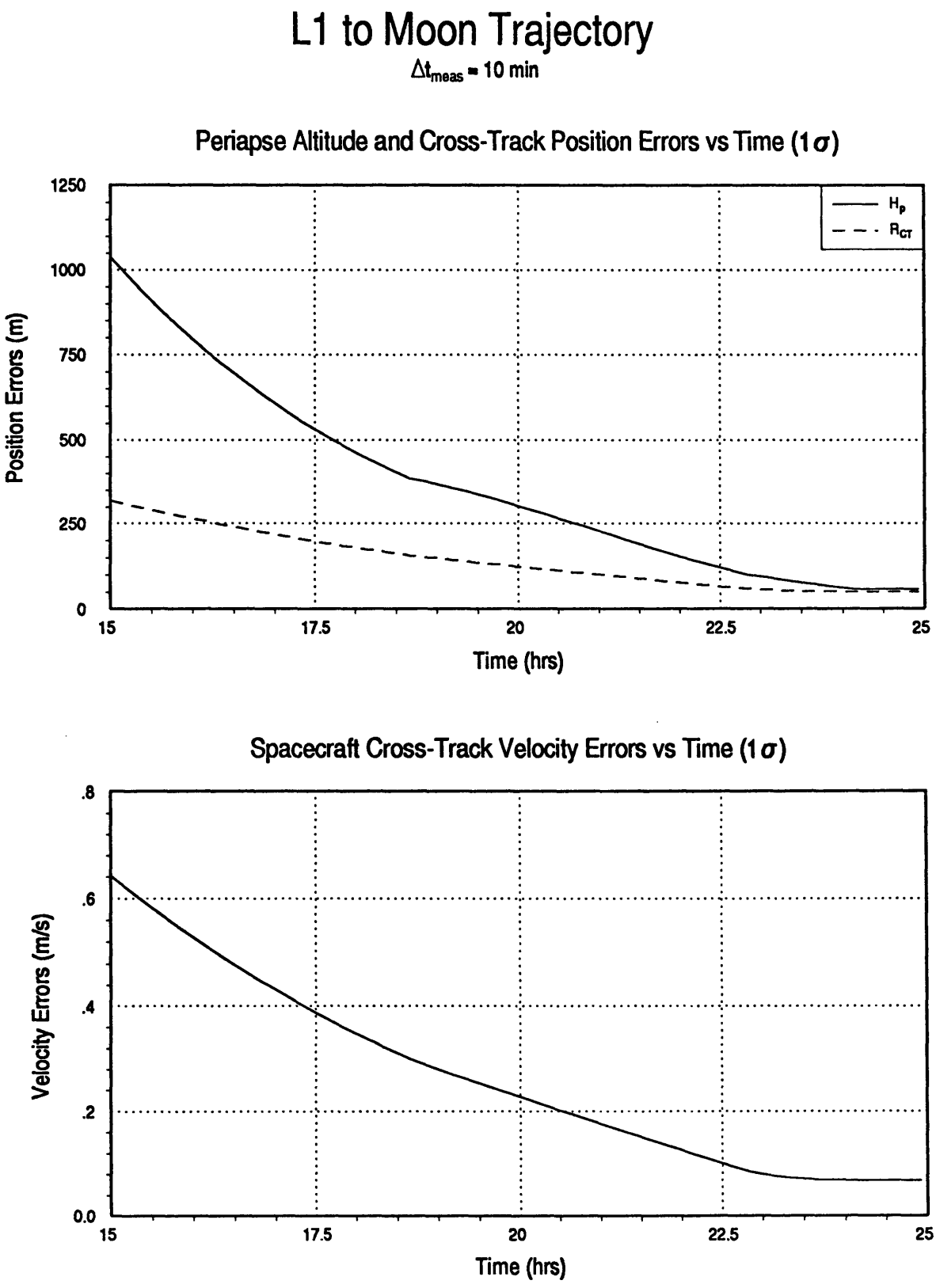

Figure A.28 : Case 3.0

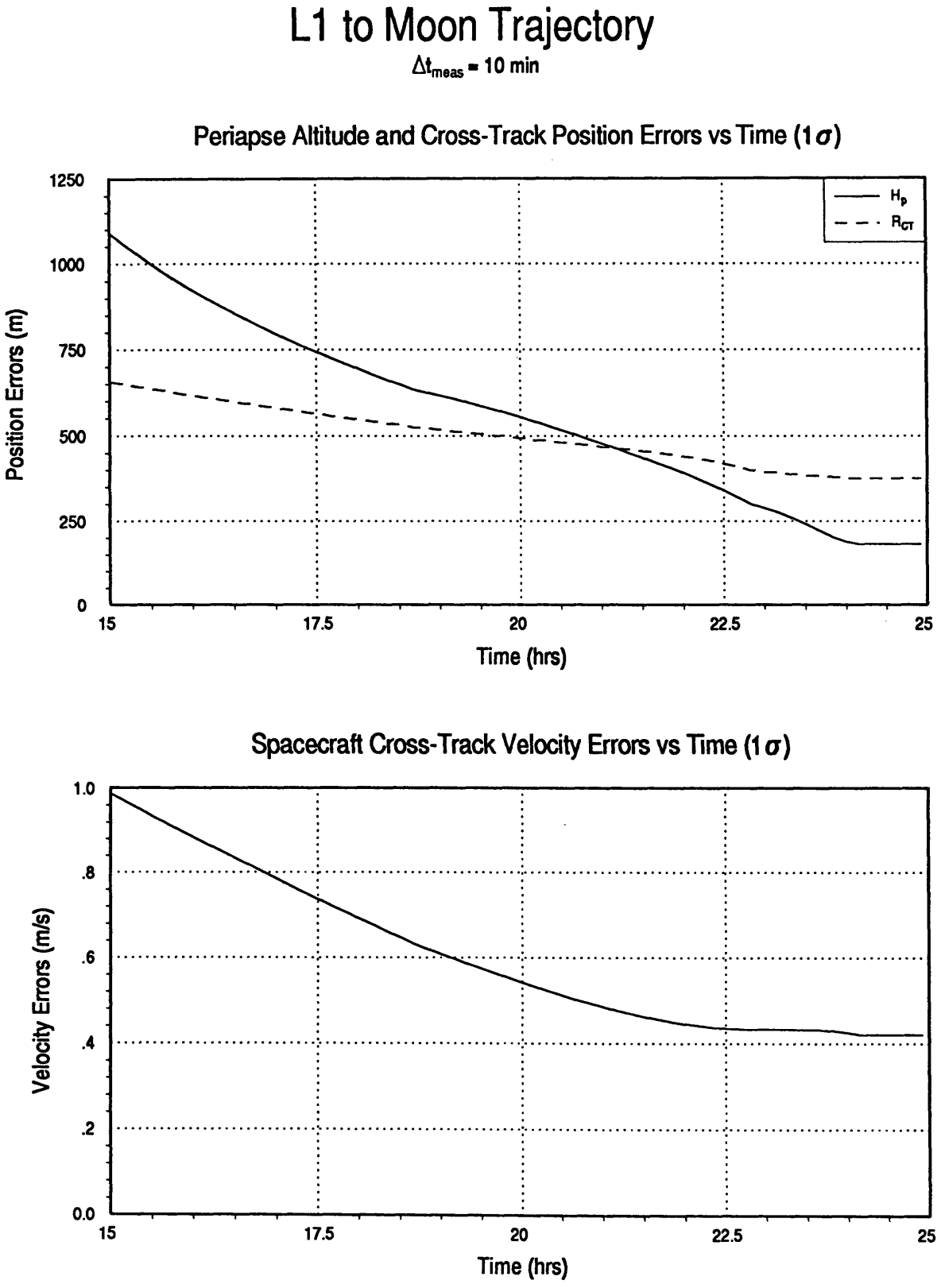

Figure A.29 : Case 3.1

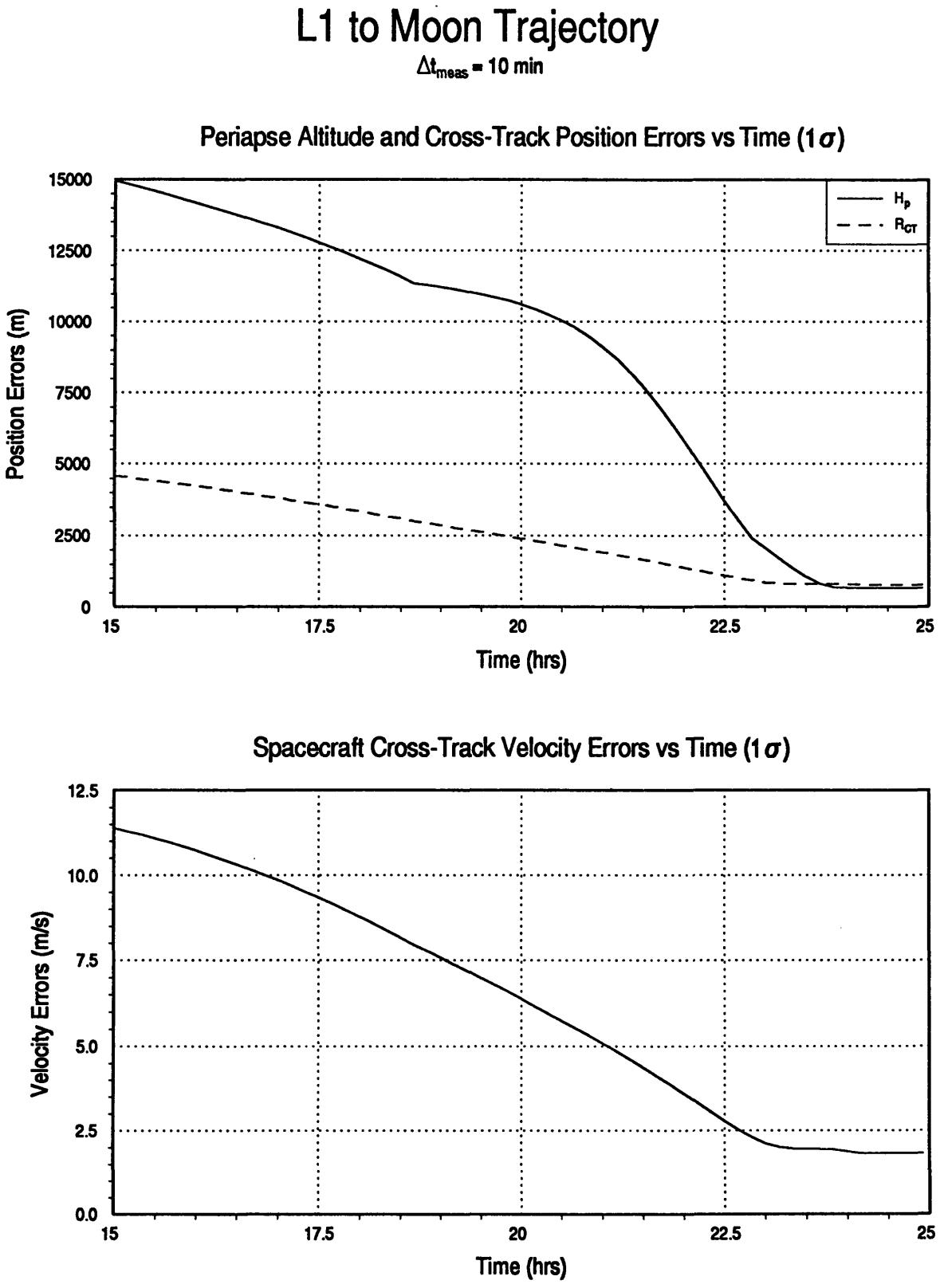

Figure A.30 : Case 3.2

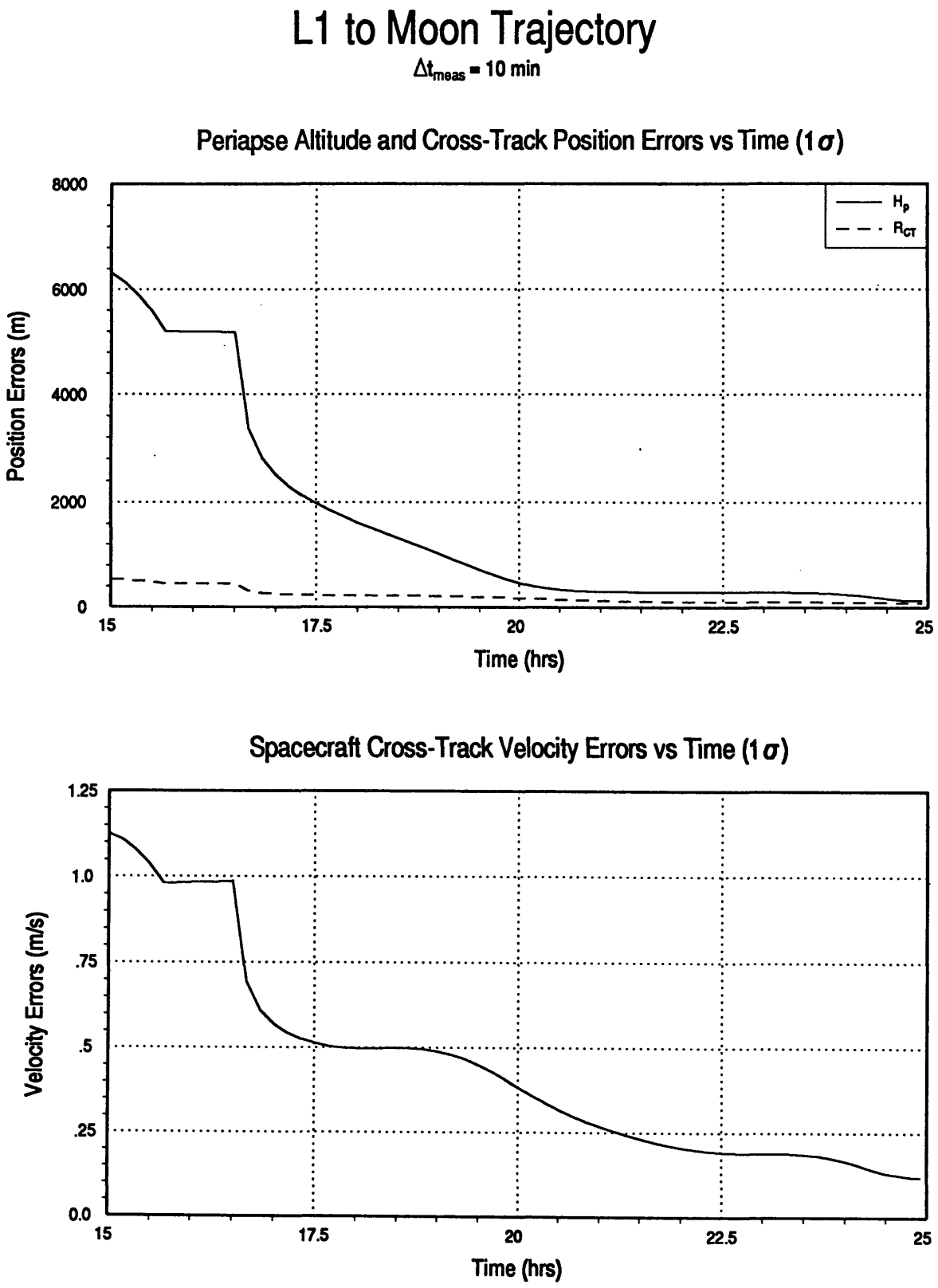

Figure A.31 : Case 3.3

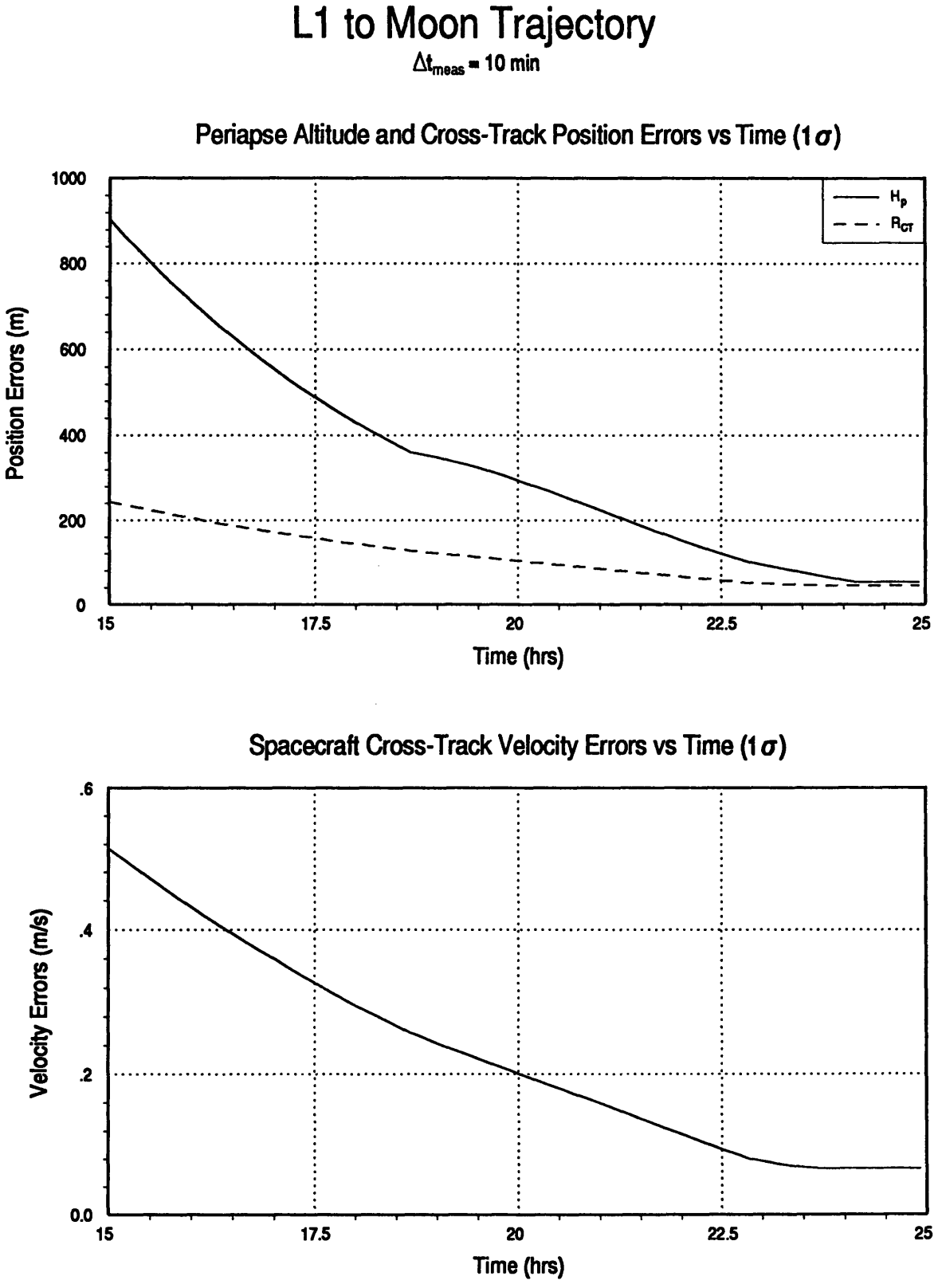

Figure A.32 : Case 3.4

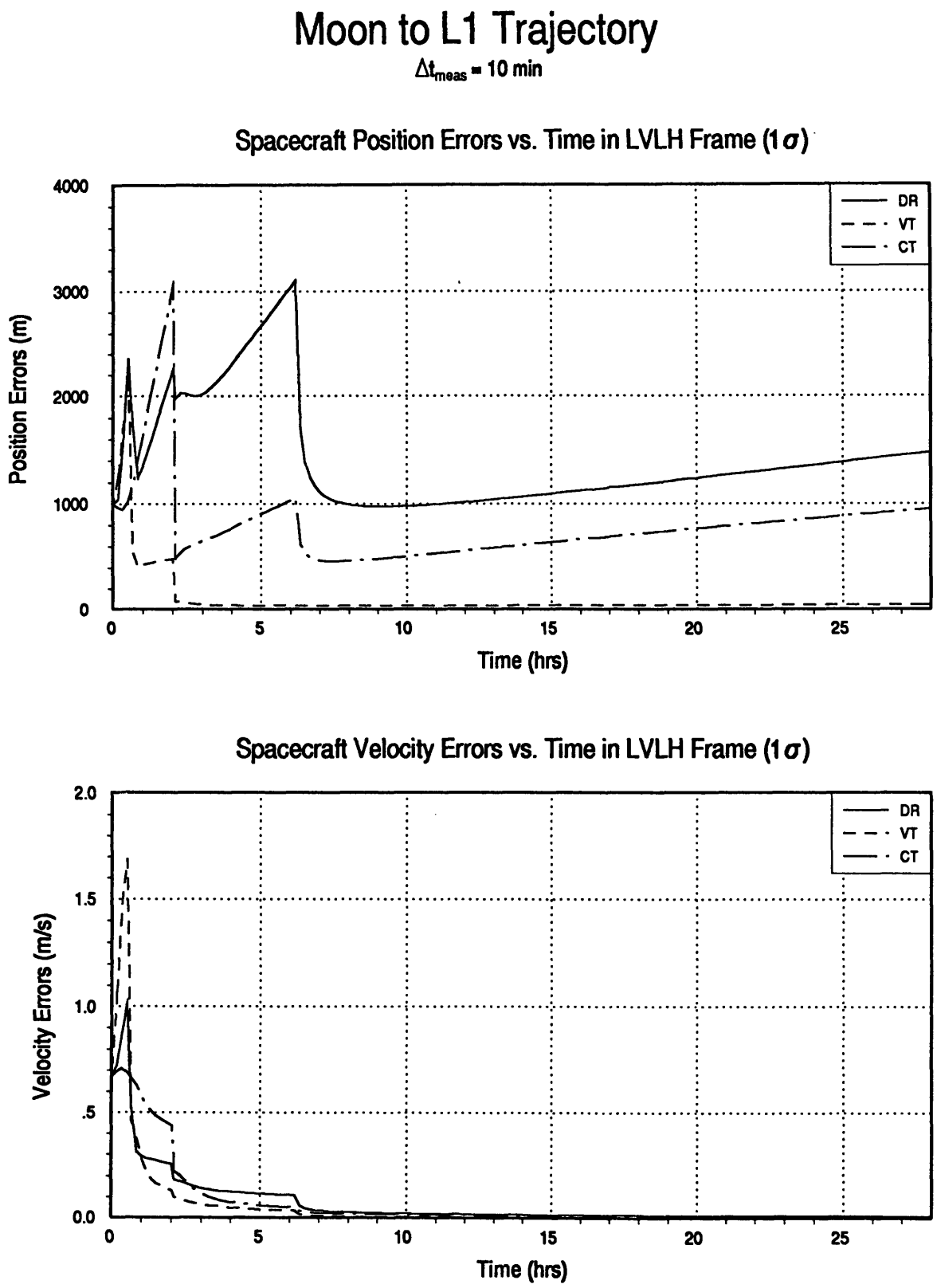

Figure A.33 : Case 4.0

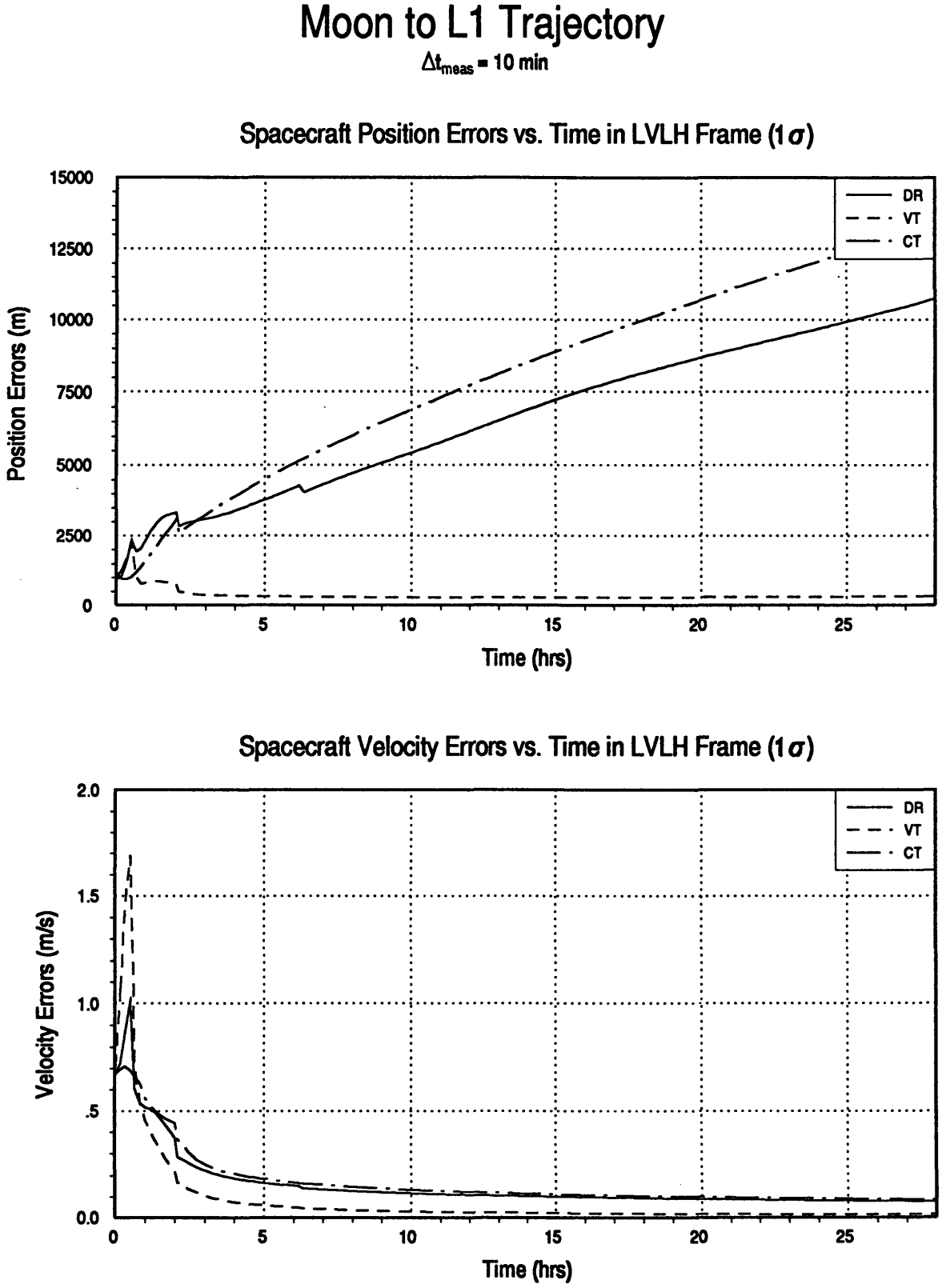

Figure A.34 : Case 4.1

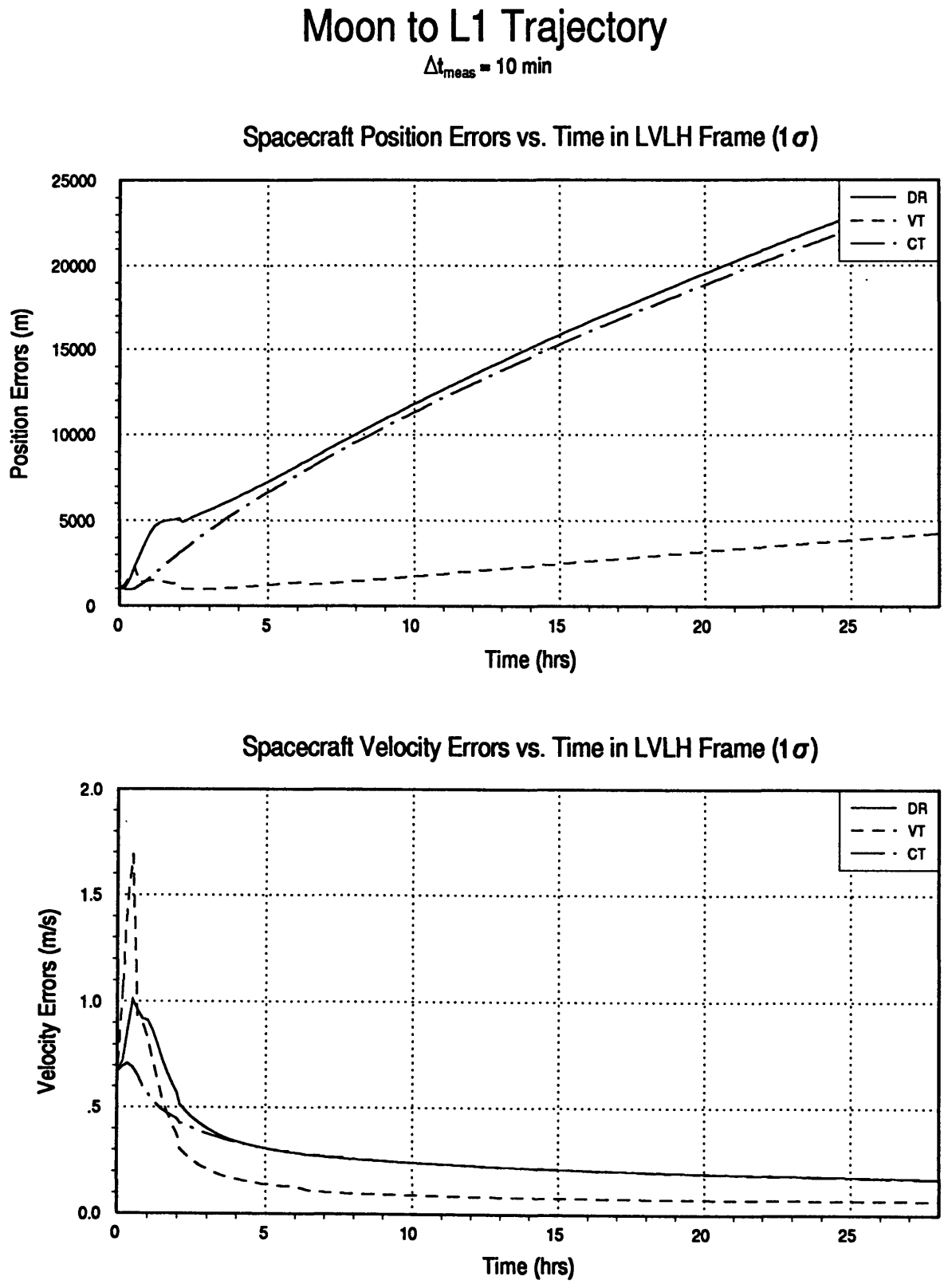

Figure A.35 : Case 4.2

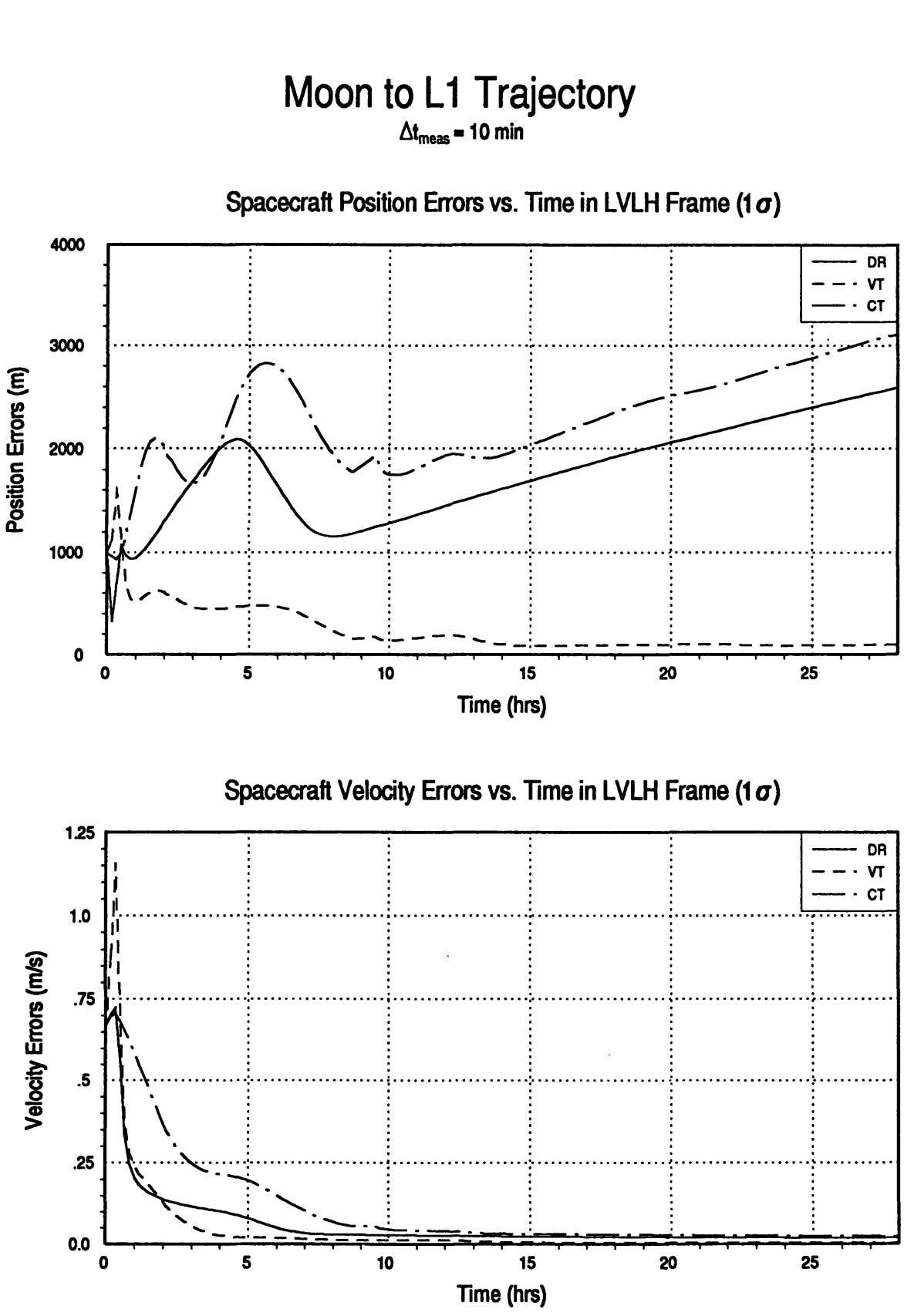

Figure A.36 : Case 4.3

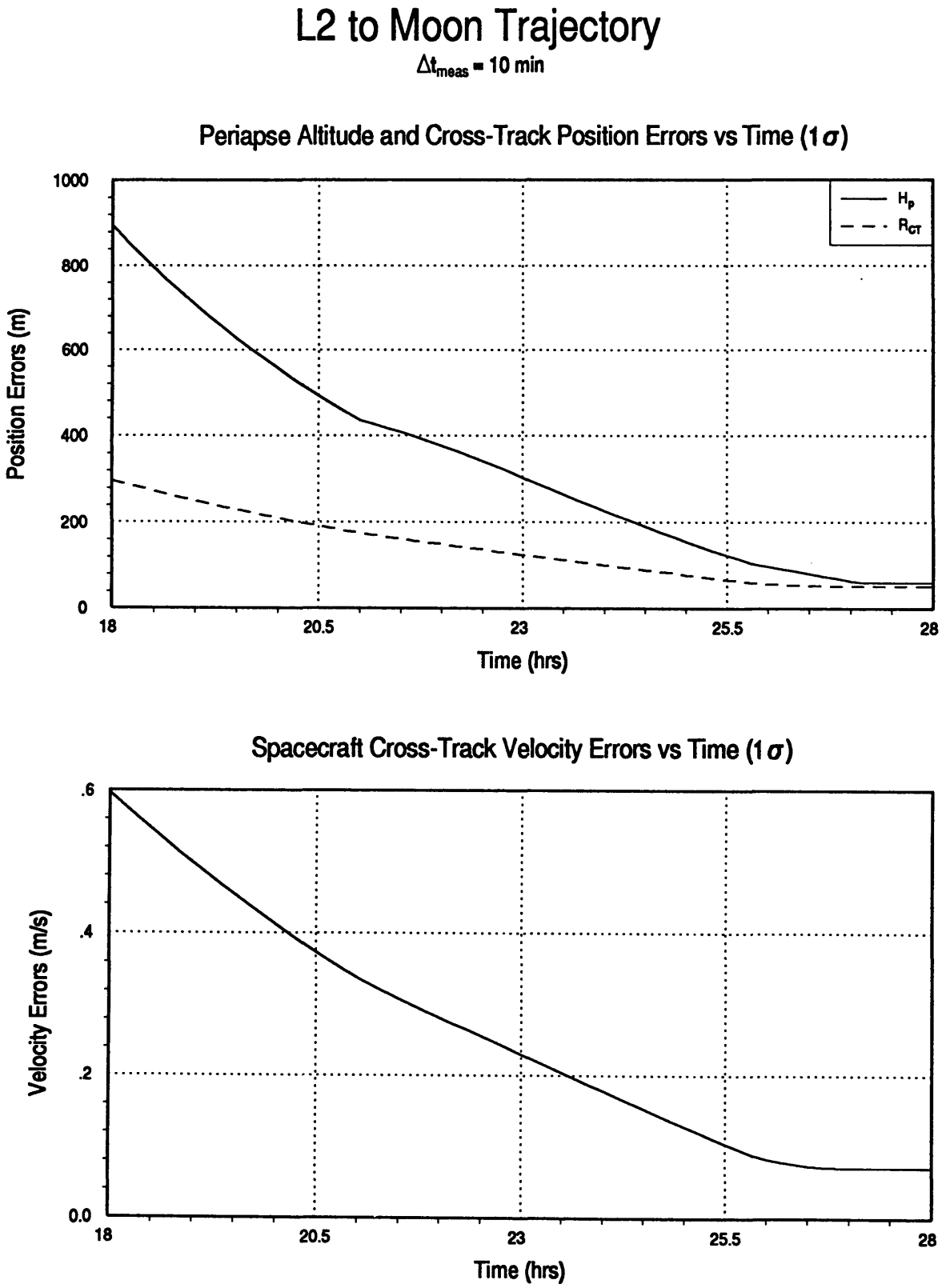

Figure A.37 : Case 5.0

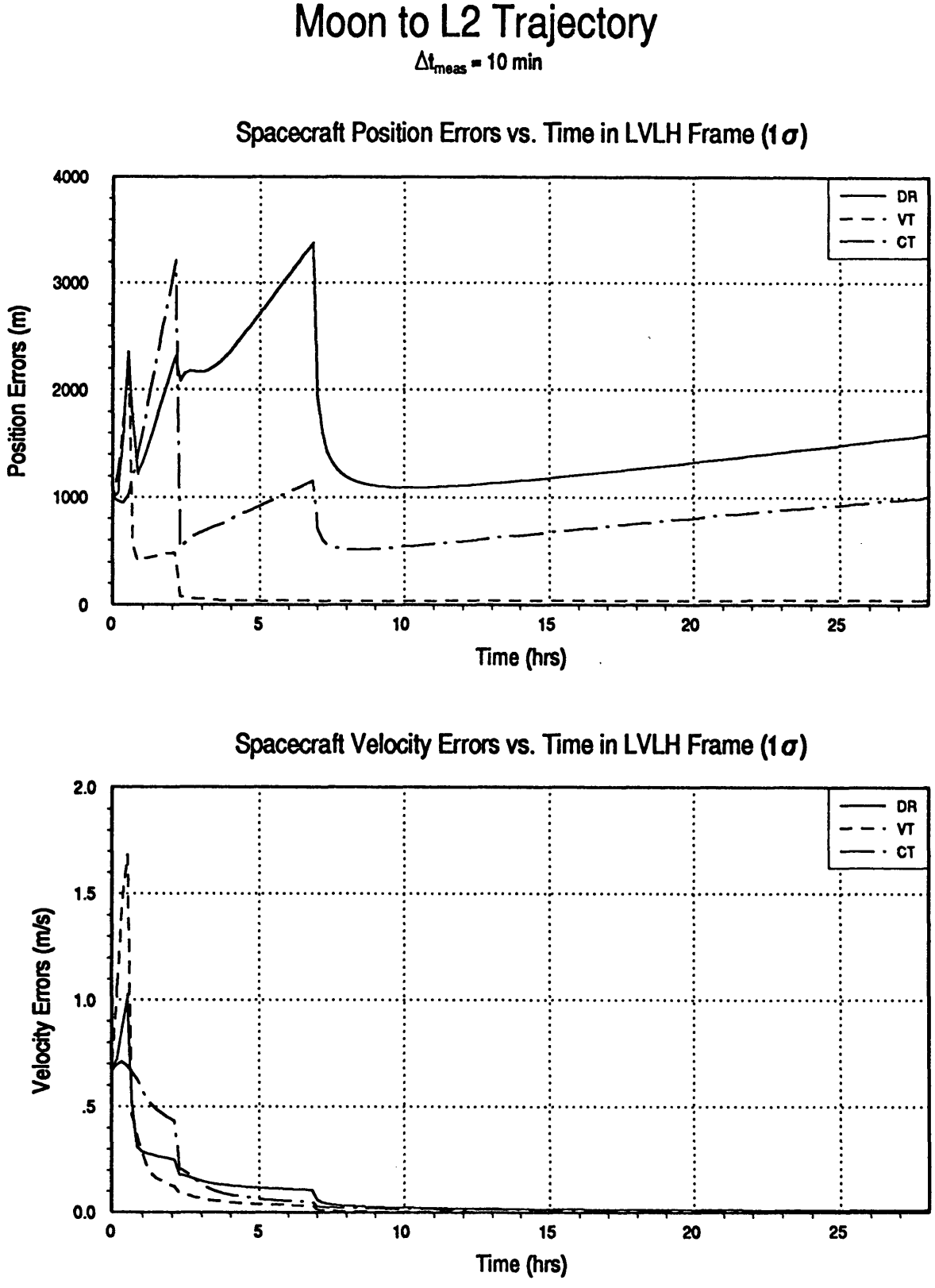

Figure A.38 : Case 6.0

APPENDIX B
List of Constants

Constant	Description	Value	
μ_{Moon}	Lunar gravitational constant	4902.78	km^3/s^2
r_{Moon}	Equatorial radius of Moon	1738.39	km
ω_{Moon}	Rotation rate of Moon	$2.66532227 \times 10^{-6}$	rad/s
i_M	Inclination of the Moon's orbital plane wrt the Earth's equator	18.28-28.58	deg
i_M^e	Inclination of the Moon's orbital plane wrt the ecliptic	5.15	deg
i_M'	Inclination of the Moon's rotation axis wrt it's orbital plane	≈ 1	deg
μ_{Earth}	Earth gravitational constant	398600.64	km^3/s^2
r_{Earth}	Equatorial radius of Earth	6378.135	km
ω_{Earth}	Rotation rate of Earth	$7.29212352 \times 10^{-5}$	rad/s
i_E	Inclination of the Earth's rotation axis to the ecliptic plane	23.45	deg
H_{atmo}	Height of Earth's atmosphere	121.920	km
R_{EM}	Earth-Moon distance	384399.3	km
e	Eccentricity of Earth-Moon system	0.054900489	-
$L1_{Factor}$	L1 Factor	0.849065933383	-
$L2_{Factor}$	L2 Factor	1.167832476643	-
$L3_{Factor}$	L3 Factor	0.992912093233	-
μ_{Sun}	Sun gravitational constant	1.3271244×10^{11}	km^3/s^2
R_{ES}	Earth-Sun distance	1.495979×10^{11}	km

List of References

1. *1992 Astronomical Almanac*, U.S. Government Printing Office, Washington D.C.

2. Battin, R.H. , *An Introduction to the Mathematics and Methods of Astrodynamics*, AIAA Education Series, New York, N.Y., 1987.

3. Bond ,V.R. and Fraietta, M.F. *Station Keeping Near The Unstable Libration Points Of The Restricted Three Body Problem*, Exploration Flight Mechanics Working Group June 8, 1990 - McDonnell Douglas Space Systems Company.

4. Bond,V.R., et. al, *Cislunar Libration Point as a Transportation Node for Lunar Exploration*, Paper AAS 91-103, Feb. 1991.

5. Breakwell, J.V. and Brown, J.V., *The "Halo" Family of 3-Dimensional Periodic Orbits in the Earth-Moon Restricted 3-Body Problem,* Celestial Mechanics, Vol 20, 1979, pages 389-404.

6. Breakwell, J.V., Kamel, A.A., and Ratner, M.J., *Station-Keeping for a Translunar Communication Satellite*, Celestial Mechanics Vol. 10, 1974, pages 357-373.

7. Butcher, J.C., *The Numerical Analysis of Ordinary Differential Equations*, John Wiley and Sons, New York, 1987.

8. Gelb, A., *Applied Optimal Estimation*, MIT Press, Cambridge MA, 1974.

9. Gordon, S.C., and Howell, K.C., *Orbit Determination Error Analysis and Comparison of Station-Keeping Costs for Lissajous and Halo-Type Libration Point Orbits*, Paper AAS 92-115, American Astronautical Society, San Diego CA, 1992.

10. Greenwood, D.T., *Principles of Dynamics* second edition, Prentice-Hall, Inc., Englewood Cliffs, CA, 1988.

11. Howell, K.C., and Pernicka, H.J., *Station-Keeping Methods for Libration Point Trajectories*, AIAA-90-2958-C, American Institute of Aeronautics and Astronautics, New York, N.Y., 1990.

12. Howell, K.C., *Halo Orbits and Other Libration Point Trajectories*, Purdue University, 1991.

13. Howell, K.C., Personal Communications, Purdue University, West Lafayette, IN.

14. Hughes, P.C., *Spacecraft Attitude Dynamics*, John Wiley and Sons, New York, 1986.

15. Konop, P., *Range Measurement Accuracy*, C.S.D.L. Internal Memo LMI-90-045, Aug. 28, 1990.

16. Lear, W. M. , *A Prototype, Real-Time Navigation Program For Multi-Phase Missions*, TRW 17618-6003-T0-00, Dec. 1971.

17. Miller, J.E., *Space Navigation Guidance & Control*, W. and J. Mackay and Co. Ltd., London, 1966.

18. Shepperd, S.W. , *Constant Covariance in Local Vertical Coordinates for Near-Circular Orbits*, Journal of Guidance, Control and Dynamics, Volume 14, Number 6, Nov.-Dec. 1991.

19. Shepperd, S.W. , *Universal Keplarian State Transition Matrix*, Celestial Mechanics Vol. 35, 1985, pages 129-144.

20. Shepperd, S.W. C.S. Draper Laboratory Inc., personal notes.

21. Sponaugle, S.J., et. al, *Optimal Cycling Between Cislunar and CisMartian Libration Points With Reusable Nuclear Electric Transfer Vehicles*, Paper AAS 91-104, Feb. 1991.